SUN AND SOLAR WIND Chapter: Flares and CMEs

Barbara J. Thompson[1], Noé Lugaz[2], Jiong Qiu[3], and David F. Webb[4]

[1]NASA Goddard Space Flight Center
[2]University of New Hampshire
[3]Montana State University
[4]Boston College

November 24, 2022

Abstract

This chapter describes the two major types of impulsive magnetic energy release on the sun: flares and coronal mass ejections (CMEs). The sections include a brief historical overview, a description of observational signature and detection properties, a section on theoretical considerations and outstanding problems, and a final brief section on the field of space weather and anticipated future developments in the field.

SUN AND SOLAR WIND

SUN AND SOLAR WIND

Nour E. Raouafi
Applied Physics Laboratory

Angelos Vourlidas
Applied Physics Laboratory

LOGO

Contents

Contributors

Barbara J. Thompson, NASA Goddard Space Flight Center, Greenbelt, MD, USA

Jiong Qiu, Montana State University, Bozeman, MT, USA

Noe Lugaz, University of New Hampshire, Durham, NH, USA

David F. Webb, Boston College, Chestnut Hill, MA, USA

Acknowledgments

Chapter 1

Introduction

Chapter 2

Solar Interior

Chapter 3

Solar Surface: Magnetism and Solar Radiation

Chapter 4

Solar Flares and Coronal Mass Ejections

4.1. Abstract

This chapter describes the two major types of impulsive magnetic energy release on the sun: flares and coronal mass ejections (CMEs). The sections include a brief historical overview, a description of observational signature and detection properties, a section on theoretical considerations and outstanding problems, and a final brief section on the field of space weather and anticipated future developments in the field.

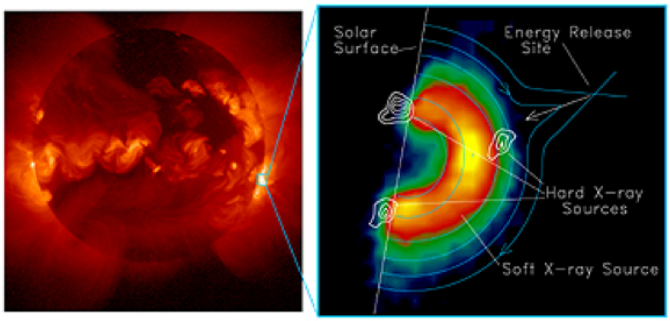

Figure 4.1: Compact flare observed in an active region off the solar limb on 13 January 1992. Left: Yohkoh Soft X-ray Telescope full-disk soft X-ray image of the Sun. The flaring region is circled. Right: Flaring region contour map of the hard X-ray emission from Yohkoh Hard X-ray Telescope, superimposed on the soft X-ray intensity map. Included are approximate magnetic field lines (with arrows indicating direction). This flare, known as the "Masuda flare" [Masuda et al., 1994] was a landmark observation because of the clarity of the coronal hard X-ray emission above flaring loops observed in profile off the solar limb. (Figure credit: Maggio [2008])

4.2. Introduction

Flares and coronal mass ejections, though often treated as separate and distinct solar phenomena, have a great deal of similarities. In fact, many researchers are coming to treat them collectively as two manifestations of a single process: large-scale magnetic reconfiguration in the solar corona.

First and foremost, both defy simple observational description. For example, when one tries to define a flare as a sudden, local, strong increase in brightness on the Sun, one has to clearly define what is meant by these descriptives, and also take into account the cases that test these general criteria.

Flares are a local brightening on the Sun, and may be observed in the photosphere, chromosphere or corona. Where the brightening is observed depends on where the magnetic energy release occurs, and also where the energy is being deposited. The definition of "local" depends on the type of flare. Compact flares (see Figure 4.1), commonly associated with active regions, are usually scaled in megameters. However, the largest long-duration, gradual flares (see Figure 4.2), which are more common in quiet Sun filament channels, can span a solar radius or more. "Local" is defined relative to the magnetic structures undergoing reconfiguration, and as flares can occur in a variety of magnetic structures, the specification of "local" evolves quite a bit. When one starts to consider "microflares" and "nanoflares," the discussion of spatial scale becomes even more complicated.

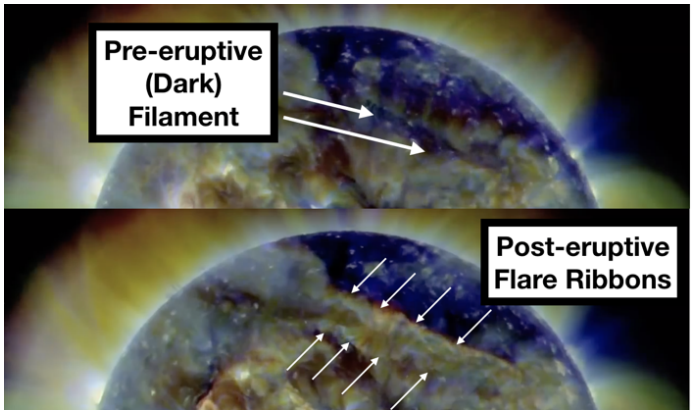

Figure 4.2: A long-duration, gradual solar flare observed in a filament channel. Above: Solar Dynamics Observatory (SDO) Atmospheric Imaging Assembly (AIA) pre-eruptive image at 02:49 UT on 1 August 2010 (Blue: 171Å, Green: 193Å, Red: 211Å). Below: post-eruptive image at 13:54 UT on 1 August 2010. The arrows in the lower image indicate the ribbons of the large-scale flare, extending across much of the visible solar surface. The dark structure in the pre-eruptive image is the filament prior to eruption (note its absence in the post-eruptive image).

Other properties such as energy, timing, and multi-spectral brightness exhibit a similar range of scales. In Section $ 4.4 we discuss the observational properties of flares in greater detail.

Coronal mass ejections (CMEs), on the other hand, are the bulk expulsion of magnetized plsama from the corona. They are typically characterized in terms of speed, acceleration, size (such as width), and brightness. It may seem that the name "CME" is not ideal: it is the magnetic field, not the mass, that forms the basis of the ejection. The mass is part of the magnetic structure (the highly conducting plasma closely follows field lines), and most of the ways CMEs are detected on the Sun depend on how the expelled magnetic fields are filled with material. A CME's observation is dependent on the detection of an apparent massive flow, but also the manifestation of a change in magnetic field structure (see Figure 4.3). The solar wind is a continuous flow of mass from the corona; it is only when the mass contains an apparent "bulk" signature, implying separate magnetic structure, that we call it a coronal mass ejection. However, CMEs can be small, faint, and often the observational viewpoint is not ideal; it is not uncommon for two observers to differ on whether a moving disturbance is a poorly-observed CME, or if it is a different evolving structure. Again, complexity arises when one looks at small CMEs, streamer puffs, or blowouts, jets or other small-scale eruptions. CME is the term used to describe the eruption and its manifestation in inner and outer coronal observations. The term interplanetary coronal mass ejection (ICME) is often used to

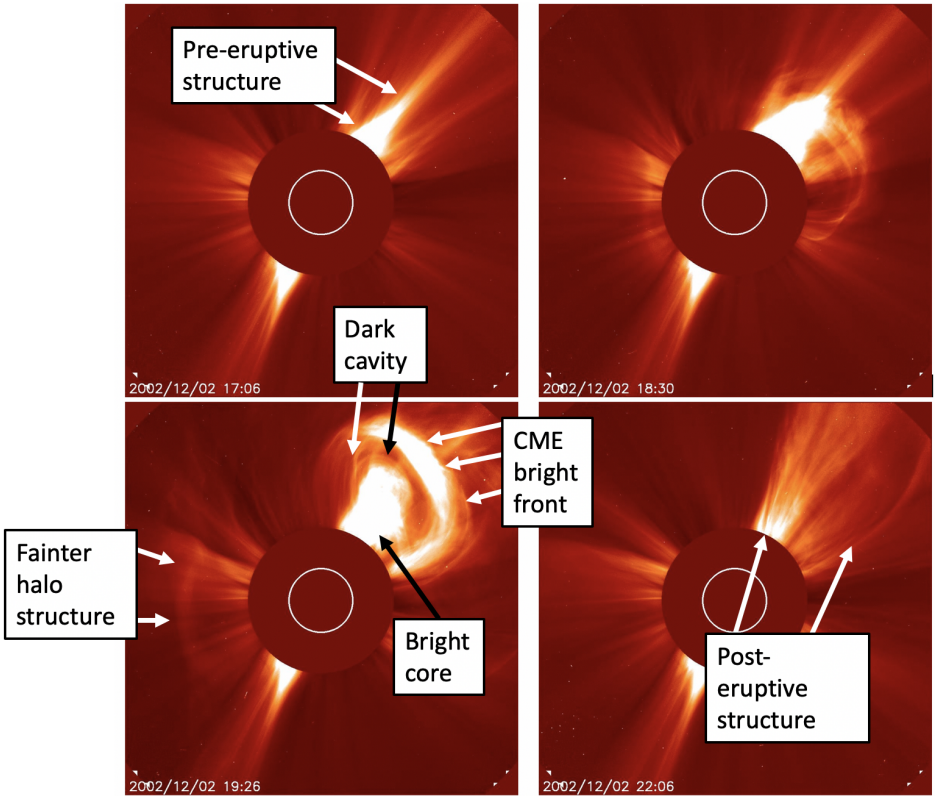

Figure 4.3: Sequence of SOHO LASCO C2 coronagraph images showing an eruption over several hours, with a clear loop CME (top), a fainter CME front (left) and some radial, non-eruptive streamer structures. (a) The "pre-event" image (at 17:06 UT on 2 December 2002) shows primarily radial structures that are typical of slowly-evolving coronal structure. (b) A relatively faint structure with a "halo component is observed, with emission observed at most angles around the disk. (c) A newer CME structure is observed, more localized to the upper right (northwest) quadrant. This CME is much more distinguishable than the first CME. (d) a few hours later, the corona has begun the return to its original, primarily radial configuration.

describe the interplanetary counterpart of CMEs. It has been historically used to describe the in situ measurements associated with these eruptions. With the development of heliospheric imaging with the Solar Mass Ejection Imager (SMEI; 2003-2011) and the STEREO mission's Heliospheric Imager (HI; 2007-present), and the availability of in situ measurements of ICMEs in the upper corona with Parker Solar Probe, the delimitation between these two terms is no longer obvious.

Forging ahead, our field has tried to pin down the key properties that observationally define both flares and CMEs. We usually start with the best examples and properties of "typical" flares and CMEs, and discuss how much these properties can vary (and why). In Section $ 4.4 we discuss observations in greater detail. This is important, as the two phenomena have been historically

defined by their observational properties; these have evolved as our physical understanding has improved and as improved measurements became available.

Flares and CMEs both require an understanding of the buildup and release of solar magnetic energy. An understanding of the physical processes behind flares and CMEs require (at least) three aspects: the buildup of surplus magnetic energy, the "trigger" or initiation of the release of that energy, and the post-flare/eruptive evolution or recovery. The interplay of "buildup" and "release" is what makes flares and CMEs so energetic and impulsive; it is also what makes them so difficult to predict. The trigger, or initiation mechanism, can be extremely subtle, serving as more of a catalyst than a driver of the energy. The trigger can simply be a small tip in the balance of energy, a transition from an eruption being "not energetically favorable" to "energetically favorable." However, once the process has been initiated, the instability can grow rapidly.

Both flares and CMEs can drive space weather in space and at Earth. Another aspect common to flares and CMEs is their impact on the surrounding corona, heliosphere, and planetary system. This is related, for the most part, to the "release" stage of an eruption. X-ray and EUV brightness increases from a flare can deposit energy in the Earth's ionosphere and cause communication disruptions. A direct hit from a CME's magnetic field on Earth can drive strong geomagnetic storms. However, space weather is complicated by a zoo of flare- and CME-associated phenomena. These are processes driven by or triggered by flares and CMEs, such as heliospheric shock waves. Energetic particles from a shock wave are one of the most important factors when predicting space weather. The associated flare and/or CME may have no direct impact on Earth, but the shock that was sparked by an eruption can cause major disruptions, including geomagnetically induced currents and drastic changes in Earths radiation belts. Therefore, it is not simply a question of what causes the release of energy; we must understand where the energy goes, and how it couples to other important phenomena.

Both flares and CMEs vary with the solar cycle and sunspot number. Flares and CMEs tend to be more energetic and frequent during (and just after) solar maximum, due to their role in helping the Sun liberate excess magnetic energy. During solar maximum, more magnetic flux is emerging from the solar interior. The opportunities to exhibit the three-fold criteria (storage, trigger, and release) are much more common. Flares and CMEs are an important means by which the Sun liberates the excess magnetic field building up during solar maximum, and help the global

solar corona transition back to a "solar minimum" configuration. During solar maximum, CME and flare-associated space weather effects are also more common.

Flare studies and CME studies are compromised by detection thresholds. It is important to note that our historical definition of flares and CMEs using observational properties imposes several limitations. For the case of flares, they are commonly defined by their X-ray peak flux, observed against an often bright and variable X-ray solar background. During solar maximum, the corona itself may exceed smaller, "A-class" and "B-class" level flares meaning that we can only detect C-class flares and above. This does not mean that there are no A-class flares during solar maximum, it just means that classical detection methods must be augmented (a similar challenge involves flares occurring on the far side of the Sun). Similarly, the mass and magnetic structure of the solar corona are more disturbed and variable during solar maximum. A faint, slow CME that would easily be detected against a more placid solar minimum corona would be more difficult to distinguish against a more active solar maximum environment. Therefore, the statistics of less energetic CMEs may be underrepresented during solar maximum, suffering a similar fate to weaker flares.

As more sophisticated measurements became available, our ability to characterize flares and CMEs dramatically improved.

They frequently occur together, suggesting that impulsive magnetic energy releases on the Sun can exhibit varying degrees of "CME-like" properties and "flare-like" properties. Several CME trigger mechanisms involve a flare-like reconfiguration (reconnection) of magnetic field that transforms confined, high-pressure magnetic flux into flux that is free to expand and leave the corona. Indeed, the famous "Aly-Sturrock" conjecture [Sturrock, 1991] stated that the magnetic energy of a given force-free boundary field is maximized when the field is open, and challenged the scientific community to explain how the apparent opening of field lines in the form of a CME could happen. The flare/CME interplay changes the boundary conditions; therefore, many CME models require a flare-like reconfiguration as part of the CME process. Additionally, open fields following a CME close back down and recover using flare-like magnetic reconnection processes.

From the other standpoint, many flare models involve the bulk motion and expulsion of magnetic flux in a CME-like manner. Even if the flux "blob" is not ejected fully from the Sun, it can be

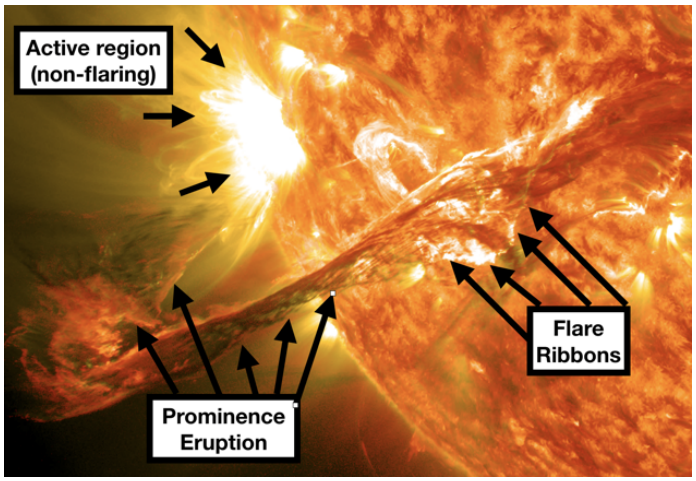

Figure 4.4: This eruption, observed by SDO/AIA on 31 August 2012 (Orange: 304Å, Yellow: 171Å) is at the time of publication one of the most common search engine results for solar flare. However, the flare-like manifestation of this event (labeled Flare Ribbons) is one of the least remarkable aspects of the image. Undoubtedly, the attraction (and confusion) is mostly due to a non-flaring (but bright) active region, and the CME (labeled Prominence Eruption.)

ejected from the flaring area and land elsewhere. Many researchers specialize in this study of "eruptive flares" and their associated "failed" eruptions, recognizing the role that flux ejection can play in flare energy release. As it turns out, most flare models contain some element of CME-like motion, and most CME models have some aspect of local flare-like energization.

They are often confused with each other. It is not at all uncommon for someone in the popular press, or even researchers in peripheral fields, to label a CME a "flare" and vice-versa. And if we are honest, can we truly blame them? With the high degree of complexity (and confusion) in defining, observing, characterizing, and understanding the two phenomena, even the most experienced observer can find it a challenge to simply call it one or the other.

Therefore, the case for treating the two collectively, as two different manifestations of a more comprehensive impulsive-magnetic-energy-release phenomenon, is compelling. Rather than specifying whether something is a "flare" or a "CME," there is a growing movement to treat the two together, and discuss how the energy release is partitioned between "flare-like" processes and "CME-like" processes. This chapter will proceed in that respect; we will discuss the "flare-like" aspect of an issue, and follow with the discussion of the "CME-like" aspect. We hope the reader will enjoy the interplay between the two.

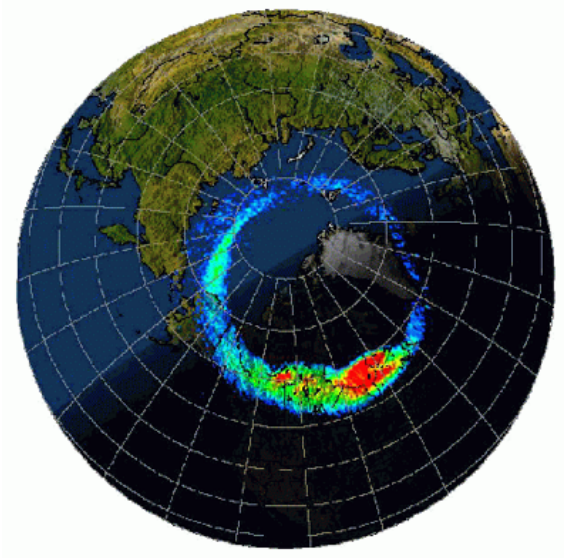

Figure 4.5: "Typical" auroral oval. Colors indicate intensity, red is strongest, blue is weakest [Holzworth and Meng, 1975] superposed over a map of the Earth. Aurorae have occurred throughout Earth's history over areas that are not heavily populated. Source credit: NASA NSSDC.

4.3. History

4.3.1. Early History

Flares and CMEs have undoubtedly been impacting the Earth for over 4 billion years. However, only recently has humanity been aware of these two phenomena. The reason for this "late realization" is because their observational properties (Section $ 4.4) are subtle, and their effects (see Section 4.6) have become more pronounced in the technological era. The one possible exception is the aurora borealis/australis. Aurorae are a beautiful manifestation of the Sun's influence on Earth (see Figure 4.5) and do not require special instrumentation to observe.

Aurorae (aurora borealis indicating north pole, aurora australis being the southern complement) have been reported throughout human history. They are observable from the ground, providing: a) the Sun's activity has impacted Earth's magnetosphere in a way that drives geomagnetic activity, b) the observer is at a latitude where aurorae are observable (primarily, high latitudes, see Figure 4.5) and c) the aurorae are visible to the observer (nighttime conditions are ideal - cloud cover and 24-hour daylight in the summer inhibit observation).

With the realization of the very ordinary conditions under which aurorae occur, and the spo-

radic conditions under which they are observed, it becomes clear why these pieces of the Sun-Earth connections puzzle were so difficult to assemble. From Earth, the Sun appeared static, constant, unchanging. Aurorae appeared at night, seemed harmless, and were a reminder of the many unknown manifestations of the power of nature.

Naked-eye observations of sunspots were reported in China starting in the 10th century [Hayakawa et al., 2016]. In the west, J. Fabricius was the first to publish a report of sunspots at the end of 1611, and shortly thereafter Galileo began recording sunspots using a new instrument - the telescope. This represents the dawn of Sun-Earth connections and space weather studies. Although sunspots are an excellent representation of the magnetic potential of the Sun, they are not a good indicator of how much Earth-impacting activity has transpired. The long-term sunspot record initiated by Galileo is invaluable; it helps us understand the Suns history and variability. But sunspot number is just one part of the puzzle.

It was not until the 19th century that evidence was clear: the Sun's activity could impact the Earth. It required two components: observations of the Sun's activity, combined with the response at Earth. The evidence began to add up. There were technological components (such as radios and telegraph machines) that provided vital clues that could be connected to the occurrence of aurorae, and there were also improved solar observations. One is left wondering how rapidly auroral (and, hence, space weather and solar activity) research would have progressed if aurorae were a commonly observed phenomenon over heavily populated areas!

To make advances in the understanding of Sun-Earth connections, humanity needed clear evidence of solar activity and of the associated response at Earth. Flares are typically observed in energetic wavelengths (X-rays and extreme ultraviolet), which are blocked by the Earth's atmosphere and are only readily observable from space. CMEs are very faint compared to the Sun's emission, and are more readily observed in the outer corona, also from space. However, the outer corona is about one billion times fainter than the Sun itself, so a definitive CME observation is a challenge. There are reports of white light (i.e. visible spectrum) flares being observed by astronomers, and CME-like structures during solar eclipses, but there not enough events to identify an association with any terrestrial response.

4.3.2. The "Carrington Event"

This all changed in 1859, when strong geomagnetic and space weather effects were observed soon after a major solar flare. It is also called the "Carrington event," after one of the astronomers who recorded the series of interactions (Richard C. Carrington and Richard Hodgson). On 29 August 1859 Carrington and Hodgson independently observed a flare in a large sunspot group. This was prior to x-ray and EUV observatories; this flare was so strong that it was easily observable in the visible spectrum. Less than 24 hours later (which is extremely fast, by CME standards), the effects were noticed at Earth. Aurorae were observed at nearly all latitudes over the globe, even locations near the equator. Telegraph systems, which are prone to space weather because they use conducting wires connected over large distances, were unable to function with the geoelectric field overload; some operators reported receiving electric shocks when they attempted operation. Additional space weather effects were observed, such as strong deviations in magnetic field measurements.

The Carrington event was significant because of two key factors: the magnitude of the storm and onset of technology affected by space weather. Modern measurements that characterize storm magnitude were not available in 1859, so a number of methods have been applied to translate the magnitude of the Carrington storm in the context of more recent events (Baker et al. [2013], Ngwira et al. [2014]). Although the estimates can vary, it is overwhelmingly agreed that there has not been as strong an impact on Earth since the Carrington event. It remains the benchmark against which all other major storms are judged.

There is little doubt that there were stronger storms prior to the Carrington event, but a key role was played by the emerging technology of the 19th century, including the improved international communication of the scientific community that allowed them to correlate global auroral observations. The accumulated evidence of solar observations, magnetic field measurements, auroral activity and anomalous telegraph behavior comprised an undeniable body of evidence: activity on the Sun has an impact on Earth.

In later years, measurements and technology both improved. We began to understand that it was not the solar flare, but the CME that travelled the 1.5×10^8 km (93 million miles) to Earth, that was responsible for the majority of the observable impacts. Storms that were weaker than the Carrington storm had much larger impacts, because radio communications, power grids, and

technology in space were much more sensitive to space weather phenomena. Still, we look to the Carrington event as a landmark event: there was no doubt that Sun-Earth connections exist, and the scientific community took up the challenge of unraveling the physics of this dynamic system.

4.3.3. Improved Observations Lead to the Modern Era

There are many measurements that led to the piecing together of the flare/CME puzzle. Not long after the Carrington event, ground-based observations of solar filaments with spectroheliographs documented their tendency to erupt [for a comprehensive review, see Parenti, 2014]. Solar magnetic field measurements from the ground, developed by George Ellery Hale in 1908, have played an important role in understanding solar dynamics. However, it was the advent of observations from space that gave the scientific community access to continuous, multi-wavelength data free of atmospheric effects.

It is important to note that observations from the ground have always provided vital information as well, such as global, synoptic H-alpha imagery obtained over many decades. New ground instruments such as the Daniel K. Inouye Solar Telescope (DKIST) in Hawaii promise to yield many more advances.

As flares were observable long before CMEs were discovered, most of the early papers focused on flares as the driver of solar activity and the subsequent effects observed at Earth. A very noteworthy discovery was the identification of coronal mass ejections by Tousey [1973] using the seventh Orbiting Solar Observatory (OSO-7). Although it was known that the solar wind existed, and that it contained transient, varying structures, the definitive observation of a CME led us to investigate the causes and effects of these phenomena. It became clear that certain effects that were attributed to flares could possibly be more clearly explained by CMEs. A famous paper by J. Gosling titled the Solar Flare Myth [Gosling, 1993] led the community to understand the tendency to believe something parallel to "ontogeny recapitulating philogeny" – or that the discovery of one phenomenon predating another phenomenon can falsely imply a causal, hierarchical relationship between the two. Gosling argued that the community needed to reevaluate the correlations between flares and certain impacts, because some effects more clearly explained as being driven by CMEs.

Švestka [1995], however, cautioned against an overemphasis on the CME aspect of magnetic

energy release. He argued that two-ribbon flares, and the study of other types of "eruptive flares", are key parts of understanding the eruption process.

Finally, Harrison [1996] led the way towards a more tempered approach, arguing that flares and CMEs are two aspects of the "same magnetic disease", and further urged against the use of simplistic terms such as "explosion" to describe the complex, interrelated process of magnetic energy liberation.

Readers are reminded that, given the long history of these studies, many excellent textbooks (e.g. Howard [2011]) and reviews are available. Fletcher et al. [2011], Hudson [2011], Benz [2017] and Webb and Howard (LRSP, 2012) provide more recent and general reviews of flare observations. A comprehensive account of flare physics is given by Tandberg-Hanssen and Emslie [1988], and Priest and Forbes [2000], Shibata and Magara [2011], Priest [2014] discuss in detail the magnetohydrodynamic processes and magnetic reconnection theory of solar flares. Yashiro et al. [2004a] and Vourlidas et al. [2017] cover the observed properties of CMEs from a single and multiple viewpoints, respectively. We recommend the papers by Gopalswamy and Thompson [2000] and Georgoulis et al. [2019] describing the early stages of CME development, and Howard [2006] for an historical overview of CME observations.

The following sections give a brief overview of observational signatures of flares and CMEs, with a particular focus to update readers with observations in the recent era.

4.4. Observational Signatures and Detection Properties

The physics of flares and CMEs is intrinsically linked; as we understand the nature of magnetic energy buildup and release, we will understand these two explosive manifestations of those processes. In this section we briefly cover the various observations that are used to study flares and CMEs. Most of them involve remote sensing - the collection of photons in the form of images and spectra. As you will read, the scientific community relies on a diverse range of observations, and each of the observations holds vital clues about the nature of the two phenomena.

4.4.1. Flares

The most prominent observational signature of a solar flare is the impulsive enhancement of radiation across the entire electromagnetic spectrum, from radio waves with the wavelength between kilometers and millimeters, through γ rays, whose extremely short wavelength is only a small fraction of the diameter of an atom. The Carrington flare was discovered as sudden brightening in the visible white-light emission from the Sun's photosphere. Nowadays, flare emissions in many wavelength ranges are recorded. Whereas modern imaging observations of flares have revealed breathtaking details down to the scale less than one thousandth of the Sun's radius, spectroscopic observations, including polarimetry measurements, remain an astrophysicist's most powerful tool to diagnose properties of plasma and magnetic field in the Sun's atmosphere.

This section is intended to focus on a few observational aspects of flares with space weather consequences, including non-thermal electrons, short-wavelength radiations, and any pertinent relationships with CMEs. Although non-thermal electrons discussed here refer to those trapped in the flare volume, they often carry a large fraction of flare energy and play a significant role to heat the flare atmosphere, which in turn produces much enhanced EUV radiation acting on Earth's upper atmosphere. In the following, only a limited description is provided to explain the basics, and readers are referred to many existing outstanding reviews for completeness and comprehensive details on flare observations.

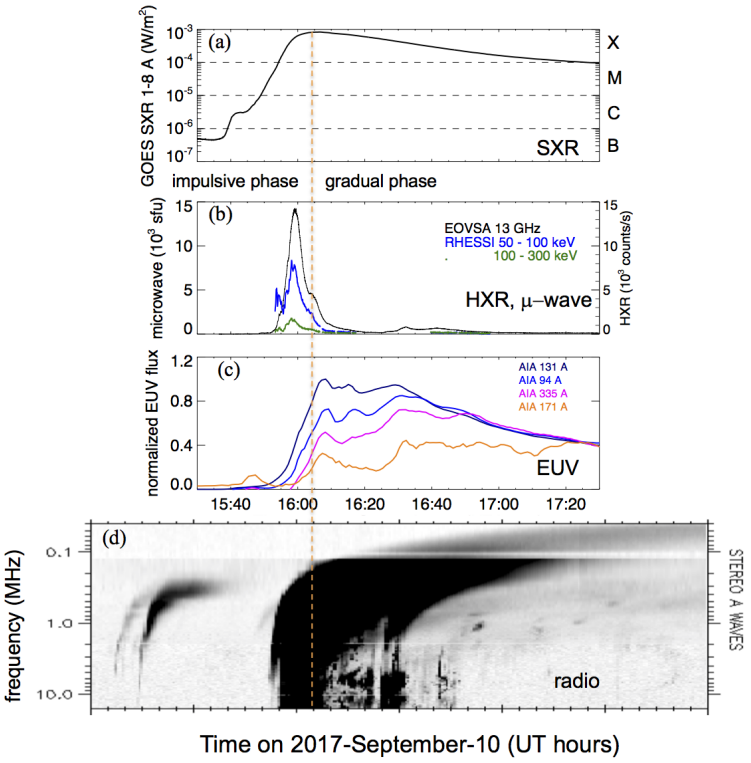

Figure 4.6: Light curves of an X8.2 flare on 10 September 2017, including (a) the soft X-ray light curve by GOES at 1-8 Å, (b) microwave light curve at 13 GHz by the Extended Owens Valley Solar Array [EOVSA; Gary et al., 2013] and hard X-ray light curves in two energy ranges by the Reuven Ramaty High Energy Solar Spectroscopic Imager [RHESSI; Lin et al., 2002], and (c) light curves of extreme-ultraviolet emissions in several pass-bands observed by the Atmospheric Imaging Assembly [AIA; Lemen et al., 2012] onboard the Solar Dynamics Observatory [SDO; Pesnell et al., 2012]. (Courtesy Dale Gary, Chunming Zhu; also see Gary et al. [2018].) (d): a strong type II radio perturbation is observed by the WAVES onboard the Solar TErrestrial RElations Observatory [STEREO; Kaiser et al., 2008] satellite. (Figure credit: `secchirh.obspm.fr`.)

4.4.1.1. Time Profiles

The time history of the flare total emission at a given wavelength is called a flare light curve. Figure 4.6a shows the soft X-ray light curve in the wavelength range 1-8 Å from a large flare, observed by the Geostationary Operational Environmental Satellite system (GOES). Flare emission at this wavelength is produced by plasma heated to more than a few million kelvin in the Sun's outer atmosphere, the corona. As a convention, this specific measurement of flare emission is used to define the magnitude of a flare: a flare is designated to be A, B, C, M, or X class when its peak soft X-ray flux is in the range of $< 10^{-7}, 10^{-7} - 10^{-6}, 10^{-6} - 10^{-5}, 10^{-5} - 10^{-4}, > 10^{-4}$ Watts per square meter, respectively. For example, the X8.2 flare illustrated in the figure produces 8.2×10^{-4}

Watts per square meter in the GOES 1-8 Å channel at its peak. Because of the logarithmic scale, X-class flares are much more energetic than C-class flares.

The soft X-ray emission of a flare is usually observed to rise rapidly on timescales of order of minutes, and then decay more gradually, sometimes lasting for hours or even days. Traditionally, we consider the flare to be in the impulsive phase during the rise of its soft X-ray emission, and in the gradual phase after the peak of the soft X-ray emission. Significant hard X-ray and microwave emissions, which are indicators of the presence of electrons accelerated to a fraction of the speed of light, are often produced in the flare's impulsive phase (Figure 4.6b). The wavelength, or energy, of hard X-ray photons is described in units of electron volts (eV). A large flare may generate many hard X-ray photons of energy from a few tens to a few hundred keV (kilo- electron volts), like shown in the figure. Microwave emissions are produced by interaction of fast electrons with plasma as well as magnetic field. Here, we start to use "frequency" in units of Hz to describe the energy of microwave photons, and the figure shows the microwave emission of the large X8.2 flare at the frequency of 13 GHz (or 13 billion Hz), which carries, at its peak, the total flux of more than 10,000 solar flux units (sfu) [1].

Following the X-ray and microwave emissions, many ion lines have flare emission in the extreme-ultraviolet (EUV) wavelengths (Figure 4.6c). These are produced by the flare plasma in the corona that cools off from more than 10 million kelvin. A flare also gives off abundant visible and ultraviolet line emission as well as enhanced continuum emission, usually produced at lower temperatures (below 100,000 kelvin) from the impulsively heated chromosphere or even photosphere. Although the amount of the Sun's radiation energy in the short wavelength is rather insignificant in comparison with its visible output, a large number of EUV photons will cause severe ionospheric responses. For this reason, over the past decade, the EUV Variability Experiments [EVE; Woods et al., 2012] has been in operation to monitor the Sun's EUV output, which increases by a few orders of magnitude during flares [Chamberlin et al., 2012, Woods, 2014].

It is worth noting that many kinds of radio emissions can be produced by or in association with a flare [see review by Pick and Vilmer, 2008]. Energetic particles escaping into interplanetary space

[1] Solar flux units describes the wave power received by a telescope detector per unit area per unit frequency range. One sfu is 10^{-22} Watts per square meter per Hz.

cause decimetric or metric type radio bursts, for example, the type III radio burst by flare produced energetic electrons. Accompanying the X8.2 flare shown in Figure 4.6, the WAVES instrument onboard the Solar TErrestrial RElations Observatory [STEREO; Kaiser et al., 2008] satellite has detected a strong type II radio burst with its frequency drifting from 10 MHz to 0.1 MHz, a signature of electrons accelerated by CME-driven shocks moving through interplanetary space. So the flare occurs together with a very fast CME, which is rapidly accelerated during the impulsive phase of the flare [Veronig et al., 2018]. Such close synchronization between the impulsive rise of flare emission and CME acceleration has been illustrated in a good number of, though not all, events, suggesting a more than casual relationship between the two [e.g. Zhang et al., 2001, Gallagher et al., 2003, Qiu et al., 2004, Temmer et al., 2010, Patsourakos et al., 2010]. Observations have further revealed the presence of a flux rope cavity [Long et al., 2018, and see Section 4.4.2 and Figure 4.11 for CME structure], significant wave transients [Liu et al., 2018, see Section 4.4.2.2 for wave transients], solar energetic particles [SEPs; Guo et al., 2018, see Chapter 8], and ground level enhancement events [GLEs; Gopalswamy et al., 2018, see Chapter 8]. So, like most X-class flares [Yashiro et al., 2004b], the illustrated X8.2 flare is one symptom of the "same magnetic disease" [Harrison, 1996] with another symptom being a fast CME, amid many others.

4.4.1.2. Spatial and Spectral Properties

Imaging observations have shown that a flare comprises a cluster of so-called flare loops[2], which are plasma tubes believed to be confined by the magnetic field. These are referred to as magnetic loops, largely residing in the tenuous corona with both ends anchored in the denser lower atmosphere. Therefore, in contrast to their outgoing CME sisters, flares are often described to be "closed", "confined", or "local" structures.

The aforementioned soft X-ray emission is from the coronal part of flare loops where plasma is heated to more than ten million kelvin. When heating is attenuated and coronal plasma cools down through a sequence of decreasing temperatures, emissions of ion lines sensitive to these temperatures

[2]For consistency in the following text, we use flare "loops" to describe observationally resolvable structures of cross-section being around 1000 km, and the term "strands" or "threads" seen elsewhere may refer to still smaller-scale fine structures resolved by only a few current instruments [See Aschwanden and Peter, 2017, for a discussion of coronal loop width].

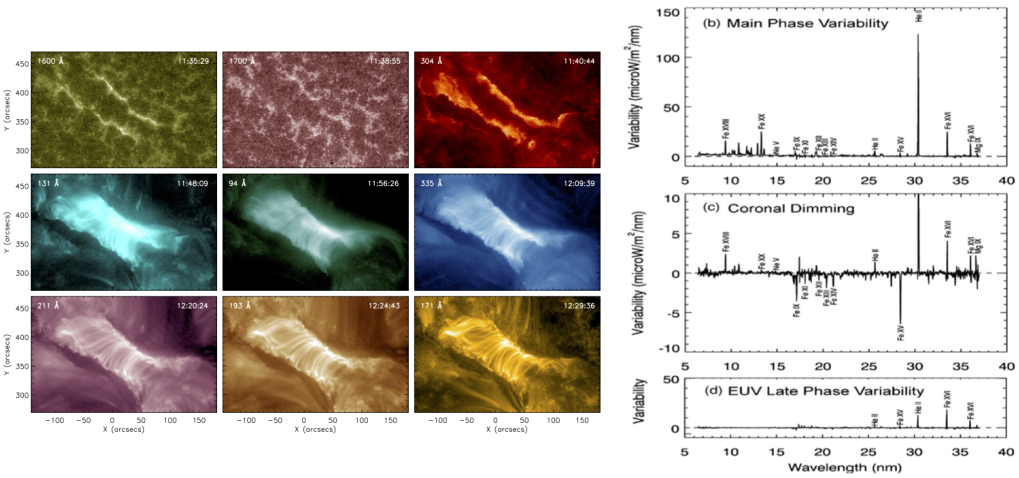

Figure 4.7: Left: an arcade of flare loops of an eruptive two-ribbon flare observed by AIA on SDO in nine ultraviolet and extreme ultraviolet passbands. The top panels show enhanced ultraviolet emission in 1600 Å, 1700 Å, and 304 Å, from the heated chromosphere and transition region, outlining the feet of flare coronal loops, which are brightened subsequently in a series of iron lines sensitive to successively lower temperatures, as shown in the middle and lower panels. (Figure credit: Cheng and Qiu [2016].) Right: EUV spectra by EVE spectrometers showing flare radiation, coronal dimming, and EUV late phase in another event. (Figure credit: Woods et al. [2011]).

arise sequentially. This is shown in Figure 4.7, where a series of Fe XXI (131 Å), Fe XVIII (94 Å), Fe XVI (335 Å), Fe XIV (211 Å), Fe XII (193 Å), and Fe IX (171 Å) lines, respectively sensitive to temperatures of 10, 6, 3, 2, 2, and 1 million kelvin, become dominant emissions in an arcade of flare loops observed by AIA. More precise diagnostics of plasma temperatures can be achieved from high-resolution spectroscopic observations obtained by spectrometers such as the EVE [Warren et al., 2013, Caspi et al., 2014, also see the right panel of Figure 4.7 for some EVE spectra]. These observations have helped establish our understanding of the heating and cooling sequence of coronal plasma in flare loops.

Analysis of these spectral line emissions also allows us to find the amount of plasma emitting at a given temperature [see Feldman et al., 1992, Del Zanna and Mason, 2018, for comprehensive tutorials of plasma diagnostics with EUV observations]. Simply put, the more plasma is emitting, the more intense the line becomes. The temperature distribution of non-isothermal coronal plasma, which is often the case during flares, is accounted for by a property called the Differential Emission Measure (DEM). $DEM(T) = n^2(T)dV/dT$, where n is the electron density, T temperature, and dV elementary volume of the plasma. The observed intensity of a specific spectral line is related to this

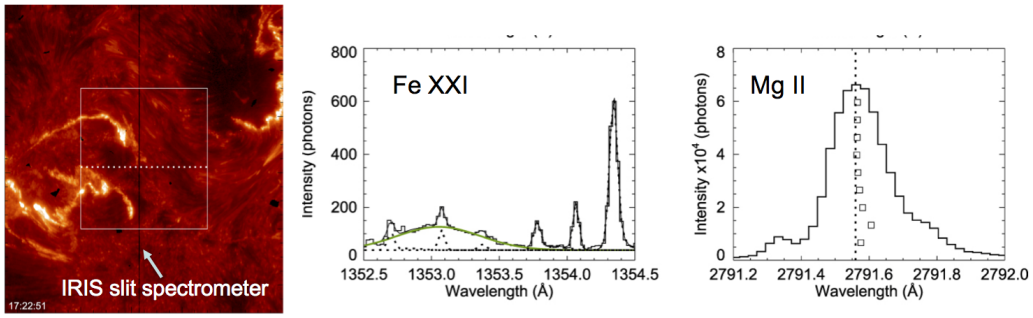

Figure 4.8: Left: Image of a flare with brightened feet of flare loops observed by the Interface Region Imaging Spectrograph (IRIS) launched in 2013. The dark vertical line shows the position of the slit spectrometer. Right: the Fe XXI and Mg II line profiles taken by the spectrometer at one location on the flare ribbon at one time. The observed hot Fe XXI line is fitted to a Gaussian profile (green), and appears to be blue-shifted from its rest wavelength 1354.1 Å, indicating hot plasma moving upward into the corona (note that dotted curves represent other lines in nearby spectral positions). The rest wavelength of the cool Mg II is at 2791.56 Å, denoted by the vertical dotted line, and black squares mark the central positions of the line from its core to the wing, which are red-shifted from the rest wavelength, indicating plasma downward motion in a complex manner in the varying depth of the chromosphere [Graham and Cauzzi, 2015].

property by $I_\lambda = \int R_\lambda(T) DEM(T) dT$ where $R_\lambda(T)$ is the combined effect of the emissivity of the line, known from atomic physics [e.g., the CHIANTI atomic database by Dere et al., 1997, and later development], and the response function of the observing instrument. Advanced inversion methods have been developed to derive the Differential Emission Measure of flare plasma from observations made at many lines sensitive to a variety of temperatures [e.g., Hannah and Kontar, 2012, Cheung et al., 2015], and the total amount of emitting plasma is then given by $EM = \int DEM(T) dT$. Interestingly, the same technique applied to coronal dimmings (signatures of a CME, see Section 4.4.2.2) yields the Emission Measure that is missing from the Sun's corona (Figure 4.7), as it is carried away by an erupting CME! When we do these, it comes as a surprise that, given its "closed" and "confined" nature, the Emission Measure of an average flare, usually of order 10^{47-50} cm^{-3} [Aschwanden et al., 2015], is indeed comparable with that of a large CME [Aschwanden, 2017]. Imaging observations give us an educated guess of the flare volume, and it then turns out that the average density of the flare coronal plasma is quite high, greater than that of the background flare-less corona by two orders of magnitude. Then, how does the flare corona become so dense apart from being hot?

The answer lies in the lower atmosphere - the chromospheric density is 10,000 times higher, and could easily act as a mass reservoir for the tenuous corona. The prevailing understanding is that the chromosphere is impulsively heated at the start of the flare, giving rise to a sudden increase of the pressure there, which drives up-flows and, therefore, transports a considerable amount of dense plasma into the corona. This is evidenced by signatures of impulsive and intense optical or ultraviolet emission at the feet of flare loops, prior to substantially increased emission in the corona, as clearly illustrated in Figure 4.7.

Yet the crucial evidence is from spectroscopic observations [see review by Milligan, 2015], which have revealed plasma upflows at speeds as large as a few hundred kilometers per second, into the tenuous corona from the impulsively brightened feet of flare loops. These are accompanied by downflows into still denser atmosphere at a few tens kilometers per second, so as to maintain momentum conservation [Canfield et al., 1987, Zarro et al., 1988]. The upward and downward motion, first discovered in the 1980s as the blue-shift of hot lines and red-shift of cool lines [e.g. Antonucci et al., 1982, Ichimoto and Kurokawa, 1984], has been called "chromospheric evaporation" and "chromospheric condensation" [Canfield, 1986, Fisher, 1989]. [Graham and Cauzzi, 2015, Figure 4.8] have demonstrated some of the most advanced spectroscopic diagnostics of flare dynamics at a high spatial resolution (of scale around 300 km) with the recently launched Interface Region Imaging Spectrograph [IRIS; De Pontieu et al., 2014] that observes the Sun's lower atmosphere, the chromosphere and transition region, in the ultraviolet spectral range. Observations of this kind remind us that the advent of next-generation, diffraction-limited high-resolution telescopes with high-sensitivity spectrometers, like the Daniel K. Inouye Solar Telescope (DKIST), will certainly increase our understanding of the fundamental scale at which flare energy is released to heat the lower atmosphere and drive chromosphere evaporation [see, e.g. Jing et al., 2016, for fine-scale structures of a flare].

Flare-accelerated electrons can deposit energy in the lower atmosphere. These electrons interact with the ambient plasma and magnetic field to produce hard X-ray and microwave emissions, and the manner of interaction much depends on the speed as well as the direction of the electrons, the latter specified by the pitch angle, the angle electrons make with magnetic field of flare loops. Kontar et al. [2011] has explained how hard X-ray observations can be used to deduce electron properties. Dulk [1985] and Bastian et al. [1998] have reviewed the physics of radio emissions in

astrophysical systems in general and in solar flares in particular.

Figure 4.9 shows that energetic hard X-ray emissions, or photons of energy more than a few tens keVs, are concentrated at two places: a compact source at the feet of the flare loop, and a weak yet more extended source above the top of the flare loop [Gary et al., 2018], similar to the "Masuda flare" in Figure 4.1. At both places, electrons collide with plasma, which produce thick-target (of the dense chromosphere) or thin-target (of the tenuous corona) bremsstrahlung radiation of hard X-ray photons [3]. Less energetic X-ray emission of photon energy below 20 keV, which is thermal bremsstrahlung emission, is found to outline hot flare loops, also visible in soft X-ray and EUV emissions.

Hard X-ray spectra can be used to calculate energy distribution of electrons based on principles governing these kinds of radiations. Figure 4.9 shows that energetic hard X-ray photons exhibit a power-law shaped spectrum, with fewer photons at higher energies. This is believed to result from the energy distribution of electrons that also follows a power-law [Brown, 1971]. The observed difference in the photon spectrum between the foot-point, thick-target source and the loop-top, thin-target source provides crucial diagnostics of physical mechanisms governing acceleration and transport of high energy electrons [e.g., Battaglia and Benz, 2007, Krucker et al., 2008, 2011].

Fast electrons subject to the magnetic Lorentz force spiral around magnetic field lines of flare loops, and produce gyrosynchrotron radiation in microwaves [Dulk, 1985]. Figure 4.9 shows the location of microwave emissions at varying frequencies from 1 to 16 GHz. In this flare, energetic electrons trapped on or above the top of the flare loop give rise to microwave emissions, and the height of the emission grows with decreasing frequency, indicating that magnetic field strength decreases with height. Therefore, spectroscopic and imaging observations of flare microwave emissions also provide unique measurements of magnetic field in the flaring corona, which may help diagnose dynamics of magnetic reconnection (see Section 4.5.1) and particle acceleration and transport mechanisms [Gary et al., 2013].

[3]For this flare observed on the limb and partially occulted, it is considered that the conjugate feet of flare loops are behind the limb, so that thick-target hard X-ray emission is visible only at the feet in front of the limb.

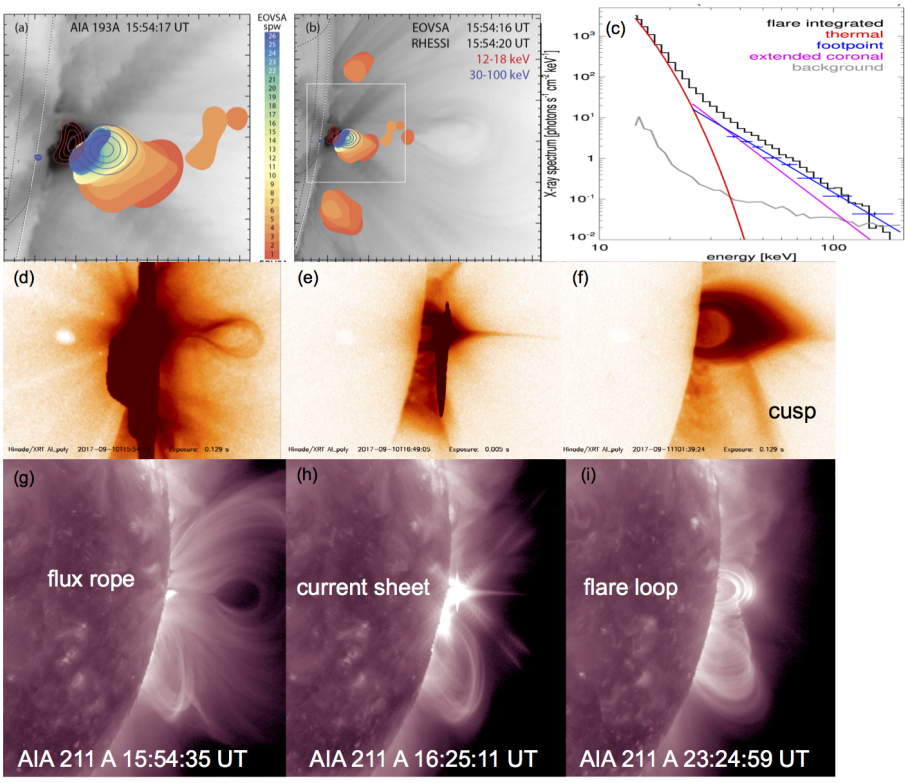

Figure 4.9: Top: X-ray emission (contours) observed by RHESSI at "soft" and "hard" energies, and microwave emission by EOVSA, in the impulsive phase during the X8.2 flare on 10 September 2017, presented in a small (a) and large (b) field of view, respectively. Background images, on reverse greyscale, are obtained from the SDO/AIA at Fe XII line at 193 Å, showing an erupting flux rope cavity above the flare (b). The box in (b) shows the field of view of (a). (Image credit: Gary et al. [2018]). (c): the spectrum of the flare X-ray emission demonstrating electron thermal bremsstrahlung emission at lower energy, and non-thermal power law distribution at higher energy of the foot-point source and coronal source, respectively. The solid black line shows the observed total photon spectrum, whereas the color curves show the model fit to different components of the X-ray emission. (Image credit: Gary et al. [2018]). Middle: soft X-ray emission by the X-ray Telescope [XRT; Golub et al., 2007] on Hinode [Kosugi et al., 2007] during the flares impulsive phase (d), gradual phase (e), when a long thin structure, considered to be a current sheet, is visible trailing the erupted flux rope CME, and many hours after the explosion (f) (Courtesy of Chunming Zhu and XRT team). Bottom (g-i): extreme ultraviolet images at Fe XIV line at 211 Å by AIA/SDO around the same times. These observations exemplify the standard eruptive flare configuration, which will be discussed in the next section.

4.4.1.3. Energetics

However particles are accelerated, and however plasma is heated, ultimately all flare energy is output in photons, by which flares are observed. Depending on the magnitude of a flare, the bolometric radiation, or the sum of electromagnetic radiation throughout the entire wavelength range, amounts to 10^{23-26} Joule, which is comparable to the energy of a CME [Emslie et al., 2012, Aschwanden et al., 2017, Aschwanden, 2017][4]. Note that the total energy of a CME includes the kinetic energy as well as the gravitational potential energy. In a flare or a CME, this large amount of energy is released on timescale of order a few tens of minutes. In terms of energy release rate, flares and CMEs are the most energetic events in the heliosphere.

Having understood mechanisms of radiation of various kinds, we may go into further details of energy distribution in a flare. In the corona, X-ray and extreme-ultraviolet spectral diagnostics tell us the temperature distribution of plasmas, so we can calculate the total thermal energy in the corona as a consequence of flare heating [Emslie et al., 2012, Aschwanden et al., 2015]. The spectral diagnostic is somewhat more complex in the dense lower atmosphere. It is estimated that the lower atmosphere holds a substantial amount of heat within the budget of flare energy [e.g., Kretzschmar, 2011, Milligan et al., 2014].

Earlier, we have discussed the possibility that the flare heating energy is originally carried in fast electrons. Then, how much is this energy? By integrating the electron spectrum inverted from the observed hard X-ray photon spectrum, it is found that a large flare produces a total number of 10^{34-36} electrons per second, and the total energy carried by non-thermal electrons can amount to more than one half of the total radiation energy of a flare [Emslie et al., 2012, Warmuth and Mann, 2016, Aschwanden et al., 2017]. If the numbers are correct, it becomes apparent that not all of the heating is done by non-thermal electrons. Flare accelerated ions may play a role in some large flares [Emslie et al., 2012, Aschwanden et al., 2017]. In the next section, some other mechanisms will be discussed.

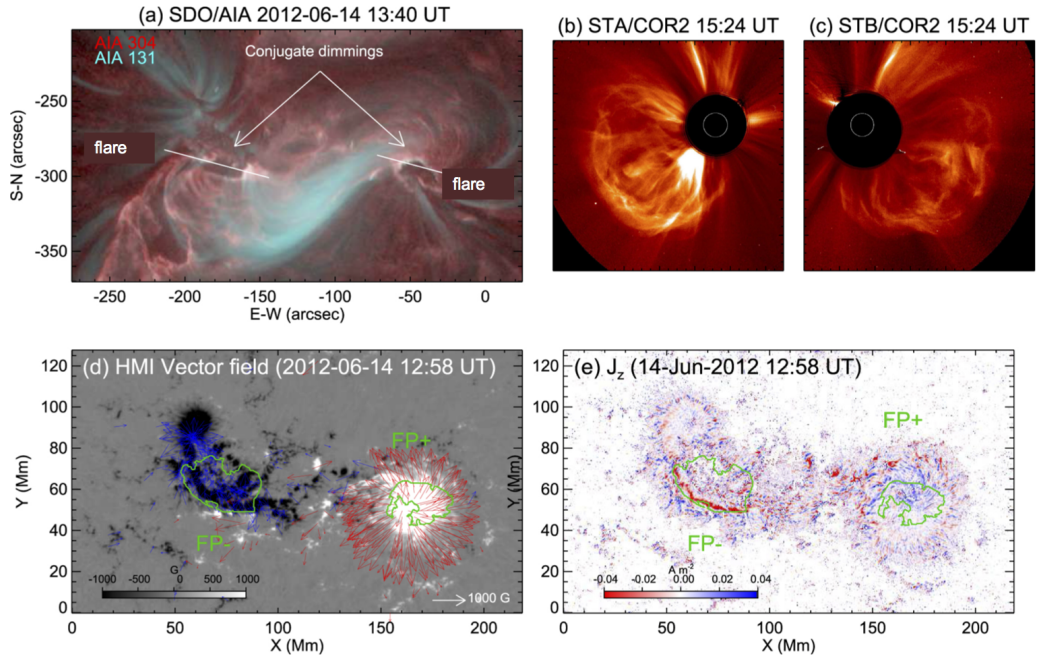

Figure 4.10: (a) An M1.9 flare observed on 14 June 2012 by SDO/AIA in 304 Å (red) and 131 Å (cyan) bands. The M1.9 flare is associated with a halo CME, which was captured by STEREO/COR2A (b) and STEREO/COR2B (c) from different perspectives. (d) A vector magnetogram obtained by the SDO/Helioseismic and Magnetic Imager [HMI Scherrer et al., 2012]; greyscale shows the longitudinal magnetic field and arrows indicate the transverse field. (e) The vertical current density calculated from the transverse magnetic field, with the positive (negative) values colored in blue (red). Two contours (green) in (d) or (e) outline the two conjugate feet of the erupting CME magnetic flux rope, which are identified by conjugate dimmings denoted in (a). (Figure credit: Wang et al. [2019], also see James et al. [2017, 2018] for this event.)

4.4.1.4. Magnetism

It has been well recognized that the source of the vast amount of energy, whether in flares or CMEs, is magnetic by nature. This knowledge has been corroborated by yet another critical observation: the polarimetric measurements of magnetic field in the Sun's atmosphere. Figure 4.10 shows an eruptive M1.9 flare residing in an active region of strong and complex magnetic field, which also hosts a sigmoid (see Section 4.4.2.2). Prior to the eruption, flux emergence, rotation of the leading sunspot carrying positive magnetic field, and strong shear motion of the other polarity have been observed in the active region. These motions have built up strong vertical electric currents (Figure 4.10e), derived as the curl of the transverse magnetic field (indicated by arrows in Figure 4.10d). Through these motions, magnetic helicity, which characterizes complexity of magnetic field, has been injected into the active region [e.g. Chae, 2001, and many following studies]. The subsequent flare and CME are found to be rooted in the areas of strong electric currents and helicity injection [James et al., 2017, 2018, Wang et al., 2019]. Note that this event was observed by SDO as well as STEREO A and B, the latter having a view angle of roughly ± 90 degrees from the former. Therefore, whereas the CME magnetic flux rope (MFR) is identified in the STEREO coronagraph observations (Figure 4.10b, c), its foot-prints on the Sun's surface are identified by coronal dimming signatures [Webb et al., 2000, see Section 4.4.2.2] observed by AIA. This event illustrates that magnetic field evolution, through flux emergence, sunspot rotation, and shear motion, builds up strong electric currents and leads to the eruption [e.g. Schrijver, 2007, Liu et al., 2017, and references therein].

A large body of observational studies, with the most recent effort using machine learning methods to analyze vector magnetic field measurements [Bobra and Couvidat, 2015b, Bobra and Ilonidis, 2016b, and references therein], have been dedicated to unravelling what magnetic field characteristics cause flares and CMEs [see, e.g., recent reviews by Green et al., 2018, Georgoulis et al., 2019]. In the meanwhile, a successful flare/CME model should lead to the understanding of how magnetic energy is abruptly released and converted to kinetic energy of particles, bulk motion, and heat. Such an understanding will not only improve our capability to predict space weather, but also shed light on mechanisms of energy release in other astrophysical systems like stellar flares and CMEs,

[4]Readers are reminded that there are flares or flare-like radiation phenomena of much smaller scales, such as microflares, nanoflares, and bright points. The energy of the smallest of these events can be as low as 10^{17} Joule [Hannah et al., 2008], depending on the detection threshold.

corona and jets from accretion disks of black holes, binaries, and proto-stars, and even γ-ray bursts.

4.4.2. Coronal Mass Ejections

CMEs are an important aspect of coronal evolution, involving vast structures of plasma and magnetic fields that are expelled from the Sun into the heliosphere. White light coronagraphs (Figure 4.3) image CMEs as bright features moving outward from the Sun with speeds ranging from tens to >3000 km/s. They can be detected in situ by their anomalous (compared to average solar wind) plasma and magnetic field characteristics [e.g. Zurbuchen and Richardson [2006]]. Much of the plasma observed in a CME is entrained on expanding magnetic field lines, which can have the form of helical field lines with changing pitch angles, i.e. a magnetic flux rope. In fast CMEs the plasma is supersonic so a detached shock forms ahead in the ambient solar wind. These shocks, in turn, can accelerate particles producing the largest SEP events (see Chapter 5) that are associated with major interplanetary disturbances and hazardous effects at Earth.

As stated previously, CMEs can be difficult to detect. Energetically, the strongest flares and CMEs are comparable: 10^{25} Joule. However, compared to the star itself, CME signatures can be very subtle. The total solar luminosity is 3.8×10^{25} Joule *per second*, whereas the CME frequency rarely exceeds ten per day. Even the outflow of the solar wind, integrated over the solar cycle, rivals the energy of flares and CMEs combined [Low, 2001]. However, the solar wind is relatively steady, and Earth can adjust and reach an equilibrium. Conversely, impulsive transients in the solar wind driven by CMEs can deposit large amounts of energy over a relatively short period, and the concomitant response of the Earth's field can drive geomagnetic currents and other space weather effects.

Even the largest CME has a small, almost inconsequential, magnetic field when compared to that of a sunspot. So how does a small ejection of flux from the solar surface have such a large impact in the corona? The reason is the large gradient in magnetic field pressure from the surface to the inner heliosphere; the magnetic pressure at the solar surface (0.5 R_{Sun}) falls off rapidly, so a CME "footnote" in the inner corona can become a dominant factor at higher altitudes (> 2 R_{Sun}). Magnetic fields on the Sun are typically tens to hundreds of Gauss, and strong sunspots can exceed several thousand Gauss. However, in space, the magnetic field is typically measured in nanotesla

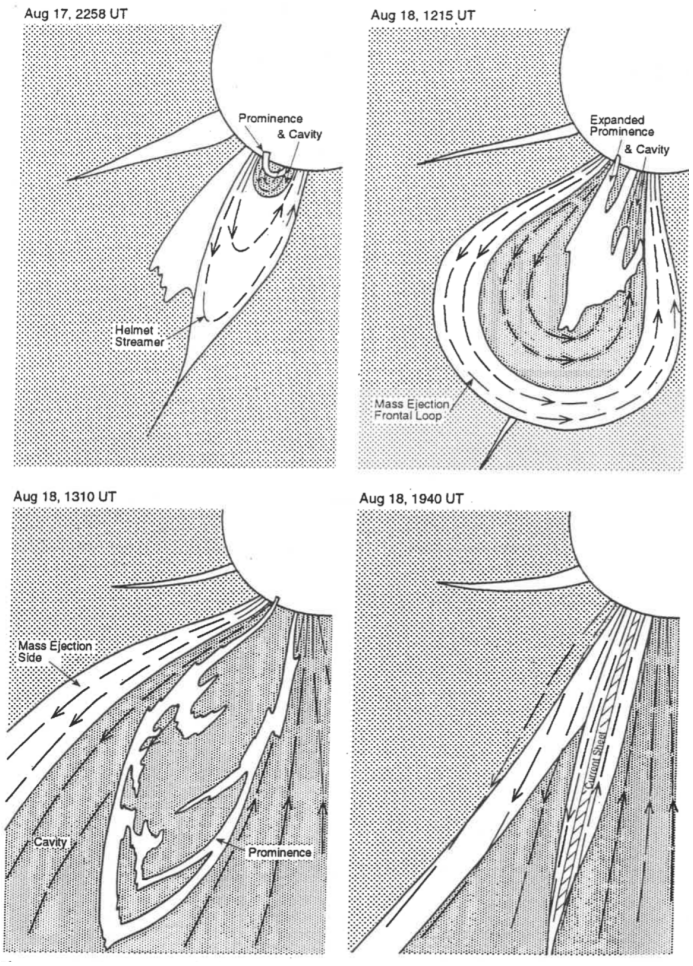

Figure 4.11: Early observations provided evidence that many CMEs have distinctive structure, consisting of a bright loop-like front, dark cavity, and dense (bright) core. Figure from Hundhausen [1999], illustrating the structure of a coronal mass ejection observed 17-18 August 1980.

(10^{-5} Gauss).

The key to detecting and observing CMEs is understanding where they have their strongest influence. In the upper corona (above 4 R_{Sun}) or the inner heliosphere (above the Alfvén surface, i.e. above about 15 R_{Sun}), local magnetic structures such as sunspots have evolved into a global structure consisting of streamers and coronal holes. The Alfvén surface is the locus where the outward speed of the accelerating solar wind passes the radial Alfvén speed, therefore any displacement of material cannot carry information back down into the corona (e.g. DeForest et al. [2014]). Thus, it is the natural outer boundary of the solar corona and the inner boundary of the heliosphere. Streamers and coronal holes are similar in that they are radially aligned, but coronal holes tend to be darker (because the plasma population is not strongly emitting in most spectral ranges, and the electron density is low) and streamers tend to be bright (plasma is more energized and emitting, and convergence of electrons in plasma flow are more effective in scattering). Both features stand in contrast to CMEs, which are more likely to take the form of easily distinguished structures (Figure 4.3). The fact that the CME is in motion, whereas the other structures are relatively static (unless disturbed by the CME), distinguishes CMEs further. However, these diagnostics are not always clear; a weak CME, or one that is not captured well by the available observations, can be difficult or ambiguous to interpret.

Usually a CME is observed via its impact on the solar atmosphere, such as evacuation of mass from the lower corona, injection of mass into the upper corona and heliosphere, dramatic magnetic field evolution, and strong interaction with the surrounding corona. Unfortunately, there are no established criteria to definitively identify a CME. Similar to flares, there are "sufficient" criteria, which when satisfied an observer may say that a CME definitely occurred. Certainly, a bright, outward-moving, loop-like structure as shown in Figure 4.3 is unambiguous evidence. However, there are no "necessary" criteria: The loop-like structure may not be observed, or the CME's direction relative to the images may make it impossible to deduce a moving structure. There are observations, and associated phenomena, that may suggest that a CME or eruption occurred.

4.4.2.1. Outer Coronal Observations

The "sufficient" observational condition for a CME is provided by a coronagraph, which is a type of imager that works as an artificial eclipse; it blocks out the Sun so that the surrounding atmosphere (which is many orders of magnitude fainter) can be observed. Coronagraph designs vary, but most extend to at least several solar radii in altitude. By this height, the solar features become more radial, and CME detection becomes less ambiguous (Figure 4.3).

Coronagraphs observe the evolution of the outer corona and the motion of density structures, typically by detecting Thomson-scattered sunlight from the free electrons in coronal and heliospheric plasma. This emission has a non-isotropic, angular dependence, which must be taken into account when interpreting the data [e.g., Billings [1966]; Vourlidas and Howard [2006], Howard and Tappin [2009]].

The two CMEs visible in Figure 4.3 exhibit a range of features. The first CME, though fainter, is more pronounced in extent (Figure 4.3b). The primary loop of the CME is visible in the upper right (northwest) portion of the image, but there is another front that is observed moving to the left (eastward). The latter CME also appears in the northwest (Figure 4.3c). Though more localized, is much brighter and more distinct. It has a bright outer loop, and within it a bright "core" structure.

Figure 4.11, an illustration from Hundhausen [1999], is based on a loop-like coronal mass ejection observed on 17-18 August 1980 by the Coronagraph/Polarimeter on the Solar Maximum Mission. The arrows indicate the direction of the magnetic field. The structure begins as a quasi-quiescent helmet streamer (first panel), expands as the interior magnetic cavity grows (second panel), erupts (third panel), and then evolves into a post-eruptive current sheet structure (last panel).

When compared to Figure 4.3, it is clear that some CMEs do exhibit this "classic" structure, but perhaps not all. Even authors of the earliest papers on CMEs recognized that there were two issues at play: 1) that not all CMEs had the same structure and dynamics, and 2) the angle of observation could have a strong impact on how a CME appeared in the image. In other words, was the earlier CME fainter, or was the second CME simply better aligned with the image direction to capture its full extent? Howard et al. [1985], surveying data from the Solwind coronagraph, described a large variety of structures: curved front, halo, complex, single spike, streamer blowout, and diffuse fan CMEs. The huge range of manifestations could not be explained by data ambiguities

alone. However, they argued that the angle of observation was a necessary consideration. CMEs with "halo" structures (eruptions that appeared with emission surrounding the occulting disk) were most likely due to a CME traveling along the observer's line of sight (i.e., toward or away the observer), rather than a CME exploding 360 degrees in all directions.

Later studies, based on coronagraphs viewing from multiple angles (the STEREO SECCHI coronagraphs [Howard et al., 2008] combined with the SOHO LASCO coronagraph [Brueckner et al., 1995]) confirmed that the varying CME manifestations were indeed a combination of the two effects. Vourlidas et al. [2017] surveyed thousands of eruptions, and strove to classify the eruptions more clearly regarding their physical nature and their observed kinematics.

However, even multiple viewing angles are limited in their ability to deduce 3-D structure. Figure 4.12 from Colaninno et al. [2013] illustrates how error or variation in identifying a point from the viewpoint of STEREO-A (blue lines), when combined with the ambiguity from STEREO-B (red lines), maps into a wide range of locations, particularly in the inner heliosphere (yellow shaded regions). The range of altitudes in the yellow shaded region is roughly proportionate with the error in position relative to the two spacecraft. However, the range of possible *longitudes* is surprising to many.

Other efforts have shed light on the subtle, but important three-dimensional properties of CMEs. For example, Kwon et al. [2015] demonstrated that there were an unusually high number of "halo" CMEs if they were considered a function of viewing angle alone. Some CMEs exhibit a halo-like structure surrounding their central emission from every direction, indicating that some halos truly were a bright structure surrounding the core CME from all directions. Thernisien et al. [2006] and Thernisien [2011] set the stage for an interpretive flux-rope CME tool that allowed the users to view a CME in the context of a consistent magnetic structure.

Another kind of telescope yielding outer coronal observations of CMEs are heliospheric imagers, beginning with Helios and the Solar Mass Ejection Imager (SMEI; Jackson et al. [2004]) and culminating in the STEREO/SECCHI HIs [Harrison et al., 2005, Eyles et al., 2009], Parker Solar Probe's Wide-Field Imager for Solar Probe Plus (WISPR; Vourlidas et al. [2016]), and Solar Orbiters Heliospheric Imager (SoloHI; Howard et al. [2019]). Their extended fields of view have allowed observers to track CMEs far from the Sun, study their evolution, and track their propagation through the heliosphere. Howard [2011] gives an comprehensive overview of many observations

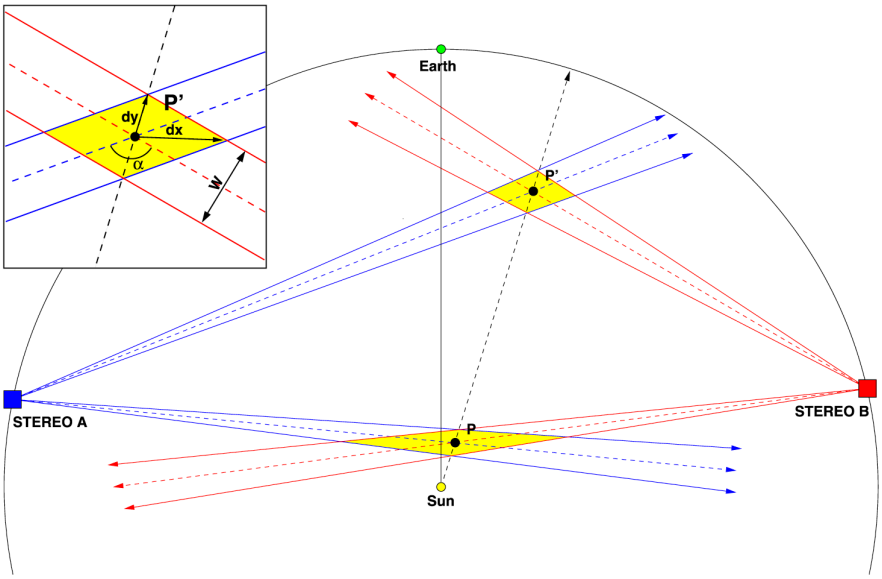

Figure 4.12: This diagram, from Colaninno et al. [2013], illustrates a difficult aspect of reconstructing 3-D CME structure using remote sensing observations. A small variation in the apparent observing angle can project to a large range of longitudes, particularly at locations close to the Sun.

and how they relate to the physical processes behind CME physics, and Green et al. [2018] incorporates multi-dimensional observations for a fully three-dimensional understanding of CME origin and initiation.

4.4.2.2. Inner Coronal Observations

There are a variety of observations in the inner corona that, when combined with coronagraph observations, shed light into the origin and structure of CMEs [e.g. Thompson et al. [1999b], Gopalswamy and Thompson [2000], Hudson and Cliver [2001]].

However, not all CMEs have inner coronal signatures [Howard and Simnett [2008], Robbrecht et al. [2009]] - the name "stealth" CME has been given to those that lack any accompanying solar surface activity. Most CMEs do have inner coronal signatures, though they have a wide variety of manifestations.

Flares, arcades and sigmoids. As flares and CMEs are related, it should not be surprising that some of the key indicators of a CME in the lower corona are provided by flare observations. Arcade

formation (as shown in Figure 4.7) provides a reliable diagnostic of the evolution of magnetic structures involved in a flare and coronal mass ejection [Hanaoka et al., 1994, Hudson and Webb, 1997]. The CME represents a topological change, and these arcades are often attributed to the re-closing of magnetic field field lines and the energization of trapped plasma along the loops. In addition, Yokoyama and Shibata [1998] discussed the ability of flare reconnection to energize adjacent, previously existing arcade loops. These correspond to the soft X-ray "long-decay enhancement" (LDE) flares, which are one of the soft X-ray signatures of a coronal mass ejection [e.g. Hudson and Webb [1997]].

Canfield et al. [1999] discovered that soft X-ray "sigmoid" eruptions, named for their S-shaped structure prior to eruption, is another type of arcade signature that correlates strongly with the presence of a coronal mass ejection. The S-shape, which forms due to the large amount of shear built up in the magnetic field, precedes an eruption; after the eruption the field evolves to a more relaxed, laminar arcade.

Many authors [Sheeley et al. [1975], Webb et al. [1976], Rust and Hildner [1976], Kahler [1992], Hudson et al. [1996]] have worked toward clarifying the relationship between LDEs, accompanying H-alpha "two-ribbon" flares, sigmoids, and CMEs. The inner coronal observations confirm these results, and the flare/arcades fitting these descriptions, when observed, are a very strong indicator of a coronal mass ejection. The converse is not necessarily true, in that a coronal mass ejection can occur without the accompanying arcade formation; however, this may correspond to a more gradual reconfiguration of magnetic field which does not result in an observable enhancement.

Coronal dimmings. EUV and soft X-ray dimmings of the corona, occurring on timescales ranging from minutes to hours, are another reliable signature of a coronal mass ejection. Such regions were called "transient coronal holes" in Skylab data and can appear as low coronal regions of reduced emission in EUV and soft X-ray emission.

Rust [1983] examined the brightest Skylab LDE events, and determined that a majority showed evidence of soft X-ray "voids" forming in association with the eruption. The voids were observed near the erupting region, either alone or in pairs, such as those shown in Figure 4.13. In general, these coronal voids lasted less than 48 hours and could decrease in emission until they were as dark as coronal holes.

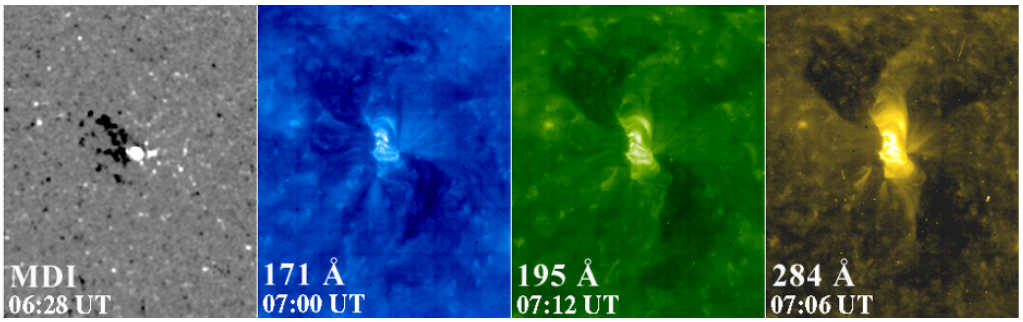

Figure 4.13: Magnetic field and EUV coronal images of a large-scale, post-eruptive dimming on 12 May 1997. First panel: SOHO MDI magnetic field, showing strong flux in the active region but weak but prevailingly unipolar flux in each of the dimming regions. The dimmings in coronal wavelengths show fairly symmetric "twin" regions. Blue: 171 Å, Green: 195 Å, Yellow: 284 Å. Figure from Thompson et al. [1998].

Rust reasoned that since the interplanetary shocks associated with eruptions "are followed by a sustained period of high speed solar wind, and recurrent high speed solar wind streams originate in long-lived coronal holes [Hundhausen, 1972], then the transient solar wind speed increases might stem from transient coronal holes." Hudson et al. [1998] determined that the dimming of the soft X-ray corona associated with a CME proceeded too rapidly to be explained by radiative or conductive cooling, leading to the conclusion that the observed decrease in emission was due mostly to the outflow of material, and not just a shift in temperature. They chose the more empirical label of "dimming." for this phenomenon.

Dimmings studies benefit from a direct comparison of the "transient" coronal hole dimmings with a more static coronal hole. Photometrically, the emission recorded in EUV and soft X-rays are comparable to that of a coronal hole [e.g. Zarro et al. [1999]], a strong indication that the decrease in emission is primarily due to a decrease in density. Additionally, Harra et al. [2007] demonstrated that coronal dimmings can exhibit Doppler shifts indicative of outflows, consistent with transient coronal hole behavior.

Sterling and Hudson [1997] demonstrated that the degree of soft X-ray dimming observed by Yohkoh SXT during a CME can only account for a fraction of the total mass of the white light CME. Thompson et al. [1998] argued that the degree of EUV dimming does not scale proportionally with the mass of the observed white light CME because a significant fraction of the CME mass source can originate from regions which are not strongly emitting in EUV or soft X-rays, such as at

higher altitudes. Harrison and Lyons [2000] included spectroscopic measurements, but Aschwanden [2016] demonstrated that a full emission measure treatment of dimmings in the EUV could account for the mass deficit.

An extensive survey of coronal dimming events and their relation to CMEs was performed by Reinard and Biesecker [2008]. They found mean lifetimes of 8 hrs, with most disappearing within a day. Reinard and Biesecker [2009] studied CMEs with and without associated dimmings, finding that those with dimmings tended to be faster and more energetic. Bewsher et al. [2008] used SOHO/CDS and LASCO data and found a 55% association rate of dimming events with CMEs, and that most CMEs were associated with dimming events. Coronal dimmings have not been observed as frequently as other associated eruptive phenomena but the recent, very sensitive results [e.g. Schrijver and Title [2011], Woods et al. [2011], Mason et al. [2016]] from SDO/AIA and SDO/EVE imply that dimmings are more common than previously thought. More recently, Krista and Reinard [2017] analyzed over 150 separate dimming events, and discussed their significance as the magnetic footprint of CMEs concluding that their magentic evolution provides essential clues of the evolution of CME eruptive topologies.

Tian et al. [2012] covered additional important factors regarding spectroscopic observations of CMEs and dimmings, shedding light on the outflow of material and mass of evacuated material. Mason et al. [2016], Aschwanden et al. [2017], and Krista and Reinard [2017] strove to connect the statistical properties of dimmings to the properties of the associated CMEs, namely their mass and velocity, finding some good correlations. Dissauer et al. [2018] investigated the relationship of dimmings to flares, then to CMEs [Dissauer et al., 2019], combining multi-viewpoint observations from the STEREO mission with those along the Earth-Sun line. These 3-D studies highlight the role of the magnetic field of a dimming region, allowing a closer examination of flare and CME manifestations of eruptions.

Filament eruptions. The presence of an erupting filament or prominence (a filament seen off the solar limb - hereafter we will refer to either as a filament) is a fairly reliable indicator of a coronal mass ejection (Figure 4.4).

As stated earlier, spectroheliograph observations of filaments began at the end of the 19th century, and they were quickly recognized to be evidence of the Sun's highly volatile nature. Filaments

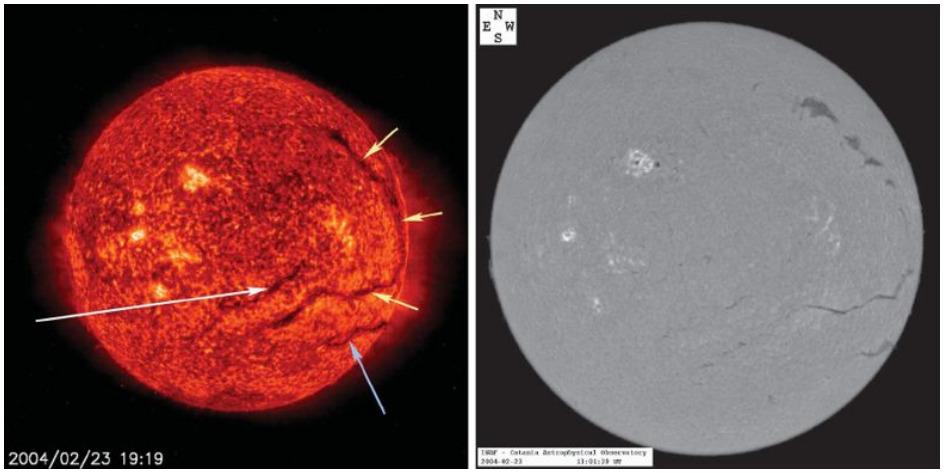

Figure 4.14: Left: SOHO Extreme Ultraviolet Telescope 304 Å(He II) image from 23 February 2004 showing several large filaments and their channels. Right: H-alpha image showing the same filament regions. Figure from Parenti [2014].

can be extremely compact (particularly filaments in an active region) or can extend for over a solar radius in length. They can remain relatively static, of quiescent, for long periods, and as they form along magnetic inversion lines they serve as excellent indicators of large-scale solar magnetic structure (Figure 4.14). For this reason, there has been a great deal of effort dedicated to studying their formation, structure, classification. evolution, and magnetic connections [see Tandberg-Hanssen [2013] and Parenti [2014] and Engvold [2015]]. For the purpose of this chapter, we briefly discuss the role filaments play in an eruption.

Filaments appear as dark masses in H_α images, and are observed in coronal emission lines as a dark profile; the dark features are due to cool dense material shadowing the bright emission behind it. In the cooler EUV 304 ÅHe II wavelength (typically estimated as representing 5 - 8 x 10e-4 K), the material can be seen either in emission or absorption (Figure 4.4). Spectrometer observations of absorption features [e.g. Kucera et al. [1998]] allow an analysis of the absorption profiles and comparisons.

Filament observations show several key aspects of a CME [Schmieder et al., 1997, 2002]. They trace out the base of the pre-eruptive structure, and continue to serve as an indicator of magnetic field evolution throughout the eruption process. Figure 4.15 highlights several important aspects of a filament's relationship to the CME magnetic field. A very clear example of a filament eruption and dimming is described by Webb et al. [2000], discussing CME properties like the magnetic flux

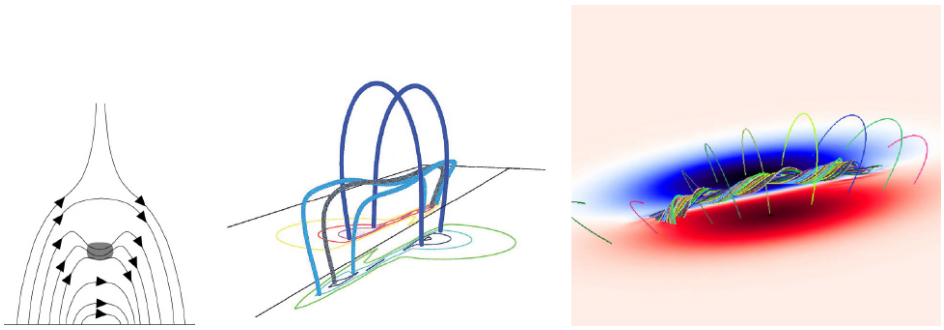

Figure 4.15: Figure 3 from Parenti [2014]. Left: A simple 2-D Kippenhahn-Schlüter magnetic field topology, showing the location of dense filament material relative to a larger loop structure [from Gilbert et al. [2001]]. Middle: A more realistic 3-D sheared arcade configuration, with dipped regions supporting filament formation [from DeVore and Antiochos [2000]]. Right: flux rope configuration [from Amari et al. [2003]].

and inferred the associated large-scale magnetic structure; through studies of many events, the picture of how filaments relate to the overall structure of CMEs becomes more clear.

Wave transients. Since their discovery by the EIT investigation on the SOHO mission [Moses et al., 1997, Thompson et al., 1998, 1999a] hundreds of papers have been written on EIT waves, which have also been called "EUV waves," Large-Scale Coronal Disturbances (LSCDs), or simply Coronal Wave Transients (see Figure 4.16). In general, studies of this phenomenon can be assigned to at least one of these broad, non-exclusive categories:

- the physical nature and appearance of EUV waves
- investigation of correlated phenomena, such as CMEs, flares, dimmings, and filament activity
- probing the origin or driver of EUV waves
- understanding the interaction with and impact on ambient coronal features.

In each of these categories, there have been major breakthroughs primarily due to the availability of high-cadence, multi-wavelength, multi-viewpoint observations from SDO, STEREO, Hinode, and other data sources [for a recent review, see Long et al., 2016]. Careful analysis has yielded a much-improved understanding of the EUV wave phenomenon, but it is clear that many outstanding questions remain.

When "EIT waves" were first observed, the assumption was that these phenomena were the coronal manifestation of Moreton waves [Moreton, 1960], which were seen as moving wave fronts

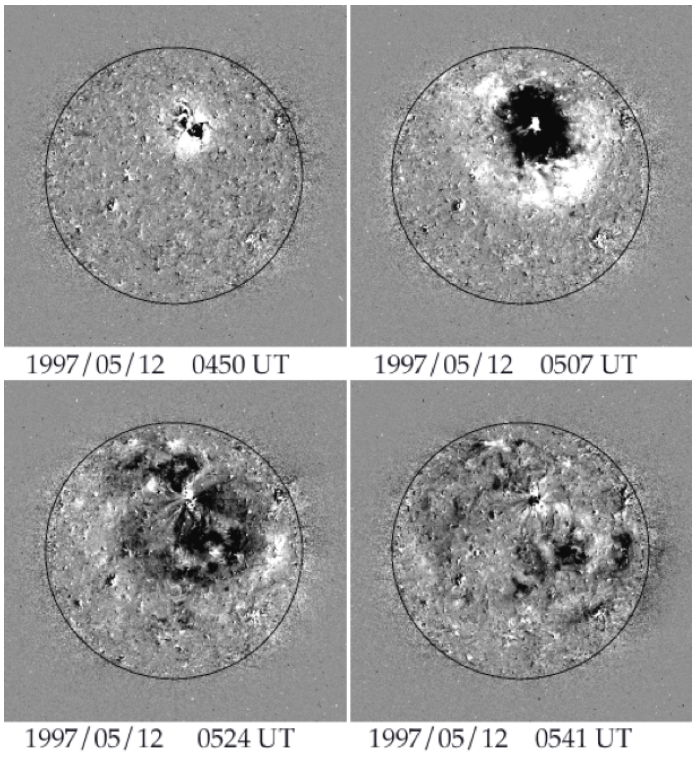

Figure 4.16: Figure from Thompson et al. [1998]. Running-difference (i.e. consecutive images subtracted) of a large-scale wave observed on 12 May 1997 by SOHO EIT 195 Å.

in H-alpha images. Among others, Uchida [1968] suggested that the Moreton wave phenomenon was not purely chromospheric in origin, but was instead the "ground track" of a three-dimensional wave front expanding in the corona. The wave shown in Figure 4.16 shows a progression in a series of running-difference images (each successive image subtracted from the next image): in less than an hour, the wave has covered almost the entire visible solar disk.

Over 100 of these wave transients were recorded by EIT, and they were interpreted as a signature of the impulse delivered to the ambient corona by the erupting field lines. There is evidence of lateral expansion during the very early stages of an eruption; this "kick" given to the corona is seen as a low-amplitude wave front propagating away from the erupting region (Figure 4.17). The discussion of Zhukov and Auchère [2004] examines the relationship between dimmings, waves and CMEs, and the analysis of Kwon et al. [2015] indicates that in general dimmings can map into the interior of a CME, while the waves generally map to the outer envelope of a CME.

Data from STEREO EUVI, with additional viewing angles, provided a significant improvement over prior observations, illuminating the complex structure and interactions of these waves [e.g. Liu

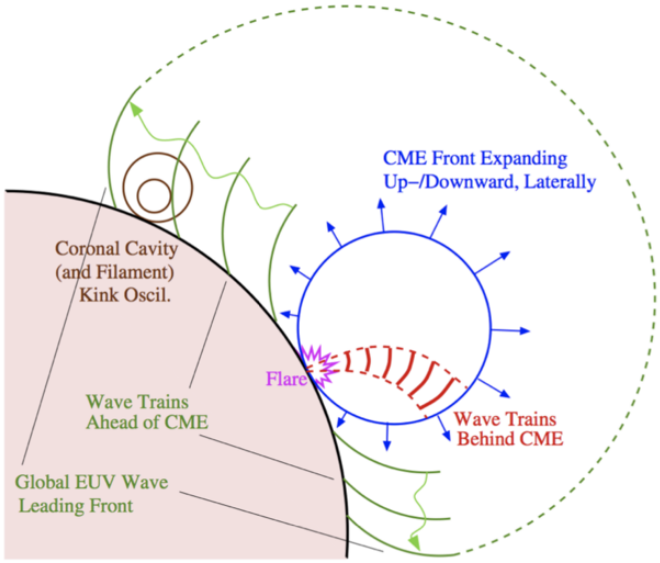

Figure 4.17: Diagram from Liu et al. [2012] summarizing the impulse from a CME (blue arrows), the expanding coronal wave front (green) and motions associated with ongoing flare activity and an affected external filament.

et al., 2012]. With these improved observations, studies of individual wave events [e.g. Long et al., 2008, Veronig et al., 2008, Long et al., 2011] as well as comprehensive studies of multiple events [Nitta et al., 2013] have augmented early kinematic studies [Wills-Davey and Thompson, 1999, Wang, 2000], thereby elucidating the initiation and subsequent deceleration of wave transients. The extensive study by Nitta et al. [2013], however, indicated that the dynamics of waves can be extremely variable, and apart from being an indicator of the presence of a CME, there is little correlation between wave kinematic properties and CME properties.

4.4.2.3. In Situ and Other Observations

There are many other observations of CMEs that have provided vital clues as to their nature. In particular, CMEs carry into the heliosphere large amounts of coronal magnetic fields and plasma, which can be detected by remote sensing and in situ spacecraft observations. In situ signatures include transient interplanetary shocks, depressed proton temperatures, cosmic ray depressions, flows with enhanced helium abundances, unusual compositions of ions and elements, and magnetic field structures consistent with looplike topologies [e.g. Vourlidas et al., 2012b, Webb and Howard,

2012, Webb et al., 1999].

In situ measurements provide the full plasma and magnetic field measurements at a single point in space. Statistical studies of CME properties measured by Helios, MESSENGER, *Venus Express*, Ulysses and spacecraft at 1 AU (ISEE, Wind, ACE, STEREO) provide average behaviors of the radial evolution of CMEs in the inner heliosphere [Bothmer and Schwenn, 1998, Liu et al., 2005, Winslow et al., 2015, Good and Forsyth, 2016, Janvier et al., 2019], giving us one of the only ways to learn from data about the changes in size, magnetic field and plasma properties inside CME with distance. Conjunction studies of specific CMEs are able to reveal the evolution and case-by-case variability of individual CME events [e.g., see Nieves-Chinchilla et al., 2012, Good et al., 2015, Winslow et al., 2016]. Recent reviews [e.g., see Manchester et al., 2017] discuss the evolution of CME in the inner heliosphere, including rotation, erosion, deflection, expansion, while Lugaz et al. [2017] discuss specifically interaction of multiple CMEs.

van Driel-Gesztelyi and Culhane [2009] trace the extensive body of research behind solar magnetic field measurements and their connections to interplanetary CMEs. Structured field configurations are often observed corresponding to the arrival of a CME. The field assumes the structure of a spiral or helix, and is accompanied by other signatures including strong magnetic field with low field variance, low plasma beta and low temperature. This substructure of a CME is referred to as a magnetic cloud [Burlaga et al., 1981], and can be modeled as a magnetic flux rope, a set of helical field lines with pitch angles increasing outward.

Heliospheric imagers have added wide-field viewing and tracking capabilities of CMEs in the heliosphere, the Solar Mass Ejection Imager (SMEI; 2003-2011) in Earth orbit and the STEREO Heliospheric Imagers (HIs; 2007 - present) in 1 AU orbits. Images of the outer heliosphere (above coronagraph altitudes) have shown great potential in connecting coronal imagery to the distances where in situ measurements are obtained [Harrison et al., 2018]. Recently, space weather models have been produced using observational CME inputs for the forecasts (see Section 4.6.1). Some insert a magnetic field structure, particularly a modeled or empirical flux rope, into the erupting CME allowing prediction of the magnetic cloud structure at 1 AU [e.g. Kay et al., 2016, Savani et al., 2017].

There are also important studies that use radio and energetic particle observations to understand shock properties of CMEs. Shocks driven by CMEs can accelerate particles to extremely high

energies, which have important impacts on their own. Chapter 8 covers Solar Energetic Particle events, a dramatic effect of solar eruptions.

4.5. Theoretical Interpretations and Key Problems

Fundamentally, the Sun's magnetic field fuels flares and CMEs. Surrounding this concept, three questions have to be answered.

First, how is energy stored in the magnetic field before its explosive release into flares and CMEs? It is well accepted that the driver is down below the photosphere, where gas density is high, and convection turbulence generates magnetic field. As the magnetic field emerges into the corona by buoyancy, it is further twisted and stressed by turbulent motions from below the photosphere. In a coronal volume, the total magnetic energy is given by $W_B = \int \frac{\vec{B}\cdot\vec{B}}{2\mu_0} dV$, where $\vec{B}$ is the magnetic field vector. It has been proven [Woltjer, 1958] that when the normal magnetic field component at the photosphere is held at fixed values (the so-called "line-tying" condition), the magnetic energy W_B is minimum if the magnetic field is current-free, namely, the current density $\vec{j} = \vec{\nabla} \times \vec{B}/\mu_0 = 0$. Such a magnetic field is called a potential field. Deviations from this potential field, such as when motions in the photosphere add shear or twist, will generate a current in the volume, associated with a higher magnetic energy. The excess magnetic energy relative to the potential field energy is called the free magnetic energy, which is the energy accessible to flares and CMEs. As the current grows and free energy accumulates, at a certain critical point, an explosion takes place to restructure the field, restoring it back into a lower-energy state.

The second question is, therefore, where is this critical point that makes the energy release possible? And at this point, what is the mechanism to suddenly change the magnetic field? Theoretically, this question has been addressed with the premise that the Sun's corona may be largely treated as an ideal conductor. This treatment means that on observed scales that are relevant to energy storage and release, plasma is tied with the magnetic field and behave as a fluid, namely, ions and electrons moving together with the magnetic field. Therefore, a magnetohydrodynamic (MHD) approach is often used to study the evolution of magnetic field and plasma. For the magnetic field and plasma to evolve steadily without explosion, the forces must (mostly) balance. In the MHD framework, the net force on plasma includes the electromagnetic Lorentz force, the plasma pressure gradient, and gravitational force. In more general terms, the critical point is reached when the system evolves into a state where no force balance can be found anymore, or when a balance, or equilibrium, is unstable, so that any small perturbation would pull the system out of the equilibrium, resulting in

explosions like a CME. Very often, it turns out that local enhancement of non-ideal MHD factors such as the plasma resistivity, which are largely unimportant in the global context, can actually help lead towards the loss of equilibrium or stability. The presence of non-ideal effects breaks the ideal condition where magnetic field is frozen in plasma, and allows the system to reach a lower energy state than in an ideal situation. This process is called magnetic reconnection, and is considered to be the governing mechanism to form flare loops and release energy therein. Reconnection also plays a vital in releasing CMEs. It is generally accepted that regardless of the initiation mechanism for a CME, the occurrence of magnetic reconnection removes restrictions bounding the CME [Aly, 1991], often also changing its structure, and helps expel the CME into interplanetary space.

Finally, the third question concerns how free magnetic energy is converted into plasma and particle energies. The answer may, at first glance, appear relatively simple for a CME, which is accelerated by the net Lorentz force against its own gravity to attain a speed from a couple hundred to a few thousand kilometers per second; then further along its path outward, drag by the ambient solar wind will eventually slow down a fast CME. However, the kinematic evolution of a CME is intrinsically tied to its structure, yet it remains largely elusive how a CME, particularly its flux rope structure, is formed in the first place. Is the flux rope born from below the photosphere or in the corona well before its eruption, or is it largely formed in situ during its eruption? Related to this notorious "nature or nurture" question of the CME flux rope, it is very puzzling whether and why an active region possessing sufficient free magnetic energy will be eruptive, converting a substantial amount of energy into CMEs. Here, the word "substantial" is meaningful when compared with the energy that goes into the associated flare. It is still trickier if we ask how energy is converted to particle kinetic energy and plasma thermal energy in a flare. For example, charged particles, electrons or ions, can be accelerated by an electric field, by waves, or by shocks; plasma in the corona and chromosphere can be heated by fast particles, in which case, plasma heating is only a secondary effect in the chain of energy conversion. But we have suggested earlier that other mechanisms may need to be invoked to heat flare plasma.

4.5.1. Magnetic Reconnection

Flares and CMEs are fueled by free magnetic energy stored in the global system. Magnetic reconnection is believed to be the primary mechanism that allows very rapid reconfiguration of the magnetic field to a lower-energy state. It forms flare loops and may also play a critical role to release CMEs into interplanetary space. Magnetic reconnection is a process of locally breaking the globally ideal condition that stressed magnetic field is frozen in plasma. For that to happen, an electric current sheet is formed at the place of strong magnetic field gradient, where a dissipation mechanism is invoked. The physics of magnetic reconnection with its application to the solar and heliospheric environment is very well explained by Priest and Forbes [2000], Biskamp [2000], and Birn and Priest [2007]. For more recent studies, Lin et al. [2015] reviewed observational signatures and numerical simulations of magnetic reconnection in the current sheet trailing CMEs, and Janvier [2017] discussed 3-D reconnection in flares and CMEs.

Back in 1947, almost a century after the discovery of the Carrington event, Giovanelli [1947] realized that flares tend to occur near sunspots at what he called the neutral point, where positive and negative magnetic fields meet, and suggested that an electric field developed there generates energetic particles responsible for observed flare radiation. In the following decades, Giovanelli's idea was developed into the theory of magnetic reconnection. Sweet [1958], Parker [1957], Petschek [1964] established steady-state 2-D reconnection models (by "steady-state", local physical quantities do not change with time). As magnetic fields of opposite sign enter the current sheet with plasma inflows v_{in} from both sides across the length of the current sheet L, due to non-ideal effects, the inflow fields of opposite signs bend, merge, and change connectivity, resulting in plasma outflows v_{out} from the other ends of the current sheet. In a 2-D steady-state configuration, $\partial\vec{B}/\partial t = -\vec{\nabla}\times\vec{E} = 0$, requiring that the advective electric field $\vec{E} = -\vec{v}\times\vec{B}$ at the outer boundary of the current sheet equals the electric field inside, generated by non-ideal effects which become important. The inflow speed v_{in} that brings in magnetic field is therefore a measure of how fast magnetic field is reconnected, and the dimensionless magnetic reconnection rate is henceforth defined as the ratio of this inflow speed to the outflow speed. By observing mass and energy conservation, the outflow speed is found to be roughly the Alfvén speed of the inflow magnetic field $v_{out} = v_a = B_{in}/\sqrt{\mu_0\rho_0}$, ρ_0 being the electron density in the current sheet. In other words, the 2-D reconnection rate is the

inflow Alfvén Mach number.

In the Sweet - Parker model, magnetic field (frozen-in to the plasma) flows in along a long current sheet to be dissipated by plasma resistivity η inside the current sheet (i.e., $\vec{E} = \eta\vec{j}$), and the derived reconnection rate is $M_a \equiv v_{in}/v_a = R_m^{-\frac{1}{2}}$, where R_m is the magnetic Reynolds number $R_m \equiv Lv_a/\eta$. Given the very low resistivity (and therefore a high magnetic Reynolds number) of the Sun's corona, the Sweet - Parker reconnection is found to be too slow to account for the observed rapid energy release in flares. Petschek [1964] changed the inflow-outflow configuration so that magnetic field flows in only along a very small length to be reconnected. Petschek's configuration introduces a vertical magnetic field component with respect to the current sheet, which can support two pairs of slow shocks spreading outward away from the current sheet. This provides an additional mechanism to carry magnetic energy away. Petschek derived the upper-limit of the reconnection rate as $M_a \sim (\ln R_m)^{-1}$. Detailed derivation and interpretation of the original Petschek model and its later development can be found in Vasyliunas [1975], Priest and Forbes [1986], Forbes et al. [2013]. The upper-limit of the Petschek reconnection rate is significantly larger than the Sweet - Parker reconnection rate, and is comparable to the observed flare energy release rate. For this reason, the Sweet - Parker model is now considered as a slow reconnection model, whereas the Petschek model represents a fast reconnection model.

Around the same time Petschek published his steady-state reconnection model, Furth et al. [1963] put forward an non-steady model, showing that the Sweet - Parker long current sheet with a finite resistivity is not stable against a long wavelength perturbation.This so-called tearing mode instability will tear the current sheet into staggered X and O configurations, or a chain of magnetic islands, and the instability growth rate is proportional to $R_m^{-\frac{3}{5}}$. In a current-carrying, circular-cylinder shaped flux tube, a finite resistivity will also give rise to a resistive kink instability, whose growth rate is proportional to $R_m^{-\frac{1}{3}}$. The continuous development of these linear instabilities may lead to non-linear growth and thinning of the current sheet, and eventually allow fast reconnection to set in [Priest and Forbes, 2000, Biskamp, 2000, Shibata and Tanuma, 2001, Pucci and Velli, 2014].

It should be noted that the above models each provide a scaling law of magnetic reconnection rate in terms of the magnetic Reynolds number defined by the resistivity due to collisions between electrons and ions. The details of the current sheet and diffusion region (where this collision is

thought to be important) in these models are very complex and usually beyond analytical approaches. From the 1980s, with development of high speed computers, numerical simulations have been conducted to examine reconnection models. These studies have found that, for fast reconnection to occur, microscopic physics below the MHD scale, treating ions and electrons as particles rather than a single fluid, has to be considered in the current sheet. These include anomalous resistivity, or other terms, apart from advective and resistive terms, in the generalized Ohm's law. There is also intriguing evidence regarding the role of "return currents" in flares, particularly relative to the role of classical or anomalous resistivity [Alaoui and Holman, 2017]. Therefore, the mechanisms causing fast reconnection is still an area of active research [Biskamp, 1986, 2000, Birn et al., 2001, Birn and Priest, 2007]. If the reconnection rate is no longer constrained by resistivity it allows fast reconnection to take place in the nearly ideal solar corona. On the other hand, depending on the problem, the detailed dissipation mechanism responsible for reconnection is perhaps not important as long as fast reconnection does occur to allow global magnetic reconfiguration and consequential energy release.

A particular challenge facing studies of reconnection theory is that most reconnection models have been two-dimensional, but reconnection is an inherently three-dimensional process. Longcope [2005], Démoulin and P. [2007], Pontin [2012] have reviewed topology of magnetic field and reconnection in three dimensions. In general, magnetic reconnection occurs at topological boundaries, called separatrices (plural of separatrix), dividing the space into domains of different magnetic field connectivities [Gorbachev and Somov, 1988]. Separatrices intersect at the null point, where magnetic field vanishes. 3-D separatrix structures have been extensively studied [e.g. Parnell et al., 1996]. Given the continuous distribution of photospheric magnetic field, Priest and Démoulin [1995] also created the concept of quasi-separatrix-layers (QSLs) in the absence of null points. Methods to determine topological features like null points, separatrices, QSLs, and bald patches (dipped magnetic field lines) have been developed and applied to analyzing magnetic field measurements and models [Demoulin et al., 1996, Titov et al., 2002]. 3-D magnetic reconnection with respect to these topological features has been studied [Lau and Finn, 1990, Priest and Titov, 1996, Aulanier et al., 2006], and flare observations have confirmed that magnetic reconnection (whose location may be mapped by flare ribbons) tends to occur at where these topological features are located [e.g. Demoulin et al., 1993, Masson et al., 2009, Savcheva et al., 2015].

Many CME eruptive models also depend heavily on the location and role of reconnection, though there is debate on what aspects are related to a flare process, and what aspects proceed independently. There are several compelling models describing the onset and early evolution of CMEs [e.g. Moore and Roumeliotis, 1992, Antiochos et al., 1999, Fan and Gibson, 2003, Lynch et al., 2005] each relating reconnecting fields to the overall eruptive topology. It is also known that a flare may accompany a CME resulting from the eruptive magnetic process rather than being a direct cause of the CME launch [Kahler, 1992, Gosling, 1993].

It has been recognized that evolution of Sun's magnetic field builds up magnetic helicity in the solar atmosphere, which characterizes the complexity of magnetic field beyond the potential field. This is discussed by Pevtsov et al. [2014]. Magnetic reconnection may redistribute magnetic helicity in coronal structures – for example, van Ballegooijen and Martens [1989], Mikic and Linker [1994], Démoulin et al. [1996], Aulanier et al. [2010], Priest and Longcope [2017] have discussed how 3-D magnetic reconnection may form or change the CME structure, by which a large part of the magnetic helicity is injected into and then carried away by CMEs [Low, 1994].

In short, the 3-D magnetic structure and its evolution determine where a current sheet forms and how rapidly reconnection can occur, which plays a role in determining the shape and energy of the associated flares and CMEs. The convergence of observations and models gives us a greater physical understanding of the two phenomena, and also provides a pathway for more accurate predictions [Green et al., 2018, Georgoulis et al., 2019].

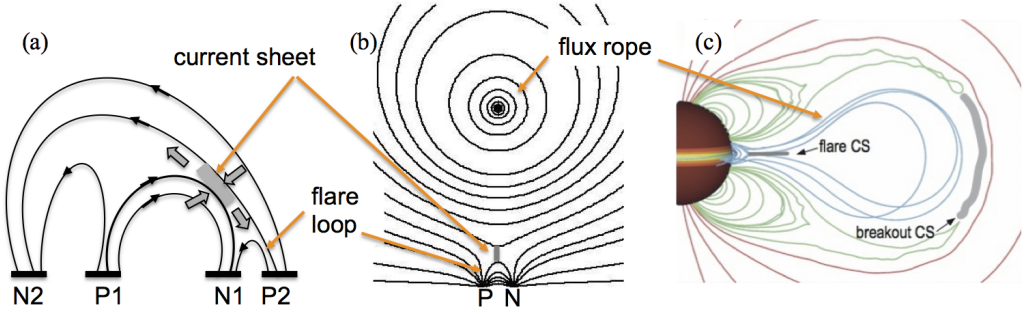

Figure 4.18: (a): magnetic flux P1-N1 emerging into pre-existing over-lying flux P2-N2 of opposite directions, forming a current sheet in between, where reconnection may occur and produce new sets of field lines, or flare loops (P1-N2 and P2-N1), after Heyvaerts et al. [1977]. (b): a current sheet below a flux rope, where reconnection may take place to form flare loops below the rope, and inject more flux into the flux rope, after Forbes and Priest [1995], Lin and Forbes [2000]. (c): a break-out configuration showing reconnection in the break-out current sheet as well as the flare current sheet (Figure credit: Karpen et al. [2012]).

4.5.2. Global Configuration and Topology

Pending knowledge of specific reconnection mechanisms acting on a tiny spot inside the diffusion region, several global configurations have been envisaged for flares and/or CMEs. In an emerging flux model [Heyvaerts et al., 1977], a current sheet forms at the boundary between magnetic field by a magnetic dipole emerging into pre-existing overlying field of opposite polarity (Figure 4.18a), where reconnection produces another set of new field lines, or flare loops.

A current sheet may also form under a rising magnetic flux rope (Figure 4.18b; Forbes and Priest [1995], Lin and Forbes [2000]), and reconnection therein generates an arcade of flare loops closing down as well as field lines curling up into the flux rope. This configuration has been known for decades as, schematically, the standard (eruptive) flare model, the Carmichael-Sturrock-Hirayama-Kopp-Pneuman (CSHKP) model [Carmichael, 1964, Sturrock, 1966, Hirayama, 1974, Kopp and Pneuman, 1976]. The standard model describes continuous generation of flare loops at progressively higher altitude, and its many features (flux rope, trailing current sheet, loop-top hard X-rays, soft X-ray cusp, hot loops on top of cool loops, and two ribbons) have been well established by decades of observations. These are demonstrated in Figure 4.9, and summarized by Lin et al. [2015]. The 3-D rendition of the standard model has been developed by Démoulin et al. [1996], Aulanier et al. [2012] (also see review by Janvier [2017]).

The standard flare configuration often also accounts for filament or CME eruption; therefore, this type of flares have been called "eruptive" flares. Moore et al. [2001] further considered that reconnection below the flux rope plays the role of "tether-cutting" to initiate the CME. In contrast, the other type of flare illustrated in Figure 4.18a has been called a "confined" flare due to its lack of apparent association with "eruptions." However, removal of the overlying flux may allow the underlying flux to further expand and even explode, corresponding to the "break-out" scenario of reconnection initiating CME eruption [Antiochos et al., 1999, Karpen et al., 2012, and Figure 4.18c].

Whereas "tether-cutting" or "break-out" reconnection may initiate CMEs, the other camp of CME initiation models rely on ideal instabilities, such as the torus instability [Bateman, 1978, Kliem and Török, 2006, Fan and Gibson, 2007, Démoulin and Aulanier, 2010] and kink instability [Newcomb, 1960, Hood and Priest, 1981, Einaudi and van Hoven, 1983, Török and Kliem, 2005, Fan and Gibson, 2007] [see recent reviews from Chen [2011], Lin et al. [2015]]. Most theories, however,

require the ejection of a magnetic flux rope (MFR) irrespective of whether the MFR existed before or formed during the eruption. In other words, all CMEs would contain a MFR, which is ejected by overcoming the constraint of the so-called "strapping" field. The stronger the "strapping" field, the more it is able to prevent an MFR from eruption [e.g. Sun et al., 2015, Amari et al., 2018, and references therein]. On the other hand, Jacobs et al. [2009] argued, on the basis of MHD simulations of quadrupolar magnetic field configurations, that eruptions could occur without the formation of an MFR.

As mentioned in Section 4.4, evidence for CME-entrained flux ropes is derived from in situ measurements of magnetic clouds [Liu et al., 2008] and from the detection of striations and 3-part morphologies in coronagraph images [Vourlidas, 2014, and references therein]. The statistics show that magnetic clouds comprise about 30% of CMEs detected at Earth [Gosling, 1990] while about 40% of CMEs show flux rope characteristics in coronagraph observations from a single viewpoint [Vourlidas et al., 2012a].

Another compelling aspect of global topology are studies of mid- and post-eruptive configuration. One interesting example is the study of "failed" or "partial" eruptions, where material that partially erupts and returns to the Sun can provide vital clues about the evolving eruptive magnetic field. One of the best examples, van Driel-Gesztelyi et al. [2014], documents falling material from a major filament eruption on 7 June 2011. The authors describe how tracing the filament material from their origin point to the locations observed after the eruption can be used as a diagnostic of global field reconfiguration. The filament plasma originated a single erupting active region, but was observed to fall at other locations on the Sun distant from the active region. The authors argue that these locations serve as an indicator of extended fields and regions that are also participating in the CME field evolution.

4.5.3. Energy Deposition in Flares

Electron acceleration. How energetic electrons are generated remains one of the biggest puzzles in flare physics. The task of a successful theory is to address the following two findings from hard X-ray and microwave observations: first, the power-law distribution of electrons, and second, the very large number of electrons produced every second during the flare, which implies that electrons

in the entire active region corona can be depleted![5]

A successful acceleration model also needs to yield the electron pitch angle distribution to help elucidate particle transport effects and understand the classic issue of electron precipitation and trapping that generate hard X-ray and microwave emissions at the flare foot-points and loop top [e.g. Melrose and Brown, 1976, Aschwanden et al., 1997, Lee and Gary, 2000, Battaglia and Benz, 2007].

Many theories have been developed to tackle these problems. Most of these theories consider the primary site of electron acceleration to be in the corona, motivated by observed hard X-ray and microwave sources at or above the flare loop top [e.g. Petrosian et al., 2002, Sui et al., 2004, Krucker et al., 2008, Gary et al., 2018, and see Figure 4.9] and also the electron time-of-flight analysis [Aschwanden et al., 1995]. Some earlier models consider electron acceleration by direct electric field in reconnection current sheet parallel to the magnetic guide field [Holman, 1985, Benka and Holman, 1994, Litvinenko, 1996]. Given the non-steady nature of magnetic reconnection that generates numerous contracting magnetic islands, electrons may likely gain energy more efficiently by interacting with these islands [Kliem et al., 2000, Drake et al., 2006, Cargill et al., 2012, Guidoni et al., 2016]. This scenario has been invoked to interpret observations of pulsating radio bursts [e.g. Kliem et al., 2000, Aurass et al., 2009, Benz et al., 2011]. More recently, quasi-periodic-pulsations (QPPs) have been found in light curves of many wavelengths than hard X-rays and microwaves [Inglis and Nakariakov, 2009, Brosius et al., 2016, Van Doorsselaere et al., 2016, for a review].The very dynamic reconnection energy release process may also generate turbulence to accelerate particles stochastically [Miller et al., 1996, Petrosian and Liu, 2004, Petrosian, 2012]. Further more, magnetic field lines from the reconnection outflow retract or shrink: Figure 4.9 nicely demonstrates the post-reconnection evolution from the soft X-ray cusp structure (panel f) to relaxed flare loops (panel i), which is a key feature of the standard flare model [e.g. Forbes and Acton, 1996]. This collapsing trap may accelerate electrons in the corona [e.g. Somov and Kosugi, 1997]. The reconnection outflow colliding with earlier formed flare loops may also produce termination shocks to accelerate particles [e.g. Forbes, 1986, Tsuneta and Naito, 1998]. Although rare, a few

[5]Let's do some math here: given an active region corona of scale size $L \sim 50$ Mm and typical electron density $n \sim 10^9$ cm^{-3}, the total number of electrons is $N_{tot} \sim 10^{38}$. Recall that a large flare may produce up to 10^{36} energetic electrons per second, so the corona is depleted in a matter of two minutes.

observations have been considered to provide evidence of the presence of the termination shock [Aurass and Mann, 2004, Mann et al., 2006, Chen et al., 2015]. Finally, to alleviate the electron number problem, Fletcher and Hudson [2008] proposed that magnetic energy is transported by Alfvén waves to the chromosphere, where electrons are accelerated.

There are not yet deterministic winners, if at all, and production of non-thermal particles remains one of the most challenging problems in flare physics. Readers are referred to Hudson and Ryan [1995], Miller et al. [1997], Aschwanden [2002], Holman et al. [2011], Klein and Dalla [2017] for thorough reviews of existing theories and challenges.

Flare heating. The very dynamic reconnection outflow region is a place with super-hot plasma or energetic particles. From this region, energy flux will be transported predominantly along the newly reconnected flare loops and heat plasma inside. Much of the energy will deposit in the dense chromosphere, which drives chromosphere evaporation, and in this way sends mass and energy back into the corona. Within this general picture, we still do not fully understand some important details. The most critical question concerns what mechanisms heat the flare plasma. Non-thermal electrons have been the most popular candidate [Somov et al., 1981, Nagai and Emslie, 1984, Mariska et al., 1989, Emslie et al., 1992]. More recently, Longcope and Guidoni [2011], Longcope et al. [2016] have proposed to heat the flare corona by slow magnetosonic shocks from reconnection, generating super-hot emission at the flare loop top [Lin et al., 1981, Caspi and Lin, 2010]. The chromosphere may be heated by thermal conduction [Gan et al., 1991], non-thermal electrons [Fisher et al., 1985a,b,c], X-ray or EUV irradiation [Hawley and Fisher, 1992], or Alfvénic waves [Kerr et al., 2016, Reep and Russell, 2016, Reep et al., 2018]. In each of these scenarios, what determines properties of chromospheric evaporation, for example, explosive versus gentle evaporation [Fisher, 1989], and the transition temperature between evaporation and condensation [e.g. Milligan and Dennis, 2009]? Furthermore, it has been known for decades that flare soft X-ray and EUV emissions often decay much more slowly than conductive and radiative cooling [Withbroe, 1978, Dere and Cook, 1979, Jiang et al., 2006, Ryan et al., 2013]; and more recently the EUV late phase emission has been discovered in EVE observations [Woods et al., 2011, Sun et al., 2013, and see Figure 4.7]. Does the extended duration of flare emission result from successive formation of and continuous heating in a multitude of flare loops (or unresolved threads) much beyond the impulsive phase [Hori et al.,

1997, Aschwanden and Alexander, 2001, Warren, 2006, Qiu and Longcope, 2016, Rubio da Costa et al., 2016, Zhu et al., 2018], or is it due to suppressed thermal conduction [Jiang et al., 2006, Wang et al., 2015, Zhu et al., 2018] or other non-equilibrium effects [see reviews by Bradshaw and Raymond, 2013, Dudík et al., 2017]?

Although reconnection is an inherently 3-D process, much of the theoretical investigation of flare heating is conducted using one-dimensional models. A major challenge in modeling flare heating is the very dynamic nature of the flare energy release and energy transport across the complex stratification of the atmosphere, particularly the sharp transition from the chromosphere to the corona. At least in the impulsive phase, equilibria or steady states cannot be assumed, posing additional difficulty in the modeling. Reale [2014] has given a comprehensive review of progress in modeling coronal heating in general, and some most recent effort particularly in heating flare loops with hydrodynamic models can be found in Reep [2014], Longcope and Klimchuk [2015, and references therein]. In the dense chromosphere, complex physical processes of absorption, emission, and scattering of photons have to be considered, by also solving radiative transfer equations. In the last decade, heating of the chromosphere has been modeled with new-generation, state-of-the-art numerical codes [Allred et al., 2005, 2015, Rubio da Costa et al., 2015, Kowalski et al., 2017]. In the mean time, advanced spectroscopic observations by EIS, EVE, and IRIS with unprecedented resolution and spectral coverage have been providing a very rich diagnostic information, through a variety of spectral lines as well as continua, to help probe physical mechanisms of flare heating or physical processes involved in energy transfer in the flare atmosphere. Finally, the (along-the-loop) one-dimensional modeling having been the mainstream, a comprehensive full-dimensional modeling taking into account both the magnetic and plasma aspects of flare evolution will be the ultimate goal, and some new progress is underway [Cheung et al., 2019, and references therein].

4.5.4. CME Mass and Energetics

For a structure containing the word mass in its name, the mass of CMEs is surprisingly not straightforward to measure. The main issue is again that of observability with coronagraph images providing a 2-D line-of-sight representation of a 3-D structure. Under a set of assumptions, including full ionization, a set ratio of heavier particles to protons, and more importantly about the geometry of the

CME itself, it is possible to derive CME mass from coronagraphic images [see e.g. Jackson and Hildner, 1978, Poland et al., 1981] following typical Thomson scattering calculation [Billings, 1966]. The typical technique requires spatial integration. The excess brightness of background-subtracted calibrated images in the area of the CME is proportional to the number of excess electrons in the CME volume. The CME mass in the middle corona is found to be 10^{15} - 10^{16} g. While CME mass has been measured starting with Skylab images, this was limited to the best observed events. With the launch of SOHO and the improved signal-over-noise ratio of the LASCO coronagraphs, the determination of CME mass from coronagraphic images has become routine.

One of the main limitations of the mass determination is that it assumes that all the measured mass is in the plane of the sky. This results in an underestimation of the CME mass (see discussion in Vourlidas et al. [2000]). On the other hand, the presence of streamers, which are often deflected during fast CMEs, may easily add spurious mass to the derived CME mass the unless the CME area is carefully delimited.

A similar method can be used for Heliospheric Imagers [DeForest et al., 2012] following early work by Jackson and Leinert [1985] using Helios data. DeForest et al. [2013] found an increase by a factor of about 2 of the CME mass from 10 $R_{\odot}$ to 0.6 AU, confirming findings from simulations [e.g. Lugaz et al., 2005]. The limitation of the mass determination can be significantly elevated by using two viewpoints, as made possible following the launch of STEREO in 2006. Assuming that the CME mass determined from both viewpoints must be the same, it is possible to determine both the CME mass and the direction of propagation [Colaninno and Vourlidas, 2009].

Determining the energetics of CMEs is once again a not straightforward problem. The driver of CME is certainly their magnetic field; however, coronal magnetic field measurements is still in its infancy. Once the CME mass and position have been derived from coronagraphic observations, it is straightforward to derive the CME kinetic and (gravitational) potential energies. To derive the magnetic energy, one needs to integrate the CME magnetic field over the volume of the magnetic ejecta. Even under the strong assumption of uniform magnetic field inside the ejecta, this requires to know the magnetic field strength or flux inside the CME as well as the CME length perpendicular to the plane of sky. In Vourlidas et al. [2000] the authors use values of the magnetic flux measured in situ at 1 AU to derive the magnetic energy. Other approaches include using the peak acceleration and derived mass to determine the magnetic flux from Newton‘s second law [DeForest et al., 2012]

or using solar measurements, as explained below. Vourlidas et al. [2010] determine the typical mass, kinetic and total energies of CMEs over all of solar cycle 23 from LASCO images, finding a median of about 10^{12} kg, 2 $\times 10^2 3$ J of kinetic energy and 4 $\times 10^2 3$ J of total mechanical energy.

Whereas coronal magnetic fields are not typically measured, solar photospheric magnetic fields are. Therefore, the amount of reconnected magnetic flux can be derived using magnetograms combined with Hα and/or EUV measurements. One technique consists in following the area of the flare ribbons and measuring the associated magnetic flux [Qiu et al., 2007, Möstl et al., 2009]. The poloidal magnetic flux in the CME is expected to be greater than the reconnected flux (as measured from ribbons), as a pre-existing flux rope may exist and (see for example the discussion in Qiu et al. [2007]. From the flux measurements, estimating the length of the flux rope (for example by assuming self-similar expansion), the CME magnetic energy can be derived.

The energy partition between flares and CMEs and other associated events during an eruption is an active area of research [Emslie et al., 2004, 2012, Feng et al., 2013]. Additional work has related flare properties, such as the flux with the CME mass or kinematics.

4.6. Space Weather and Beyond

4.6.1. Space Weather

Space weather is the study of how changes in space affect life and technology on Earth and in space. It requires an understanding of how solar and heliospheric changes interact with the Earth's system, and it requires a partnership with "end users," i.e. those whose systems are impacted by space weather processes. Like terrestrial weather, an important part of space weather is accurate forecasting, and an improved scientific understanding of the constituent processes can result in dramatic improvements in forecast capabilities.

There are three primary areas that sum up the diversity of space weather effects. Diversity of drivers (flares, CMEs, SEPs, high-speed streams), diversity of effects (such as signal interruption, spacecraft charging, orbital drag, ionospheric disturbances), and the diversity of locations (from interplanetary space to the Earth's surface). For these reasons, the scientific community works together with forecasters to advance our ability to cope with space weather impacts. Some of the advances allow a better assessment of the likelihood of an eruption or disturbance. Others deal with predicting the impact after a transient is observed, and providing an accurate "nowcast" of the space environment. As our understanding of the Sun-Earth connected system improves, so will our ability to cope with the effects of our dynamic star and the impacts it can cause.

Flares and CMEs are the two main drivers of space weather activity. Every advance in our observational and theoretical understanding of flares and CMEs can be harnessed to improve our ability to predict the impact on Earth and technology in space. The other consistent cause of space weather is high-speed streams (see Chapter 7), which originate from coronal holes and travel faster than the relatively slower ambient solar wind. As the high-speed stream propagates into slower plasma, a compression region forms. Compression, along with southward interplanetary magnetic field (IMF), are the main space weather drivers of heliospheric transient disturbances. Southward IMF from high-speed streams allows merging of the IMF and Earth's magnetic field and transfer of solar wind energy and mass into the magnetosphere. Such compression regions, with higher density and magnetic field than typical solar wind, can drive geomagnetic activity at Earth and generate radiation belt activity. However, the largest and most dramatic storms are associated with CME

impacts.

CMEs and their associated coronal activity cause the largest disturbances in the corona and subsequently in the heliosphere. CMEs can contain long-duration flows of southward IMF and fast CMEs compress any southward field ahead. CMEs can drive interplanetary shocks, a key source of solar energetic particles (SEPs; see Chapter 8), which are one of the most difficult space weather effects to predict. CMEs drive space weather not only at Earth but also other planets and locations in the heliosphere and, therefore, can have a significant impact on society.

Flares are important for space weather because of their ability to produce sudden dramatic enhancements in a broad range of wavelengths. The X-ray, EUV and radio emission from flares can drive myriad processes in the Earth's atmosphere, disrupting communication, causing sudden ionospheric disturbances (SIDs), and heating of the upper layers of the atmosphere to increase drag on spacecraft.

Flare impacts are difficult to forecast because of their impulsive nature; light from the Sun takes 8 minutes to reach Earth, and the same light that drives space weather impacts is also used to detect flares in the first place! By the time we are aware that a flare is transpiring, Earth is already experiencing space weather effects. Therefore, much of flare space weather strategy focuses on improving our ability to predict whether a region is likely to produce a flare.

Fast CMEs can reach Earth in 1-2 days, but the majority take at least three days to reach Earth. This may seem like a long time, but the shock-driven particles can travel much faster. The observed kinematic parameters of CMEs are typically inserted into propagation forecast models as a spherical shape, or cone. Cone models approximate initial CME parameters assuming isoptropic expansion, radial propagation and constant width of the CME. Two popular models are Wang-Sheeley-Arge (WSA)-ENLIL+Cone [Odstrcil et al., 2004] and EUHFORIA (EUropean Heliospheric FORecasting Information Asset) [Pomoell and Poedts, 2018]). The Drag-based Model [Vršnak et al., 2013] has also been extensively used with STEREO CME observations.

Additionally, the difficulty in resolving the exact direction of propagation (see Figure 4.12), combined with the delayed availability of many critical types of data, mean that it can take over a day to produce a complete CME forecast. A common strategy is ensemble modeling of CME propagation to Earth, which harnesses the ambiguity in model inputs to produce a range of possible outputs. Recent papers summarizing CME impact forecasting include: Lee et al. [2013], Möstl et al.

[2014], Mays et al. [2015], Wold et al. [2018], Verbeke et al. [2019]. Verifications and validations of forecasts using the above models typically yield errors in CME arrival times on the order of 8-14 hours.

The National Oceanic and Atmospheric Administration (NOAA) Space Weather Prediction Center (SWPC) coordinates the space weather forecasts for assets in the United States. SWPC and many others have chosen (rather pragmatically) to categorize space weather impacts through a consideration of both the drivers and their effects. The three categories of "NOAA Scales" are radio blackouts, geomagnetic storms and energetic particles/radiation. Radio blackouts are a function of flare flux; photons of higher energies deposit in the Earth's upper atmosphere and ionosphere and inhibit communications, radio signals, GPS, etc. Geomagnetic storms are the CME counterpart to flare effects. While flare effects are due to photons, when a CMEs plasma and magnetic fields arrive at Earth, they can drive a large magnetospheric reaction. The response time is longer; light takes 8 minutes to get to Earth, independent of wavelength, while the fastest CMEs take nearly a day to reach us. This can be viewed as inconvenient (many effects are distributed over time, so it is difficult to call an "all clear" forecast), or one may see the separation of effects as a scientific opportunity.

The "NOAA Scales" focus areas were chosen based on how drivers and impacts are clustered. The key to the first (radio blackouts) requires us to understand how magnetic energy stored on the Sun is converted to different emissions in the electromagnetic spectrum. As photons of different wavelengths are deposited into the Earth's upper atmosphere and ionosphere, we are better able to understand how the local structure influences radio signal propagation. The second area (geomagnetic storms) require the deliberate study of solar transients or CMEs leaving the Sun, propagating through the heliosphere and impacting geospace. Observations in space over the last several solar activity cycles have allowed us to accumulate important evidence. It is important to understand how the Earth responds to a CME, but the Earth's state prior to the CME can also play a role. Nonetheless, definitive, deterministic models have shown great potential over the past decade. Finally, the third area (energetic particles and radiation) includes energetic particles in both the solar wind and the Earths radiation belts. While SEP events can develop quickly, their associated radiation storms at Earth can last for days and can have major impacts on spacecraft at geosynchronous orbit as well as in lower orbits.

4.6.2. Exoplanet impacts

Recent attention has focused on the impact of stellar activity on exoplanets. Like Earth, planets can feel the impact of stellar activity, and this can influence the way life evolves on exoplanets.

There have been studies of flares on other stars, and that has helped us understand stellar activity in the context of our star's activity. It has also helped us understand the range of potential behavior of Sun-like stars. X-ray and EUV radiation can heat or ionize the upper atmosphere leading to increased atmospheric loss [Lammer et al., 2007]. As the presence of a steady atmosphere is an important factor in habitability, Scalo et al. [2007] discuss how a strong planetary magnetic field may help mitigate loss effects.

We have come to understand that it is not only flares, but also CMEs that can determine this habitability. An important clue was the study by Jakosky [2015] that indicated CMEs may have affected the evolution of the Martian atmosphere. Just as space weather research at Earth has elucidated the role that CMEs and flares play, researchers are attempting to recognize the potential effects that solar transients may have in other stellar systems.

Khodachenko et al. [2007] show that in the case of a significant planetary magnetic field, the atmosphere can still be eroded when CME impacts compress the planetary magnetosphere. Kay et al. [2016] adapted their terrestrial space weather model to investigate the potential impacts of CMEs on habitability on other systems. They found that the planets in what is thought to be the "habitable zone" of magnetically active M dwarf stars may experience more extreme space weather than at Earth. Interestingly, this leads to increased flare impact as well; frequent CME impacts can lead to atmospheric erosion, leaving the surface exposed to extreme flare activity.

The first observation of a CME on another star has been recently reported [Argiroffi et al., 2019]. However, Harra et al. [2016] reviewed the different observational properties of CMEs discussed in Section 4.4 and found that coronal dimmings show great promise as an indicator of CMEs on other stars. The consideration of space weather for exoplanet habitability is a fairly recent development, there are many exciting new results that are sure to come in the future.

4.6.3. Enabling Predictions Using Machine Learning

We close this chapter with a brief mention of an exciting new frontier in flare/CME studies. Many researchers are examining models and forecasts using new methods derived from data science, advanced statistics, and machine learning. In particular, space weather events are amenable to machine learning problems because the data are already labeled and easily used with methods such as logistic regression (e.g., flare/no flare).

Many authors (e.g. Bobra and Couvidat [2015a]) have found that machine learning methods such as neural nets, support vector machines, and random forests have been successful in improving predictive accuracy. Others have focused on impacts. For example, McGranaghan et al. [2018] address the high-latitude ionospheric impact with a data-driven discovery machine learning approach. Not only did they find improved predictive performance, but they were able to analyze the various data input parameters, or "features," to determine which played the greatest role in driving space weather effects.

Similar efforts have focused on CME prediction (e.g. Bobra and Ilonidis [2016a]) and classification (e.g. Heidrich-Meisner and Wimmer-Schweingruber [2018]). The book "Machine Learning Techniques for Space Weather" by Camporeale et al. [2018] summarizes many space weather concepts that are advanced by machine learning. Beyond simple forecasts and predictions, machine learning studies are revolutionizing our ability to identify important features, classify phenomena, and derive correlations between physical processes that have thus far eluded classical methods. The HelioML online book by Bobra et al. [2019] demonstrates the prospects of machine learning combined with the potential represented by the open source/open code ethic. These expanded capabilities, combined with classical methods and models, present an exciting new frontier for space weather research.

Acknowledgments

The authors would like to thank Dr. Christina D. Kay for her guidance on exoplanet studies.

Bibliography

Meriem Alaoui and Gordon D. Holman. Understanding Breaks in Flare X-Ray Spectra: Evaluation of a Cospatial Collisional Return-current Model. *The Astrophysical Journal*, 851(2):78, 12 2017. ISSN 1538-4357. doi: 10.3847/1538-4357/aa98de. URL http://stacks.iop.org/0004-637X/851/i=2/a=78.

J. C. Allred, S. L. Hawley, W. P. Abbett, and M. Carlsson. Radiative Hydrodynamic Models of the Optical and Ultraviolet Emission from Solar Flares. *Astrophysical Journal*, 630:573–586, September 2005. doi: 10.1086/431751.

J. C. Allred, A. F. Kowalski, and M. Carlsson. A Unified Computational Model for Solar and Stellar Flares. *Astrophysical Journal*, 809:104, August 2015. doi: 10.1088/0004-637X/809/1/104.

J. J. Aly. How Much Energy Can Be Stored in a Three-dimensional Force-free Magnetic Field? *Astrophyiscal Journal Letters*, 375:L61, 7 1991. doi: 10.1086/186088.

T. Amari, J. F. Luciani, J. J. Aly, Z. Mikic, and J. Linker. Coronal Mass Ejection: Initiation, Magnetic Helicity, and Flux Ropes. II. Turbulent Diffusiondriven Evolution. *The Astrophysical Journal*, 595(2):1231–1250, 10 2003. ISSN 0004-637X. doi: 10.1086/377444. URL http://stacks.iop.org/0004-637X/595/i=2/a=1231.

Tahar Amari, Aurélien Canou, Jean-Jacques Aly, Francois Delyon, and Fréderic Alauzet. Magnetic cage and rope as the key for solar eruptions. *Nature*, 554(7691):211–215, Feb 2018. doi: 10.1038/nature24671.

S. K. Antiochos, C. R. DeVore, and J. A. Klimchuk. A Model for Solar Coronal Mass Ejections. *Astrophysical Journal*, 510:485–493, January 1999. doi: 10.1086/306563.

E. Antonucci, A. H. Gabriel, L. W. Acton, J. L. Culhane, J. G. Doyle, J. W. Leibacher, M. E. Machado, L. E. Orwig, and C. G. Rapley. Impulsive phase of flares in soft X-ray emission. *Solar Physics*, 78:107–123, May 1982. doi: 10.1007/BF00151147.

C. Argiroffi, F. Reale, J. J. Drake, A. Ciaravella, P. Testa, R. Bonito, M. Miceli, S. Orlando, and G. Peres. A stellar flare-coronal mass ejection event revealed by X-ray plasma motions. *Nature Astronomy*, page 328, May 2019. doi: 10.1038/s41550-019-0781-4.

M. J. Aschwanden. *Particle Acceleration and Kinematics in Solar Flares*. Kluwer Academic Publishers, Dordrecht, September 2002.

Markus J. Aschwanden. GLOBAL ENERGETICS OF SOLAR FLARES. IV. CORONAL MASS EJECTION ENERGETICS. *The Astrophysical Journal*, 831 (1):105, 10 2016. ISSN 1538-4357. doi: 10.3847/0004-637X/831/1/105. URL `http://stacks.iop.org/0004-637X/831/i=1/a=105`.

Markus J. Aschwanden. Global Energetics of Solar Flares. VI. Refined Energetics of Coronal Mass Ejections. *Astrophysical Journal*, 847(1):27, Sep 2017. doi: 10.3847/1538-4357/aa8952.

Markus J. Aschwanden and David Alexander. Flare Plasma Cooling from 30 MK down to 1 MK modeled from Yohkoh, GOES, and TRACE observations during the Bastille Day Event (14 July 2000). *Solar Physics*, 204:91–120, Dec 2001. doi: 10.1023/A:1014257826116.

Markus J. Aschwanden and Hardi Peter. The Width Distribution of Loops and Strands in the Solar Corona—Are We Hitting Rock Bottom? *Astrophysical Journal*, 840(1):4, May 2017. doi: 10.3847/1538-4357/aa6b01.

Markus J. Aschwanden, Richard A. Schwartz, and Daniel M. Alt. Electron Time-of-Flight Differences in Solar Flares. *Astrophysical Journal*, 447:923, Jul 1995. doi: 10.1086/175930.

Markus J. Aschwanden, Robert M. Bynum, Takeo Kosugi, Hugh S. Hudson, and Richard A. Schwartz. Electron Trapping Times and Trap Densities in Solar Flare Loops Measured

with COMPTON and YOHKOH. *Astrophysical Journal*, 487(2):936–955, Oct 1997. doi: 10.1086/304633.

Markus J. Aschwanden, Paul Boerner, Daniel Ryan, Amir Caspi, James M. McTiernan, and Harry P. Warren. Global Energetics of Solar Flares: II. Thermal Energies. *Astrophysical Journal*, 802(1):53, Mar 2015. doi: 10.1088/0004-637X/802/1/53.

Markus J. Aschwanden, Amir Caspi, Christina M. S. Cohen, Gordon Holman, Ju Jing, Matthieu Kretzschmar, Eduard P. Kontar, James M. McTiernan, Richard A. Mewaldt, and Aidan O'Flannagain. Global Energetics of Solar Flares. V. Energy Closure in Flares and Coronal Mass Ejections. *Astrophysical Journal*, 836(1):17, Feb 2017. doi: 10.3847/1538-4357/836/1/17.

Markus J. Aschwanden, Amir Caspi, Christina M. S. Cohen, Gordon Holman, Ju Jing, Matthieu Kretzschmar, Eduard P. Kontar, James M. McTiernan, Richard A. Mewaldt, Aidan O'Flannagain, Ian G. Richardson, Daniel Ryan, Harry P. Warren, and Yan Xu. Global Energetics of Solar Flares: V. Energy Closure in Flares and Coronal Mass Ejections. *The Astrophysical Journal*, 836(1):17, 1 2017. ISSN 1538-4357. doi: 10.3847/1538-4357/836/1/17. URL `http://dx.doi.org/10.3847/1538-4357/836/1/17`.

G. Aulanier, E. Pariat, P. Démoulin, and C. R. DeVore. Slip-Running Reconnection in Quasi-Separatrix Layers. *Solar Physics*, 238(2):347–376, Nov 2006. doi: 10.1007/s11207-006-0230-2.

G. Aulanier, T. Török, P. Démoulin, and E. E. DeLuca. Formation of Torus-Unstable Flux Ropes and Electric Currents in Erupting Sigmoids. *Astrophysical Journal*, 708:314–333, January 2010. doi: 10.1088/0004-637X/708/1/314.

G. Aulanier, M. Janvier, and B. Schmieder. The standard flare model in three dimensions. I. Strong-to-weak shear transition in post-flare loops. *Astronomy and Astrophysics*, 543:A110, July 2012. doi: 10.1051/0004-6361/201219311.

H. Aurass and G. Mann. Radio Observation of Electron Acceleration at Solar Flare Reconnection Outflow Termination Shocks. *Astrophysical Journal*, 615:526–530, November 2004. doi: 10.1086/424374.

H. Aurass, F. Landini, and G. Poletto. Coronal current sheet signatures during the 17 May 2002 CME-flare. *Astronomy and Astrophysics*, 506(2):901–911, Nov 2009. doi: 10.1051/0004-6361/200912229.

D. N. Baker, X. Li, A. Pulkkinen, C. M. Ngwira, M. L. Mays, A. B. Galvin, and K. D. C. Simunac. A major solar eruptive event in July 2012: Defining extreme space weather scenarios. *Space Weather*, 11(10):585–591, 10 2013. ISSN 15427390. doi: 10.1002/swe.20097. URL `http://doi.wiley.com/10.1002/swe.20097`.

T. S. Bastian, A. O. Benz, and D. E. Gary. Radio Emission from Solar Flares. *Annual Reviews*, 36:131–188, Jan 1998. doi: 10.1146/annurev.astro.36.1.131.

G. Bateman. *MHD instabilities*. Cambridge, Mass., MIT Press, 1978.

M. Battaglia and A. O. Benz. Exploring the connection between coronal and footpoint sources in a thin-thick target solar flare model. *Astronomy and Astrophysics*, 466(2):713–716, May 2007. doi: 10.1051/0004-6361:20077144.

Stephen G. Benka and Gordon D. Holman. A Thermal/Nonthermal Model for Solar Hard X-Ray Bursts. *Astrophysical Journal*, 435:469, Nov 1994. doi: 10.1086/174829.

A. O. Benz. Flare Observations. *Living Reviews in Solar Physics*, 14:2, December 2017. doi: 10.1007/s41116-016-0004-3.

Arnold O. Benz, Marina Battaglia, and Nicole Vilmer. Location of Decimetric Pulsations in Solar Flares. *Solar Physics*, 273(2):363–375, Nov 2011. doi: 10.1007/s11207-011-9760-3.

D. Bewsher, R. A. Harrison, and D. S. Brown. The relationship between EUV dimming and coronal mass ejections. *Astronomy & Astrophysics*, 478(3):897–906, 2 2008. ISSN 0004-6361. doi: 10.1051/0004-6361:20078615. URL `http://www.aanda.org/10.1051/0004-6361:20078615`.

D. E. Billings. *A Guide to the Solar Corona*. Academic Press, New York; London, 1966.

J. Birn and E. R. Priest. *Reconnection of Magnetic Fields*. Cambridge, UK: Cambridge University Press, January 2007.

J. Birn, J. F. Drake, M. A. Shay, B. N. Rogers, R. E. Denton, M. Hesse, M. Kuznetsova, Z. W. Ma, A. Bhattacharjee, A. Otto, and P. L. Pritchett. Geospace Environmental Modeling (GEM) magnetic reconnection challenge. *Journal of Geophysical Research*, 106:3715–3720, March 2001. doi: 10.1029/1999JA900449.

D. Biskamp. Magnetic reconnection via current sheets. *Physics of Fluids*, 29:1520–1531, May 1986. doi: 10.1063/1.865670.

D. Biskamp. *Magnetic Reconnection in Plasmas*. Cambridge, UK: Cambridge University Press, September 2000.

M. G. Bobra and S. Couvidat. Solar Flare Prediction Using SDO/HMI Vector Magnetic Field Data with a Machine-learning Algorithm. *Astrophysical Journal*, 798(2):135, Jan 2015a. doi: 10.1088/0004-637X/798/2/135.

M. G. Bobra and S. Couvidat. Solar Flare Prediction Using SDO/HMI Vector Magnetic Field Data with a Machine-learning Algorithm. *Astrophysical Journal*, 798(2):135, Jan 2015b. doi: 10.1088/0004-637X/798/2/135.

M. G. Bobra and S. Ilonidis. Predicting Coronal Mass Ejections Using Machine Learning Methods. *Astrophysical Journal*, 821(2):127, Apr 2016a. doi: 10.3847/0004-637X/821/2/127.

M. G. Bobra and S. Ilonidis. Predicting Coronal Mass Ejections Using Machine Learning Methods. *Astrophysical Journal*, 821(2):127, Apr 2016b. doi: 10.3847/0004-637X/821/2/127.

Monica Bobra, Chris Holdgraf, James Mason, Paul Wright, Carlos Jos Daz Baso, and Ariel Rokem. Helioml/helioml: Helioml 0.2.0 (2019-02-22), February 2019. URL `https://doi.org/10.5281/zenodo.2575738`.

V. Bothmer and R. Schwenn. The structure and origin of magnetic clouds in the solar wind. *Annales Geophysicae*, 16(1):1–24, 1 1998. ISSN 1432-0576. doi: 10.1007/s00585-997-0001-x. URL `http://www.ann-geophys.net/16/1/1998/`.

Stephen J. Bradshaw and John Raymond. Collisional and Radiative Processes in Optically Thin Plasmas. *Space Science Reviews*, 178(2-4):271–306, Oct 2013. doi: 10.1007/s11214-013-9970-0.

Jeffrey W. Brosius, Adrian N. Daw, and Andrew R. Inglis. Quasi-periodic Fluctuations and Chromospheric Evaporation in a Solar Flare Ribbon Observed by Hinode/EIS, IRIS, and RHESSI. *Astrophysical Journal*, 830(2):101, Oct 2016. doi: 10.3847/0004-637X/830/2/101.

J. C. Brown. The Deduction of Energy Spectra of Non-Thermal Electrons in Flares from the Observed Dynamic Spectra of Hard X-Ray Bursts. *Solar Physics*, 18:489–502, July 1971. doi: 10.1007/BF00149070.

G. E. Brueckner, R. A. Howard, M. J. Koomen, C. M. Korendyke, D. J. Michels, J. D. Moses, D. G. Socker, K. P. Dere, P. L. Lamy, and A. Llebaria. The Large Angle Spectroscopic Coronagraph (LASCO). *Solar Physics*, 162(1-2):357–402, Dec 1995. doi: 10.1007/BF00733434.

L. Burlaga, E. Sittler, F. Mariani, and R. Schwenn. Magnetic loop behind an interplanetary shock: Voyager, Helios, and IMP 8 observations. *Journal of Geophysical Research*, 86(A8):6673, 1981. ISSN 0148-0227. doi: 10.1029/JA086iA08p06673. URL `http://doi.wiley.com/10.1029/JA086iA08p06673`.

E. Camporeale, S. Wing, and J. R. Johnson. *Machine Learning Techniques for Space Weather*. Elsevier Press, 2018. ISBN 978-0-12-811788-0. doi: 110.1016/C2016-0-01976-9. URL `https://www.sciencedirect.com/book/9780128117880/machine-learning-techniques-for-space-weathe`

R. C. Canfield, T. R. Metcalf, K. T. Strong, and D. M. Zarro. A novel observational test of momentum balance in a solar flare. *Nature*, 326:165, March 1987. doi: 10.1038/326165a0.

Richard C. Canfield. Impulsive phase explosive dynamics. *Advances in Space Research*, 6(6):167–176, 1 1986. ISSN 02731177. doi: 10.1016/0273-1177(86)90140-7. URL `https://linkinghub.elsevier.com/retrieve/pii/0273117786901407`.

Richard C. Canfield, Hugh S. Hudson, and David E. McKenzie. Sigmoidal morphology and eruptive solar activity. *Geophysical Research Letters*, 26(6):627–630, Jan 1999. doi: 10.1029/1999GL900105.

P. J. Cargill, L. Vlahos, G. Baumann, J. F. Drake, and Å. Nordlund. Current Fragmentation and Particle Acceleration in Solar Flares. *Space Science Reviews*, 173(1-4):223–245, Nov 2012. doi: 10.1007/s11214-012-9888-y.

H. Carmichael. A Process for Flares. *NASA Special Publication*, 50:451, 1964.

A. Caspi and R. P. Lin. RHESSI Line and Continuum Observations of Super-hot Flare Plasma. *Astrophysical Journal*, 725(2):L161–L166, Dec 2010. doi: 10.1088/2041-8205/725/2/L161.

Amir Caspi, James M. McTiernan, and Harry P. Warren. Constraining Solar Flare Differential Emission Measures with EVE and RHESSI. *Astrophysical Journal Letters*, 788(2):L31, Jun 2014. doi: 10.1088/2041-8205/788/2/L31.

Jongchul Chae. Observational Determination of the Rate of Magnetic Helicity Transport through the Solar Surface via the Horizontal Motion of Field Line Footpoints. *Astrophysical Journal Letters*, 560(1):L95–L98, Oct 2001. doi: 10.1086/324173.

P. C. Chamberlin, R. O. Milligan, and T. N. Woods. Thermal Evolution and Radiative Output of Solar Flares Observed by the EUV Variability Experiment (EVE). *Solar Physics*, 279:23–42, July 2012. doi: 10.1007/s11207-012-9975-y.

B. Chen, T. S. Bastian, C. Shen, D. E. Gary, S. Krucker, and L. Glesener. Particle acceleration by a solar flare termination shock. *Science*, 350:1238–1242, December 2015. doi: 10.1126/science.aac8467.

P. F. Chen. Coronal Mass Ejections: Models and Their Observational Basis. *Living Reviews in Solar Physics*, 8(1):1, 2011. ISSN 1614-4961. doi: 10.12942/lrsp-2011-1. URL `http://link.springer.com/10.12942/lrsp-2011-1`.

J. X. Cheng and J. Qiu. The Nature of CME-flare-Associated Coronal Dimming. *Astrophysical Journal*, 825:37, July 2016. doi: 10.3847/0004-637X/825/1/37.

M. C. M. Cheung, P. Boerner, C. J. Schrijver, P. Testa, F. Chen, H. Peter, and A. Malanushenko. Thermal Diagnostics with the Atmospheric Imaging Assembly on board the Solar Dynamics Observatory: A Validated Method for Differential Emission Measure Inversions. *Astrophysical Journal*, 807:143, July 2015. doi: 10.1088/0004-637X/807/2/143.

M. C. M. Cheung, M. Rempel, G. Chintzoglou, F. Chen, P. Testa, J. Martínez-Sykora, A. Sainz Dalda, M. L. DeRosa, A. Malanushenko, V. Hansteen, B. De Pontieu, M. Carlsson, B. Gudik-

sen, and S. W. McIntosh. A comprehensive three-dimensional radiative magnetohydrodynamic simulation of a solar flare. *Nature Astronomy*, 3:160–166, January 2019. doi: 10.1038/s41550-018-0629-3.

R. C. Colaninno, A. Vourlidas, and C. C. Wu. Quantitative comparison of methods for predicting the arrival ofcoronal mass ejections at earth based on multiview imaging. *Journal of Geophysical Research: Space Physics*, 118(11):6866–6879, 2013. doi: 10.1002/2013JA019205. URL `https://agupubs.onlinelibrary.wiley.com/doi/abs/10.1002/2013JA019205`.

Robin C Colaninno and Angelos Vourlidas. First Determination of the True Mass of Coronal Mass Ejections: A Novel Approach to Using the Two STEREO Viewpoints. *Astrophysical Journal*, 698(1):852–858, 6 2009. doi: 10.1088/0004-637X/698/1/852.

B. De Pontieu, A. M. Title, J. R. Lemen, G. D. Kushner, D. J. Akin, B. Allard, T. Berger, P. Boerner, M. Cheung, C. Chou, J. F. Drake, D. W. Duncan, S. Freeland, G. F. Heyman, C. Hoffman, N. E. Hurlburt, R. W. Lindgren, D. Mathur, R. Rehse, D. Sabolish, R. Seguin, C. J. Schrijver, T. D. Tarbell, J.-P. Wülser, C. J. Wolfson, C. Yanari, J. Mudge, N. Nguyen-Phuc, R. Timmons, R. van Bezooijen, I. Weingrod, R. Brookner, G. Butcher, B. Dougherty, J. Eder, V. Knagenhjelm, S. Larsen, D. Mansir, L. Phan, P. Boyle, P. N. Cheimets, E. E. DeLuca, L. Golub, R. Gates, E. Hertz, S. McKillop, S. Park, T. Perry, W. A. Podgorski, K. Reeves, S. Saar, P. Testa, H. Tian, M. Weber, C. Dunn, S. Eccles, S. A. Jaeggli, C. C. Kankelborg, K. Mashburn, N. Pust, L. Springer, R. Carvalho, L. Kleint, J. Marmie, E. Mazmanian, T. M. D. Pereira, S. Sawyer, J. Strong, S. P. Worden, M. Carlsson, V. H. Hansteen, J. Leenaarts, M. Wiesmann, J. Aloise, K.-C. Chu, R. I. Bush, P. H. Scherrer, P. Brekke, J. Martinez-Sykora, B. W. Lites, S. W. McIntosh, H. Uitenbroek, T. J. Okamoto, M. A. Gummin, G. Auker, P. Jerram, P. Pool, and N. Waltham. The Interface Region Imaging Spectrograph (IRIS). *Solar Physics*, 289:2733–2779, July 2014. doi: 10.1007/s11207-014-0485-y.

C. E. DeForest, T. A. Howard, and D. J. McComas. Disconnecting Open Solar Magnetic Flux. *Astrophysical Journal*, 745(1):36, Jan 2012. doi: 10.1088/0004-637X/745/1/36.

C. E. DeForest, T. A. Howard, and D. J. McComas. Tracking Coronal Features from the Low

Corona to Earth: A Quantitative Analysis of the 2008 December 12 Coronal Mass Ejection. *Astrophysical Journal*, 769(1):43, May 2013. doi: 10.1088/0004-637X/769/1/43.

C. E. DeForest, T. A. Howard, and D. J. McComas. INBOUND WAVES IN THE SOLAR CORONA: A DIRECT INDICATOR OF ALFVÉN SURFACE LOCATION. *The Astrophysical Journal*, 787(2):124, 5 2014. ISSN 0004-637X. doi: 10.1088/0004-637X/787/2/124. URL `http://stacks.iop.org/0004-637X/787/i=2/a=124`.

Giulio Del Zanna and Helen E. Mason. Solar UV and X-ray spectral diagnostics. *Living Reviews in Solar Physics*, 15(1):5, Aug 2018. doi: 10.1007/s41116-018-0015-3.

P. Démoulin and G. Aulanier. Criteria for Flux Rope Eruption: Non-equilibrium Versus Torus Instability. *Astrophysical Journal*, 718:1388–1399, August 2010. doi: 10.1088/0004-637X/718/2/1388.

P. Démoulin and P. Where will efficient energy release occur in 3-D magnetic configurations? *Advances in Space Research*, 39(9):1367–1377, 1 2007. ISSN 02731177. doi: 10.1016/j.asr.2007.02.046. URL `https://linkinghub.elsevier.com/retrieve/pii/S0273117707001482`.

P. Demoulin, L. van Driel-Gesztelyi, B. Schmieder, J. C. Hemoux, G. Csepura, and M. J. Hagyard. Evidence for magnetic reconnection in solar flares. *Astronomy and Astrophysics*, 271:292, Apr 1993.

P. Demoulin, J. C. Henoux, E. R. Priest, and C. H. Mandrini. Quasi-Separatrix layers in solar flares. I. Method. *Astronomy and Astrophysics*, 308:643–655, April 1996.

P. Démoulin, E. R. Priest, and D. P. Lonie. Three-dimensional magnetic reconnection without null points 2. Application to twisted flux tubes. *Journal of Geophysical Research*, 101:7631–7646, April 1996. doi: 10.1029/95JA03558.

K. P. Dere and J. W. Cook. The decay of the 1973 August 9 flare. *Astrophysical Journal*, 229:772–787, April 1979. doi: 10.1086/157013.

K. P. Dere, E. Landi, H. E. Mason, B. C. Monsignori Fossi, and P. R. Young. CHIANTI - an atomic database for emission lines. *Astronomy and Astrophysics, Supplement*, 125:149–173, Oct 1997. doi: 10.1051/aas:1997368.

C. Richard DeVore and Spiro K. Antiochos. Dynamical Formation and Stability of Helical Prominence Magnetic Fields. *The Astrophysical Journal*, 539(2):954–963, 8 2000. ISSN 0004-637X. doi: 10.1086/309275. URL http://stacks.iop.org/0004-637X/539/i=2/a=954.

K. Dissauer, A. M. Veronig, M. Temmer, and T. Podladchikova. Statistics of Coronal Dimmings Associated with Coronal Mass Ejections. II. Relationship between Coronal Dimmings and Their Associated CMEs. *The Astrophysical Journal*, 874(2):123, 3 2019. ISSN 0004-637X. doi: 10.3847/1538-4357/AB0962. URL https://iopscience.iop.org/article/10.3847/1538-4357/ab0962.

Karin Dissauer, Astrid M. Veronig, Manuela Temmer, Tatiana Podladchikova, and Kamalam Vanninathan. On the detection of coronal dimmings and the extraction of their characteristic properties. *The Astrophysical Journal, Volume 855, Issue 2, article id. 137, 13 pp. (2018).*, 855, 2 2018. ISSN 0004-637X. doi: 10.3847/1538-4357/aaadb5. URL http://arxiv.org/abs/1802.03185 http://dx.doi.org/10.3847/1538-4357/aaadb5.

J. F. Drake, M. Swisdak, H. Che, and M. A. Shay. Electron acceleration from contracting magnetic islands during reconnection. *Nature*, 443:553–556, October 2006. doi: 10.1038/nature05116.

Jaroslav Dudík, Elena Dzifčáková, Nicole Meyer-Vernet, Giulio Del Zanna, Peter R. Young, Alessandra Giunta, Barbara Sylwester, Janusz Sylwester, Mitsuo Oka, and Helen E. Mason. Nonequilibrium Processes in the Solar Corona, Transition Region, Flares, and Solar Wind (Invited Review). *Solar Physics*, 292(8):100, Aug 2017. doi: 10.1007/s11207-017-1125-0.

G. A. Dulk. Radio emission from the sun and stars. *Annual Reviews*, 23:169–224, 1985. doi: 10.1146/annurev.aa.23.090185.001125.

G. Einaudi and G. van Hoven. The stability of coronal loops - Finite-length and pressure-profile limits. *Solar Physics*, 88:163–177, October 1983. doi: 10.1007/BF00196185.

A. G. Emslie, P. Li, and J. T. Mariska. Diagnostics of electron-heated solar flare models. III - Effects of tapered loop geometry and preheating. *Astrophysical Journal*, 399:714–723, November 1992. doi: 10.1086/171964.

A. G. Emslie, H. Kucharek, B. R. Dennis, N. Gopalswamy, G. D. Holman, G. H. Share, A. Vourlidas, T. G. Forbes, P. T. Gallagher, G. M. Mason, T. R. Metcalf, R. A. Mewaldt, R. J. Murphy, R. A. Schwartz, and T. H. Zurbuchen. Energy partition in two solar flare/CME events. *Journal of Geophysical Research*, 109(A10):A10104, 10 2004. ISSN 0148-0227. doi: 10.1029/2004JA010571. URL `http://doi.wiley.com/10.1029/2004JA010571`.

A. G. Emslie, B. R. Dennis, A. Y. Shih, P. C. Chamberlin, R. A. Mewaldt, C. S. Moore, G. H. Share, A. Vourlidas, and B. T. Welsch. Global Energetics of Thirty-eight Large Solar Eruptive Events. *Astrophysical Journal*, 759:71, November 2012. doi: 10.1088/0004-637X/759/1/71.

A. G. Emslie, B. R. Dennis, A. Y. Shih, P. C. Chamberlin, R. A. Mewaldt, C. S. Moore, G. H. Share, A. Vourlidas, and B. T. Welsch. GLOBAL ENERGETICS OF THIRTY-EIGHT LARGE SOLAR ERUPTIVE EVENTS. *The Astrophysical Journal*, 759(1):71, 11 2012. ISSN 0004-637X. doi: 10.1088/0004-637X/759/1/71. URL `http://stacks.iop.org/0004-637X/759/i=1/a=71`.

Oddbjrn Engvold. Description and Classification of Prominences. In *Solar Prominences*, pages 31–60. Springer International Publishing, 2015. doi: 10.1007/978-3-319-10416-4{_}2. URL `http://link.springer.com/10.1007/978-3-319-10416-4_2`.

C. J. Eyles, R. A. Harrison, C. J. Davis, N. R. Waltham, B. M. Shaughnessy, H. C. A. Mapson-Menard, D. Bewsher, S. R. Crothers, J. A. Davies, and G. M. Simnett. The Heliospheric Imagers Onboard the STEREO Mission. *Solar Physics*, 254(2):387–445, Feb 2009. doi: 10.1007/s11207-008-9299-0.

Y. Fan and S. E. Gibson. The Emergence of a Twisted Magnetic Flux Tube into a Preexisting Coronal Arcade. *The Astrophysical Journal*, 589(2):L105–L108, 6 2003. ISSN 0004-637X. doi: 10.1086/375834. URL `http://stacks.iop.org/1538-4357/589/i=2/a=L105`.

Y. Fan and S. E. Gibson. Onset of Coronal Mass Ejections Due to Loss of Confinement of Coronal Flux Ropes. *Astrophysical Journal*, 668:1232–1245, October 2007. doi: 10.1086/521335.

U. Feldman, P. Mandelbaum, J. F. Seely, G. A. Doschek, and H. Gursky. The Potential for Plasma Diagnostics from Stellar Extreme-Ultraviolet Observations. *Astrophysical Journal Supplement*, 81:387, Jul 1992. doi: 10.1086/191698.

L. Feng, T. Wiegelmann, Y. Su, B. Inhester, Y. P. Li, X. D. Sun, and W. Q. Gan. MAGNETIC ENERGY PARTITION BETWEEN THE CORONAL MASS EJECTION AND FLARE FROM AR 11283. *The Astrophysical Journal*, 765(1):37, 2 2013. ISSN 0004-637X. doi: 10.1088/0004-637X/765/1/37. URL `http://stacks.iop.org/0004-637X/765/i=1/a=37`.

G. H. Fisher. Dynamics of flare-driven chromospheric condensations. *Astrophysical Journal*, 346: 1019–1029, November 1989. doi: 10.1086/168084.

G. H. Fisher, R. C. Canfield, and A. N. McClymont. Flare loop radiative hydrodynamics. V - Response to thick-target heating. VI - Chromospheric evaporation due to heating by nonthermal electrons. VII - Dynamics of the thick-target heated chromosphere. *Astrophysical Journal*, 289: 414–441, February 1985a. doi: 10.1086/162901.

G. H. Fisher, R. C. Canfield, and A. N. McClymont. Flare Loop Radiative Hydrodynamics - Part Six - Chromospheric Evaporation due to Heating by Nonthermal Electrons. *Astrophysical Journal*, 289:425, February 1985b. doi: 10.1086/162902.

G. H. Fisher, R. C. Canfield, and A. N. McClymont. Flare Loop Radiative Hydrodynamics - Part Seven - Dynamics of the Thick Target Heated Chromosphere. *Astrophysical Journal*, 289:434, February 1985c. doi: 10.1086/162903.

L. Fletcher and H. S. Hudson. Impulsive Phase Flare Energy Transport by Large-Scale Alfvén Waves and the Electron Acceleration Problem. *Astrophysical Journal*, 675:1645–1655, March 2008. doi: 10.1086/527044.

L. Fletcher, B. R. Dennis, H. S. Hudson, S. Krucker, K. Phillips, A. Veronig, M. Battaglia, L. Bone, A. Caspi, Q. Chen, P. Gallagher, P. T. Grigis, H. Ji, W. Liu, R. O. Milligan, and M. Temmer. An Observational Overview of Solar Flares. *Space Science Reviews*, 159:19–106, September 2011. doi: 10.1007/s11214-010-9701-8.

T. G. Forbes. Fast-shock formation in line-tied magnetic reconnection models of solar flares. *Astrophysical Journal*, 305:553–563, June 1986. doi: 10.1086/164268.

T. G. Forbes and L. W. Acton. Reconnection and Field Line Shrinkage in Solar Flares. *Astrophysical Journal*, 459:330, Mar 1996. doi: 10.1086/176896.

T. G. Forbes and E. R. Priest. Photospheric Magnetic Field Evolution and Eruptive Flares. *Astrophysical Journal*, 446:377, Jun 1995. doi: 10.1086/175797.

T. G. Forbes, E. R. Priest, D. B. Seaton, and Y. E. Litvinenko. Indeterminacy and instability in Petschek reconnection. *Physics of Plasmas*, 20(5):052902, May 2013. doi: 10.1063/1.4804337.

H. P. Furth, J. Killeen, and M. N. Rosenbluth. Finite-Resistivity Instabilities of a Sheet Pinch. *Physics of Fluids*, 6:459–484, April 1963. doi: 10.1063/1.1706761.

P. T. Gallagher, G. R. Lawrence, and B. R. Dennis. Rapid Acceleration of a Coronal Mass Ejection in the Low Corona and Implications for Propagation. *Astrophysical Journal Letters*, 588:L53–L56, May 2003. doi: 10.1086/375504.

W. Q. Gan, H. Q. Zhang, and C. Fang. A hydrodynamic model of the impulsive phase of a solar flare loop. *Astronomy and Astrophysics*, 241:618–624, January 1991.

D. E. Gary, G. D. Fleishman, and G. M. Nita. Magnetography of Solar Flaring Loops with Microwave Imaging Spectropolarimetry. *Solar Physics*, 288(2):549–565, Dec 2013. doi: 10.1007/s11207-013-0299-3.

D. E. Gary, B. Chen, B. R. Dennis, G. D. Fleishman, G. J. Hurford, S. Krucker, J. M. McTiernan, G. M. Nita, A. Y. Shih, S. M. White, and S. Yu. Microwave and Hard X-Ray Observations of the 2017 September 10 Solar Limb Flare. *Astrophysical Journal*, 863:83, August 2018. doi: 10.3847/1538-4357/aad0ef.

Manolis K. Georgoulis, Alexander Nindos, and Hongqi Zhang. The source and engine of coronal mass ejections. *Philosophical Transactions of the Royal Society of London Series A*, 377(2148): 20180094, Jul 2019. doi: 10.1098/rsta.2018.0094.

H. R. Gilbert, B. J. Thompson, T. E. Holzer, and J. T. Burkepile. A Comparison of CME-associated atmospheric waves observed in coronal (19.5 nm) and chromospheric (He I 1083 nm and H-alpha 656 nm) lines. In *AGU Fall Meeting Abstracts*, volume 2001, pages SH12B–0746, 12 2001.

R. G. Giovanelli. Magnetic and Electric Phenomena in the Sun's Atmosphere associated with Sunspots. *Monthly Notices of the Royal Astronomical Society*, 107:338, 1947. doi: 10.1093/mnras/107.4.338.

L. Golub, E. Deluca, G. Austin, J. Bookbinder, D. Caldwell, P. Cheimets, J. Cirtain, M. Cosmo, P. Reid, and A. Sette. The X-Ray Telescope (XRT) for the Hinode Mission. *Solar Physics*, 243 (1):63–86, Jun 2007. doi: 10.1007/s11207-007-0182-1.

S. W. Good and R. J. Forsyth. Interplanetary Coronal Mass Ejections Observed by MESSENGER and Venus Express. *Solar Physics*, 291(1):239–263, 1 2016. ISSN 0038-0938. doi: 10.1007/s11207-015-0828-3. URL http://arxiv.org/abs/1511.07749 http://dx.doi.org/10.1007/s11207-015-0828-3 http://link.springer.com/10.1007/s11207-015-0828-3.

S. W. Good, R. J. Forsyth, J. M. Raines, D. J. Gershman, J. A. Slavin, and T. H. Zurbuchen. RADIAL EVOLUTION OF A MAGNETIC CLOUD: ¡i¿MESSENGER¡/i¿ , ¡i¿STEREO¡/i¿ , AND ¡i¿VENUS EXPRESS¡/i¿ OBSERVATIONS. *The Astrophysical Journal*, 807(2):177, 7 2015. ISSN 1538-4357. doi: 10.1088/0004-637X/807/2/177. URL http://stacks.iop.org/0004-637X/807/i=2/a=177.

N. Gopalswamy and B. J. Thompson. Early life of coronal mass ejections. *Journal of Atmospheric and Solar-Terrestrial Physics*, 62(16):1457–1469, Nov 2000. doi: 10.1016/S1364-6826(00)00079-1.

N Gopalswamy and B. J. Thompson. Early life of coronal mass ejections. *Journal of Atmospheric and Solar-Terrestrial Physics*, 62(16):1457–1469, 11 2000. doi: 10.1016/S1364-6826(00)00079-1.

N. Gopalswamy, S. Yashiro, P. Mäkelä, H. Xie, S. Akiyama, and C. Monstein. Extreme Kinematics of the 2017 September 10 Solar Eruption and the Spectral Characteristics of the Associated Energetic Particles. *Astrophysical Journal Letters*, 863(2):L39, Aug 2018. doi: 10.3847/2041-8213/aad86c.

V. S. Gorbachev and B. V. Somov. Photospheric Vortex Flows as a Cause for Two-Ribbon Flares - a Topological Model. *Solar Physics*, 117(1):77–88, Mar 1988. doi: 10.1007/BF00148574.

J. T. Gosling. Coronal mass ejections and magnetic flux ropes in interplanetary space. *Washington DC American Geophysical Union Geophysical Monograph Series*, 58:343–364, Jan 1990. doi: 10.1029/GM058p0343.

J. T. Gosling. The solar flare myth. *Journal of Geophysical Research*, 98(A11):18937–18950, Nov 1993. doi: 10.1029/93JA01896.

J. T. Gosling. The solar flare myth. *Journal of Geophysical Research*, 98(A11):18937–18950, 11 1993. doi: 10.1029/93JA01896.

D. R. Graham and G. Cauzzi. Temporal Evolution of Multiple Evaporating Ribbon Sources in a Solar Flare. *Astrophysical Journal Letters*, 807:L22, July 2015. doi: 10.1088/2041-8205/807/2/L22.

L. M. Green, T. Török, B. Vršnak, W. Manchester, and A. Veronig. The Origin, Early Evolution and Predictability of Solar Eruptions. *Space Science Reviews*, 214:46, February 2018. doi: 10.1007/s11214-017-0462-5.

S. E. Guidoni, C. R. DeVore, J. T. Karpen, and B. J. Lynch. Magnetic-island Contraction and Particle Acceleration in Simulated Eruptive Solar Flares. *Astrophysical Journal*, 820(1):60, Mar 2016. doi: 10.3847/0004-637X/820/1/60.

Jingnan Guo, Mateja Dumbović, Robert F. Wimmer-Schweingruber, Manuela Temmer, Henning Lohf, Yuming Wang, Astrid Veronig, Donald M. Hassler, Leila M. Mays, and Cary Zeitlin. Modeling the Evolution and Propagation of 10 September 2017 CMEs and SEPs Arriving at Mars Constrained by Remote Sensing and In Situ Measurement. *Space Weather*, 16(8):1156–1169, Aug 2018. doi: 10.1029/2018SW001973.

Yoichiro Hanaoka, Hiroki Kurokawa, Shinzo Enome, Hiroshi Nakajima, Kiyoto Shibasaki, Masanori Nishio, Toshiaki Takano, Chikayoshi Torii, Hideaki Sekiguchi, and Susumu Kawashima. Simultaneous Observations of a Prominence Eruption Followed by a Coronal Arcade Formation in Radio, Soft X-Rays, and Hα. *Publications of the ASJ*, 46:205–216, Apr 1994.

I. G. Hannah and E. P. Kontar. Differential emission measures from the regularized inversion of Hinode and SDO data. *Astronomy and Astrophysics*, 539:A146, Mar 2012. doi: 10.1051/0004-6361/201117576.

I. G. Hannah, S. Christe, S. Krucker, G. J. Hurford, H. S. Hudson, and R. P. Lin. RHESSI Microflare

Statistics. II. X-Ray Imaging, Spectroscopy, and Energy Distributions. *Astrophysical Journal*, 677:704–718, April 2008. doi: 10.1086/529012.

Louise K. Harra, Hirohisa Hara, Shinsuke Imada, Peter R. Young, David R. Williams, Alphonse C. Sterling, Clarence Korendyke, and Gemma D. R. Attrill. Coronal Dimming Observed with Hinode: Outflows Related to a Coronal Mass Ejection. *Publications of the Astronomical Society of Japan*, 59(sp3):S801–S806, 11 2007. ISSN 0004-6264. doi: 10.1093/pasj/59.sp3.S801. URL `https://academic.oup.com/pasj/article-lookup/doi/10.1093/pasj/59.sp3.S801`.

Louise K. Harra, Carolus J. Schrijver, Miho Janvier, Shin Toriumi, Hugh Hudson, Sarah Matthews, Magnus M. Woods, Hirohisa Hara, Manuel Guedel, Adam Kowalski, Rachel Osten, Kanya Kusano, and Theresa Lueftinger. The Characteristics of Solar X-Class Flares and CMEs: A Paradigm for Stellar Superflares and Eruptions? *Solar Physics*, 291(6):1761–1782, 8 2016. ISSN 0038-0938. doi: 10.1007/s11207-016-0923-0. URL `http://link.springer.com/10.1007/s11207-016-0923-0`.

R. A. Harrison and M. Lyons. A spectroscopic study of coronal dimming associated with a coronal mass ejection. *Astronomy and Astrophysics*, 358:1097, 6 2000.

R. A. Harrison, C. J. Davis, and C. J. Eyles. The STEREO heliospheric imager: how to detect CMEs in the heliosphere. *Advances in Space Research*, 36(8):1512–1523, Jan 2005. doi: 10.1016/j.asr.2005.01.024.

R. A. Harrison, J. A. Davies, D. Barnes, J. P. Byrne, C. H. Perry, V. Bothmer, J. P. Eastwood, P. T. Gallagher, E. K. J. Kilpua, C. Möstl, L. Rodriguez, A. P. Rouillard, and D. Odstrčil. CMEs in the Heliosphere: I. A Statistical Analysis of the Observational Properties of CMEs Detected in the Heliosphere from 2007 to 2017 by STEREO/HI-1. *Solar Physics*, 293(5):77, 5 2018. doi: 10.1007/S11207-018-1297-2. URL `https://ui.adsabs.harvard.edu/abs/2018SoPh..293...77H/abstract`.

Richard A. Harrison. Coronal Magnetic Storms: a New Perspective on Flares and the 'Solar Flare Myth' Debate. *Solar Physics*, 166(2):441–444, Jul 1996. doi: 10.1007/BF00149411.

S. L. Hawley and G. H. Fisher. X-ray-heated models of stellar flare atmospheres - Theory and

comparison with observations. *Astrophysical Journal Supplement*, 78:565–598, February 1992. doi: 10.1086/191640.

Hisashi Hayakawa, Kiyomi Iwahashi, Harufumi Tamazawa, Hiroaki Isobe, Ryuho Kataoka, Yusuke Ebihara, Hiroko Miyahara, Akito Davis Kawamura, and Kazunari Shibata. East Asian observations of low-latitude aurora during the Carrington magnetic storm. *Publications of the ASJ*, 68 (6):99, Dec 2016. doi: 10.1093/pasj/psw097.

Verena Heidrich-Meisner and Robert F. Wimmer-Schweingruber. Solar Wind Classification Via k-Means Clustering Algorithm. *Machine Learning Techniques for Space Weather*, pages 397–424, 1 2018. doi: 10.1016/B978-0-12-811788-0.00016-0. URL

J. Heyvaerts, E. R. Priest, and D. M. Rust. An emerging flux model for the solar flare phenomenon. *Astrophysical Journal*, 216:123–137, August 1977. doi: 10.1086/155453.

T. Hirayama. Theoretical Model of Flares and Prominences. I: Evaporating Flare Model. *Solar Physics*, 34:323–338, February 1974. doi: 10.1007/BF00153671.

G. D. Holman. Acceleration of runaway electrons and Joule heating in solar flares. *Astrophysical Journal*, 293:584–594, Jun 1985. doi: 10.1086/163263.

G. D. Holman, M. J. Aschwanden, H. Aurass, M. Battaglia, P. C. Grigis, E. P. Kontar, W. Liu, P. Saint-Hilaire, and V. V. Zharkova. Implications of X-ray Observations for Electron Acceleration and Propagation in Solar Flares. *Space Science Reviews*, 159(1-4):107–166, Sep 2011. doi: 10.1007/s11214-010-9680-9.

R. H. Holzworth and C. I. Meng. Mathematical representation of the auroral oval. *Geophysical Research Letters*, 2(9):377–380, Sep 1975. doi: 10.1029/GL002i009p00377.

A. W. Hood and E. R. Priest. Critical conditions for magnetic instabilities in force-free coronal loops. *Geophysical and Astrophysical Fluid Dynamics*, 17:297–318, 1981. doi: 10.1080/03091928108243687.

K. Hori, T. Yokoyama, T. Kosugi, and K. Shibata. Pseudo-Two-dimensional Hydrodynamic Modeling of Solar Flare Loops. *Astrophysical Journal*, 489:426–441, November 1997. doi: 10.1086/304754.

R. A. Howard. A Historical Perspective on Coronal Mass Ejections. *Washington DC American Geophysical Union Geophysical Monograph Series*, 165:7, October 2006. doi: 10.1029/165GM03.

R. A. Howard, N. R. Sheeley Jr., M. J. Koomen, and D. J. Michels. Coronal mass ejections: 19791981. *Journal of Geophysical Research: Space Physics*, 90(A9):8173–8191, 1985. doi: 10.1029/JA090iA09p08173. URL https://agupubs.onlinelibrary.wiley.com/doi/abs/10.1029/JA090iA09p08173.

R. A. Howard, J. D. Moses, A. Vourlidas, J. S. Newmark, D. G. Socker, S. P. Plunkett, C. M. Korendyke, J. W. Cook, A. Hurley, and J. M. Davila. Sun Earth Connection Coronal and Heliospheric Investigation (SECCHI). *Space Science Reviews*, 136(1-4):67–115, Apr 2008. doi: 10.1007/s11214-008-9341-4.

Russell Howard, A Vourlidas, R.C. Colaninno, C.M. Korendyke, S.P. Plunkett, M.T. Carter, Dennis Wang, Nathan Rich, S Lynch, A Thurn, D Socker, A Thernisien, and Damien Chua. The solar orbiter heliospheric imager (solohi). *Astronomy and Astrophysics*, 06 2019. doi: 10.1051/0004-6361/201935202.

T. A. Howard and G. M. Simnett. Interplanetary coronal mass ejections that are undetected by solar coronagraphs. *Journal of Geophysical Research: Space Physics*, 113(A8), 2008. doi: 10.1029/2007JA012920. URL https://agupubs.onlinelibrary.wiley.com/doi/abs/10.1029/2007JA012920.

Timothy Howard. *Introduction*, pages 1–18. Springer New York, New York, NY, 2011. ISBN 978-1-4419-8789-1. doi: 10.1007/978-1-4419-8789-1_1. URL https://doi.org/10.1007/978-1-4419-8789-1$_1$.

Timothy A. Howard and S. James Tappin. Interplanetary coronal mass ejections observed inthehe-liosphere: 1. review of theory. *Space Science Reviews*, 147(1):31–54, Oct 2009. ISSN 1572-9672. doi: 10.1007/s11214-009-9542-5. URL https://doi.org/10.1007/s11214-009-9542-5.

H. Hudson and J. Ryan. High-Energy Particles In Solar Flares. *Annual Reviews*, 33:239–282, Jan 1995. doi: 10.1146/annurev.aa.33.090195.001323.

H. S. Hudson and E. W. Cliver. Observing coronal mass ejections without coronagraphs. *Journal of Geophysical Research: Space Physics*, 106(A11):25199–25213, 11 2001. ISSN 01480227. doi: 10.1029/2000JA904026. URL http://doi.wiley.com/10.1029/2000JA904026.

H. S. Hudson, L. W. Acton, and S. L. Freeland. A Long-Duration Solar Flare with Mass Ejection and Global Consequences. *The Astrophysical Journal*, 470:629, 10 1996. ISSN 0004-637X. doi: 10.1086/177894. URL http://adsabs.harvard.edu/doi/10.1086/177894.

H. S. Hudson, J. R. Lemen, O. C. St. Cyr, A. C. Sterling, and D. F. Webb. X-ray coronal changes during Halo CMEs. *Geophysical Research Letters*, 25(14):2481–2484, 7 1998. ISSN 00948276. doi: 10.1029/98GL01303. URL http://doi.wiley.com/10.1029/98GL01303.

Hugh S. Hudson. Global Properties of Solar Flares. *Space Science Reviews*, 158(1):5–41, Jan 2011. doi: 10.1007/s11214-010-9721-4.

Hugh S. Hudson and David F. Webb. *Soft X-Ray Signatures of Coronal Ejections*, pages 27–38. American Geophysical Union (AGU), 1997. ISBN 9781118664377. doi: 10.1029/GM099p0027. URL https://agupubs.onlinelibrary.wiley.com/doi/abs/10.1029/GM099p0027.

A. Hundhausen. Coronal Mass Ejections. In Keith T. Strong, Julia L. R. Saba, Bernhard M. Haisch, and Joan T. Schmelz, editors, *The many faces of the sun: a summary of the results from NASA's Solar Maximum Mission.*, page 143, Jan 1999.

A. J. Hundhausen. High-Speed Plasma Streams and Magnetic Sectors. In *Coronal Expansion and Solar Wind*, pages 121–168. Springer, Berlin, Heidelberg, 1972. doi: 10.1007/978-3-642-65414-5{_}5. URL http://link.springer.com/10.1007/978-3-642-65414-5$_5$.

K. Ichimoto and H. Kurokawa. H-alpha red asymmetry of solar flares. *Solar Physics*, 93:105–121, June 1984. doi: 10.1007/BF00156656.

A. R. Inglis and V. M. Nakariakov. A multi-periodic oscillatory event in a solar flare. *Astronomy and Astrophysics*, 493(1):259–266, Jan 2009. doi: 10.1051/0004-6361:200810473.

B. V. Jackson and E. Hildner. Forerunners: outer rims of solar coronal transients. *Solar Physics*, 60(1):155–170, Nov 1978. doi: 10.1007/BF00152340.

B. V. Jackson and C. Leinert. Helios images of solar mass ejections. *Journal of Geophysical Research*, 90(A11):10759–10764, Nov 1985. doi: 10.1029/JA090iA11p10759.

B. V. Jackson, A. Buffington, P. P. Hick, R. C. Altrock, S. Figueroa, P. E. Holladay, J. C. Johnston, S. W. Kahler, J. B. Mozer, and S. Price. The Solar Mass-Ejection Imager (SMEI) Mission. *Solar Physics*, 225(1):177–207, Nov 2004. doi: 10.1007/s11207-004-2766-3.

C. Jacobs, I. I. Roussev, N. Lugaz, and S. Poedts. THE INTERNAL STRUCTURE OF CORONAL MASS EJECTIONS: ARE ALL REGULAR MAGNETIC CLOUDS FLUX ROPES? *The Astrophysical Journal*, 695(2):L171–L175, 4 2009. ISSN 0004-637X. doi: 10.1088/0004-637X/695/2/L171. URL `http://stacks.iop.org/1538-4357/695/i=2/a=L171`.

Bruce M Jakosky. MAVEN GOES TO MARS. MAVEN Explores the Martian Upper Atmosphere. Introduction. *Science (New York, N.Y.)*, 350(6261):643, 11 2015. ISSN 1095-9203. doi: 10.1126/science.aad3443. URL `http://www.ncbi.nlm.nih.gov/pubmed/26542563`.

A. W. James, L. M. Green, E. Palmerio, G. Valori, H. A. S. Reid, D. Baker, D. H. Brooks, L. van Driel-Gesztelyi, and E. K. J. Kilpua. On-Disc Observations of Flux Rope Formation Prior to Its Eruption. *Solar Physics*, 292:71, May 2017. doi: 10.1007/s11207-017-1093-4.

Alexander W. James, Gherardo Valori, Lucie M. Green, Yang Liu, Mark C. M. Cheung, Yang Guo, and Lidia van Driel-Gesztelyi. An Observationally Constrained Model of a Flux Rope that Formed in the Solar Corona. *Astrophysical Journal Letters*, 855(2):L16, Mar 2018. doi: 10.3847/2041-8213/aab15d.

Miho Janvier. Three-dimensional magnetic reconnection and its application to solar flares. *Journal of Plasma Physics*, 83(1):535830101, Feb 2017. doi: 10.1017/S0022377817000034.

Miho Janvier, Reka M. Winslow, Simon Good, Elise Bonhomme, Pascal Démoulin, Sergio Dasso, Christian Möstl, No Lugaz, Tanja Amerstorfer, Elie Soubrié, and Peter D. Boakes. Generic Magnetic Field Intensity Profiles of Interplanetary Coronal Mass Ejections at Mercury, Venus, and Earth From Superposed Epoch Analyses. *Journal of Geophysical Research: Space Physics*, 124(2):812–836, 2 2019. ISSN 2169-9380. doi: 10.1029/2018JA025949.

URL http://arxiv.org/abs/1901.09921 http://dx.doi.org/10.1029/2018JA025949 https://onlinelibrary.wiley.com/doi/abs/10.1029/2018JA025949.

Yan Wei Jiang, Siming Liu, Wei Liu, and Vahé Petrosian. Evolution of the Loop-Top Source of Solar Flares: Heating and Cooling Processes. *Astrophysical Journal*, 638(2):1140–1153, Feb 2006. doi: 10.1086/498863.

Ju Jing, Yan Xu, Wenda Cao, Chang Liu, Dale Gary, and Haimin Wang. Unprecedented Fine Structure of a Solar Flare Revealed by the 1.6 m New Solar Telescope. *Scientific Reports*, 6: 24319, Apr 2016. doi: 10.1038/srep24319.

S. W. Kahler. Solar Flares and Coronal Mass Ejections. *Annual Review of Astronomy and Astrophysics*, 30(1):113–141, 9 1992. ISSN 0066-4146. doi: 10.1146/annurev.aa.30.090192.000553. URL http://www.annualreviews.org/doi/10.1146/annurev.aa.30.090192.000553.

M. L. Kaiser, T. A. Kucera, J. M. Davila, O. C. St. Cyr, M. Guhathakurta, and E. Christian. The STEREO Mission: An Introduction. *Space Science Reviews*, 136:5–16, April 2008. doi: 10.1007/s11214-007-9277-0.

J. T. Karpen, S. K. Antiochos, and C. R. DeVore. The Mechanisms for the Onset and Explosive Eruption of Coronal Mass Ejections and Eruptive Flares. *Astrophysical Journal*, 760:81, November 2012. doi: 10.1088/0004-637X/760/1/81.

C. Kay, M. Opher, and M. Kornbleuth. PROBABILITY OF CME IMPACT ON EXOPLANETS ORBITING M DWARFS AND SOLAR-LIKE STARS. *The Astrophysical Journal*, 826(2):195, 7 2016. ISSN 1538-4357. doi: 10.3847/0004-637X/826/2/195. URL http://stacks.iop.org/0004-637X/826/i=2/a=1955.

Graham S. Kerr, Lyndsay. Fletcher, Alexand er J. B. Russell, and Joel C. Allred. Simulations of the Mg II k and Ca II 8542 lines from an AlfvÉn Wave-heated Flare Chromosphere. *Astrophysical Journal*, 827(2):101, Aug 2016. doi: 10.3847/0004-637X/827/2/101.

M.L. Khodachenko, H. Lammer, H.I.M. Lichtenegger, D. Langmayr, N.V. Erkaev, J-M. Grießmeier, M. Leitner, T. Penz, H.K. Biernat, U. Motschmann, and H.O. Rucker. Mass loss of Hot

JupitersImplications for CoRoT discoveries. Part I: The importance of magnetospheric protection of a planet against ion loss caused by coronal mass ejections. *Planetary and Space Science*, 55(5):631–642, 4 2007. ISSN 00320633. doi: 10.1016/j.pss.2006.07.010. URL `https://linkinghub.elsevier.com/retrieve/pii/S0032063306002583`.

Karl-Ludwig Klein and Silvia Dalla. Acceleration and Propagation of Solar Energetic Particles. *Space Science Reviews*, 212(3-4):1107–1136, Nov 2017. doi: 10.1007/s11214-017-0382-4.

B. Kliem and T. Török. Torus Instability. *Physical Review Letters*, 96(25):255002, June 2006. doi: 10.1103/PhysRevLett.96.255002.

B. Kliem, M. Karlický, and A. O. Benz. Solar flare radio pulsations as a signature of dynamic magnetic reconnection. *Astronomy and Astrophysics*, 360:715–728, Aug 2000.

E. P. Kontar, J. C. Brown, A. G. Emslie, W. Hajdas, G. D. Holman, G. J. Hurford, J. Kašparová, P. C. V. Mallik, A. M. Massone, and M. L. McConnell. Deducing Electron Properties from Hard X-ray Observations. *Space Science Reviews*, 159(1-4):301–355, Sep 2011. doi: 10.1007/s11214-011-9804-x.

R. A. Kopp and G. W. Pneuman. Magnetic reconnection in the corona and the loop prominence phenomenon. *Solar Physics*, 50:85–98, October 1976. doi: 10.1007/BF00206193.

T. Kosugi, K. Matsuzaki, T. Sakao, T. Shimizu, Y. Sone, S. Tachikawa, T. Hashimoto, K. Minesugi, A. Ohnishi, and T. Yamada. The Hinode (Solar-B) Mission: An Overview. *Solar Physics*, 243 (1):3–17, Jun 2007. doi: 10.1007/s11207-007-9014-6.

Adam F. Kowalski, Joel C. Allred, Adrian Daw, Gianna Cauzzi, and Mats Carlsson. The Atmospheric Response to High Nonthermal Electron Beam Fluxes in Solar Flares. I. Modeling the Brightest NUV Footpoints in the X1 Solar Flare of 2014 March 29. *Astrophysical Journal*, 836 (1):12, Feb 2017. doi: 10.3847/1538-4357/836/1/12.

M. Kretzschmar. The Sun as a star: observations of white-light flares. *Astronomy and Astrophysics*, 530:A84, Jun 2011. doi: 10.1051/0004-6361/201015930.

Larisza D. Krista and Alysha A. Reinard. Statistical study of solar dimmings using CoDiT. *The Astrophysical Journal*, 839(1):50, 5 2017. ISSN 1538-4357. doi: 10.3847/1538-4357/aa6626. URL http://dx.doi.org/10.3847/1538-4357/aa6626.

S. Krucker, M. Battaglia, P. J. Cargill, L. Fletcher, H. S. Hudson, A. L. MacKinnon, S. Masuda, L. Sui, M. Tomczak, A. L. Veronig, L. Vlahos, and S. M. White. Hard X-ray emission from the solar corona. *Astronomy and Astrophysics Reviews*, 16:155–208, October 2008. doi: 10.1007/s00159-008-0014-9.

Säm Krucker, H. S. Hudson, N. L. S. Jeffrey, M. Battaglia, E. P. Kontar, A. O. Benz, A. Csillaghy, and R. P. Lin. High-resolution Imaging of Solar Flare Ribbons and Its Implication on the Thick-target Beam Model. *Astrophysical Journal*, 739(2):96, Oct 2011. doi: 10.1088/0004-637X/739/2/96.

T.A. Kucera, A.I. Poland, J.E. Wiik, B. Schmieder, and G. Simnett. Helical Structure in an Eruptive Prominence Related to a CME (SUMER, CDS, LASCO). *International Astronomical Union Colloquium*, 167:318–321, 4 1998. ISSN 0252-9211. doi: 10.1017/S0252921100047825.

Ryun-Young Kwon, Jie Zhang, and Angelos Vourlidas. Are Halo-like Solar Coronal Mass Ejections Merely a Matter of Geometric Projection Effects? *Astrophysical Journal*, 799(2):L29, Jan 2015. doi: 10.1088/2041-8205/799/2/L29.

Ryun-Young Kwon, Jie Zhang, and Angelos Vourlidas. Are Halo-like Solar Coronal Mass Ejections Merely a Matter of Geometric Projection Effects? *Astrophysical Journal Letters*, 799(2):L29, 1 2015. doi: 10.1088/2041-8205/799/2/L29.

Helmut Lammer, Herbert I.M. Lichtenegger, Yuri N. Kulikov, Jean-Mathias Grießmeier, N. Terada, Nikolai V. Erkaev, Helfried K. Biernat, Maxim L. Khodachenko, Ignasi Ribas, Thomas Penz, and Franck Selsis. Coronal Mass Ejection (CME) Activity of Low Mass M Stars as An Important Factor for The Habitability of Terrestrial Exoplanets. II. CME-Induced Ion Pick Up of Earth-like Exoplanets in Close-In Habitable Zones. *Astrobiology*, 7(1):185–207, 2 2007. ISSN 1531-1074. doi: 10.1089/ast.2006.0128. URL http://www.liebertpub.com/doi/10.1089/ast.2006.0128.

Y.-T. Lau and J. M. Finn. Three-dimensional kinematic reconnection in the presence of field nulls and closed field lines. *Astrophysical Journal*, 350:672–691, February 1990. doi: 10.1086/168419.

C. O. Lee, C. N. Arge, D. Odstrčil, G. Millward, V. Pizzo, J. M. Quinn, and C. J. Henney. Ensemble Modeling of CME Propagation. *Solar Physics*, 285(1-2):349–368, 7 2013. ISSN 0038-0938. doi: 10.1007/s11207-012-9980-1. URL `http://link.springer.com/10.1007/s11207-012-9980-1`.

J. Lee and Dale E. Gary. Solar Microwave Bursts and Injection Pitch-Angle Distribution of Flare Electrons. *Astrophysical Journal*, 543(1):457–471, Nov 2000. doi: 10.1086/317080.

James R. Lemen, Alan M. Title, David J. Akin, Paul F. Boerner, Catherine Chou, Jerry F. Drake, Dexter W. Duncan, Christopher G. Edwards, Frank M. Friedlaender, and Gary F. Heyman. The Atmospheric Imaging Assembly (AIA) on the Solar Dynamics Observatory (SDO). *Solar Physics*, 275(1-2):17–40, Jan 2012. doi: 10.1007/s11207-011-9776-8.

J. Lin and T. G. Forbes. Effects of reconnection on the coronal mass ejection process. *Journal of Geophysical Research*, 105(A2):2375–2392, Feb 2000. doi: 10.1029/1999JA900477.

Jun Lin, Nicholas A. Murphy, Chengcai Shen, John C. Raymond, Katharine K. Reeves, Jiayong Zhong, Ning Wu, and Yan Li. Review on Current Sheets in CME Development: Theories and Observations. *Space Science Reviews*, 194(1-4):237–302, Nov 2015. doi: 10.1007/s11214-015-0209-0.

R. P. Lin, R. A. Schwartz, R. M. Pelling, and K. C. Hurley. A new component of hard X-rays in solar flares. *Astrophysical Journal Letters*, 251:L109–L114, December 1981. doi: 10.1086/183704.

R. P. Lin, B. R. Dennis, G. J. Hurford, D. M. Smith, A. Zehnder, P. R. Harvey, D. W. Curtis, D. Pankow, P. Turin, and M. Bester. The Reuven Ramaty High-Energy Solar Spectroscopic Imager (RHESSI). *Solar Physics*, 210(1):3–32, Nov 2002. doi: 10.1023/A:1022428818870.

Y. E. Litvinenko. Particle Acceleration in Reconnecting Current Sheets with a Nonzero Magnetic Field. *Astrophysical Journal*, 462:997, May 1996. doi: 10.1086/177213.

Wei Liu, Leon Ofman, Nariaki V. Nitta, Markus J. Aschwanden, Carolus J. Schrijver, Alan M. Title, and Theodore D. Tarbell. Quasi-periodic Fast-mode Wave Trains Within a Global EUV Wave and Sequential Transverse Oscillations Detected by SDO/AIA. *The Astrophysical Journal, Volume 753, Issue 1, article id. 52, 17 pp. (2012).*, 753, 4 2012. ISSN

0004-637X. doi: 10.1088/0004-637X/753/1/52. URL http://arxiv.org/abs/1204.5470 http://dx.doi.org/10.1088/0004-637X/753/1/52.

Wei Liu, Meng Jin, Cooper Downs, Leon Ofman, Mark C. M. Cheung, and Nariaki V. Nitta. A Truly Global Extreme Ultraviolet Wave from the SOL2017-09-10 X8.2+ Solar Flare-Coronal Mass Ejection. *Astrophysical Journal Letters*, 864(2):L24, Sep 2018. doi: 10.3847/2041-8213/aad77b.

Y. Liu, J.D. Richardson, and J.W. Belcher. A statistical study of the properties of interplanetary coronal mass ejections from 0.3 to 5.4AU. *Planetary and Space Science*, 53(1-3):3–17, 1 2005. ISSN 00320633. doi: 10.1016/j.pss.2004.09.023. URL https://linkinghub.elsevier.com/retrieve/pii/S0032063304001631.

Y. Liu, X. Sun, T. Török, V. S. Titov, and J. E. Leake. Electric-current Neutralization, Magnetic Shear, and Eruptive Activity in Solar Active Regions. *Astrophysical Journal Letters*, 846:L6, September 2017. doi: 10.3847/2041-8213/aa861e.

Y. C. Liu, A. B. Galvin, K. D. Simunac, L. M. Kistler, M. A. Popecki, C. F. Farrugia, L Ellis, E Mobius, M. A. Lee, T. H. Zurbuchen, S Lepri, L. M. Blush, P Bochsler, H Daoudi, P Wurz, R. F. Wimmer-Schweingruber, B Klecker, and B Thompson. Oxygen Observations by STEREO/PLASTIC in the Slow Solar Wind. In *AGU Fall Meeting Abstracts*, volume 2008, pages SH51B–1604, 12 2008.

David M. Long, Peter T. Gallagher, R. T. James McAteer, and D. Shaun Bloomfield. The Kinematics of a Globally Propagating Disturbance in the Solar Corona. *The Astrophysical Journal Letters, Volume 680, Issue 1, pp. L81 (2008).*, 680:L81, 5 2008. ISSN 0004-637X. doi: 10.1086/589742. URL http://arxiv.org/abs/0805.2023 http://dx.doi.org/10.1086/589742.

David M. Long, Edward E. DeLuca, and Peter T. Gallagher. The Wave Properties of Coronal Bright Fronts Observed Using SDO/AIA. *The Astrophysical Journal Letters, Volume 741, Issue 1, article id. L21, 6 pp. (2011).*, 741, 9 2011. ISSN 0004-637X. doi: 10.1088/2041-8205/741/1/L21. URL http://arxiv.org/abs/1109.5897 http://dx.doi.org/10.1088/2041-8205/741/1/L21.

David M. Long, D. Shaun Bloomfield, Peng-Fei Chen, Cooper Downs, Peter T. Gallagher, Ryun Young Kwon, Kamalam Vanninathan, Astrid M. Veronig, Angelos Vourlidas, Bojan

Vrsnak, Alexander Warmuth, and Tomislav Zic. Understanding the Physical Nature of Coronal "EIT Waves". *Solar Physics*, 292(1):7, 11 2016. ISSN 0038-0938. doi: 10.1007/s11207-016-1030-y. URL http://link.springer.com/10.1007/s11207-016-1030-y http://arxiv.org/abs/1611.05505 http://dx.doi.org/10.1007/s11207-016-1030-y.

David M. Long, Louise K. Harra, Sarah A. Matthews, Harry P. Warren, Kyoung-Sun Lee, George A. Doschek, Hirohisa Hara, and Jack M. Jenkins. Plasma Evolution within an Erupting Coronal Cavity. *Astrophysical Journal*, 855(2):74, Mar 2018. doi: 10.3847/1538-4357/aaad68.

D. Longcope, J. Qiu, and J. Brewer. A Reconnection-driven Model of the Hard X-Ray Loop-top Source from Flare 2004-Feb-26. *Astrophysical Journal*, 833:211, December 2016. doi: 10.3847/1538-4357/833/2/211.

D. W. Longcope and S. E. Guidoni. A Model for the Origin of High Density in Looptop X-Ray Sources. *Astrophysical Journal*, 740:73, October 2011. doi: 10.1088/0004-637X/740/2/73.

D. W. Longcope and J. A. Klimchuk. How Gas-dynamic Flare Models Powered by Petschek Reconnection Differ from Those with Ad Hoc Energy Sources. *Astrophysical Journal*, 813(2):131, Nov 2015. doi: 10.1088/0004-637X/813/2/131.

Dana W. Longcope. Topological Methods for the Analysis of Solar Magnetic Fields. *Living Reviews in Solar Physics*, 2(1):7, Nov 2005. doi: 10.12942/lrsp-2005-7.

B. C. Low. Magnetohydrodynamic processes in the solar corona: Flares, coronal mass ejections, and magnetic helicity. *Physics of Plasmas*, 1(5):1684–1690, 5 1994. doi: 10.1063/1.870671.

B. C. Low. Coronal mass ejections, magnetic flux ropes, and solar magnetism. *Journal of Geophysical Research*, 106(A11):25141–25164, Nov 2001. doi: 10.1029/2000JA004015.

N. Lugaz, IV Manchester, W. B., and T. I. Gombosi. The Evolution of Coronal Mass Ejection Density Structures. *Astrophysical Journal*, 627(2):1019–1030, Jul 2005. doi: 10.1086/430465.

No Lugaz, Manuela Temmer, Yuming Wang, and Charles J. Farrugia. The Interaction of Successive Coronal Mass Ejections: A Review. *Solar Physics*, 292(4):64, 4 2017. ISSN 0038-0938. doi: 10.1007/s11207-017-1091-6. URL

http://arxiv.org/abs/1612.02398 http://dx.doi.org/10.1007/s11207-017-1091-6 http://link.springer.com/10.1007/s11207-017-1091-6.

B. J. Lynch, J. R. Gruesbeck, T. H. Zurbuchen, and S. K. Antiochos. Solar cycle-dependent helicity transport by magnetic clouds. *Journal of Geophysical Research: Space Physics*, 110(A8), 8 2005. ISSN 01480227. doi: 10.1029/2005JA011137. URL http://doi.wiley.com/10.1029/2005JA011137.

A. Maggio. Non-thermal hard X-ray emission from stellar coronae. , 79:186, Jan 2008.

Ward Manchester, Emilia K. J. Kilpua, Ying D. Liu, No Lugaz, Pete Riley, Tibor Török, and Bojan Vršnak. The Physical Processes of CME/ICME Evolution. *Space Science Reviews*, 212(3-4):1159–1219, 11 2017. ISSN 0038-6308. doi: 10.1007/s11214-017-0394-0. URL http://link.springer.com/10.1007/s11214-017-0394-0.

G. Mann, H. Aurass, and A. Warmuth. Electron acceleration by the reconnection outflow shock during solar flares. *Astronomy and Astrophysics*, 454(3):969–974, Aug 2006. doi: 10.1051/0004-6361:20064990.

J. T. Mariska, A. G. Emslie, and P. Li. Numerical simulations of impulsively heated solar flares. *Astrophysical Journal*, 341:1067–1074, June 1989. doi: 10.1086/167564.

James Paul Mason, Thomas N Woods, David F Webb, Barbara J Thompson, Robin C Colaninno, and Angelos Vourlidas. Relationship of EUV Irradiance Coronal Dimming Slope and Depth to Coronal Mass Ejection Speed and Mass. *Astrophysical Journal*, 830(1):20, 10 2016. doi: 10.3847/0004-637X/830/1/20.

S. Masson, E. Pariat, G. Aulanier, and C. J. Schrijver. The Nature of Flare Ribbons in Coronal Null-Point Topology. *Astrophysical Journal*, 700:559–578, July 2009. doi: 10.1088/0004-637X/700/1/559.

S. Masuda, T. Kosugi, H. Hara, S. Tsuneta, and Y. Ogawara. A loop-top hard X-ray source in a compact solar flare as evidence for magnetic reconnection. *Nature*, 371(6497):495–497, Oct 1994. doi: 10.1038/371495a0.

M. L. Mays, A. Taktakishvili, A. Pulkkinen, P. J. MacNeice, L. Rastätter, D. Odstrcil, L. K. Jian, I. G. Richardson, J. A. LaSota, Y. Zheng, and M. M. Kuznetsova. Ensemble Modeling of CMEs Using the WSAENLIL+Cone Model. *Solar Physics*, 290(6):1775–1814, 6 2015. ISSN 0038-0938. doi: 10.1007/s11207-015-0692-1. URL http://arxiv.org/abs/1504.04402 http://dx.doi.org/10.1007/s11207-015-0692-1 http://link.springer.com/10.1007/s11207-015-0692-1.

Ryan M. McGranaghan, Anthony J. Mannucci, Brian Wilson, Chris A Mattmann, and Richard Chadwick. New Capabilities for Prediction of High-Latitude Ionospheric Scintillation: A Novel Approach With Machine Learning. *Space Weather*, 16(11):1817–1846, 11 2018. ISSN 15427390. doi: 10.1029/2018SW002018. URL http://doi.wiley.com/10.1029/2018SW002018.

D. B. Melrose and J. C. Brown. Precipitation in trap models for solar hard X-ray bursts. *Monthly Notices of the Royal Astronomical Society*, 176:15–30, Jul 1976. doi: 10.1093/mnras/176.1.15.

Zoran Mikic and Jon A. Linker. Disruption of Coronal Magnetic Field Arcades. *Astrophysical Journal*, 430:898, Aug 1994. doi: 10.1086/174460.

J. A. Miller, T. N. Larosa, and R. L. Moore. Stochastic Electron Acceleration by Cascading Fast Mode Waves in Impulsive Solar Flares. *Astrophysical Journal*, 461:445, April 1996. doi: 10.1086/177072.

J. A. Miller, P. J. Cargill, A. G. Emslie, G. D. Holman, B. R. Dennis, T. N. LaRosa, R. M. Winglee, S. G. Benka, and S. Tsuneta. Critical issues for understanding particle acceleration in impulsive solar flares. *Journal of Geophysical Research*, 102:14631–14660, July 1997. doi: 10.1029/97JA00976.

Ryan O. Milligan. Extreme Ultra-Violet Spectroscopy of the Lower Solar Atmosphere During Solar Flares (Invited Review). *Solar Physics*, 290(12):3399–3423, Dec 2015. doi: 10.1007/s11207-015-0748-2.

Ryan O. Milligan and Brian R. Dennis. Velocity Characteristics of Evaporated Plasma Using Hinode/EUV Imaging Spectrometer. *Astrophysical Journal*, 699(2):968–975, Jul 2009. doi: 10.1088/0004-637X/699/2/968.

Ryan O. Milligan, Graham S. Kerr, Brian R. Dennis, Hugh S. Hudson, Lyndsay Fletcher, Joel C. Allred, Phillip C. Chamberlin, Jack Ireland, Mihalis Mathioudakis, and Francis P. Keenan. The Radiated Energy Budget of Chromospheric Plasma in a Major Solar Flare Deduced from Multi-wavelength Observations. *Astrophysical Journal*, 793(2):70, Oct 2014. doi: 10.1088/0004-637X/793/2/70.

Ronald L. Moore and George Roumeliotis. Triggering of eruptive flares: Destabilization of the preflare magnetic field configuration. In *Eruptive Solar Flares*, pages 69–78. Springer Berlin Heidelberg, Berlin, Heidelberg, 1992. doi: 10.1007/3-540-55246-4{_}79. URL http://link.springer.com/10.1007/3-540-55246-4$_7$9.

Ronald L. Moore, Alphonse C. Sterling, Hugh S. Hudson, and James R. Lemen. Onset of the Magnetic Explosion in Solar Flares and Coronal Mass Ejections. *Astrophysical Journal*, 552(2): 833–848, May 2001. doi: 10.1086/320559.

G. E. Moreton. Hα Observations of Flare-Initiated Disturbances with Velocities ˜1000 km/sec. *The Astronomical Journal*, 65:494, 1960. ISSN 00046256. doi: 10.1086/108346. URL http://adsabs.harvard.edu/cgi-bin/bib$_q$$uery$?1960$AJ$.....65$U$.494$M$.

D Moses, F Clette, J P. Delaboudinière, G. E. Artzner, M Bougnet, J Brunaud, C Carabetian, A. H. Gabriel, J. F. Hochedez, F Millier, X. Y. Song, B Au, K. P. Dere, R. A. Howard, R Kreplin, D. J. Michels, J. M. Defise, C Jamar, P Rochus, J. P. Chauvineau, J. P. Marioge, R. C. Catura, J. R. Lemen, L Shing, R. A. Stern, J. B. Gurman, W. M. Neupert, J Newmark, B Thompson, A Maucherat, F Portier-Fozzani, D Berghmans, P Cugnon, E. L. van Dessel, and J. R. Gabryl. EIT Observations of the Extreme Ultraviolet Sun. *Solar Physics*, 175(2):571–599, 10 1997. doi: 10.1023/A:1004902913117.

C. Möstl, C. J. Farrugia, M. Temmer, C. Miklenic, A. M. Veronig, A. B. Galvin, M. Leitner, and H. K. Biernat. LINKING REMOTE IMAGERY OF A CORONAL MASS EJECTION TO ITS IN SITU SIGNATURES AT 1 AU. *The Astrophysical Journal*, 705 (2):L180–L185, 11 2009. ISSN 0004-637X. doi: 10.1088/0004-637X/705/2/L180. URL http://stacks.iop.org/1538-4357/705/i=2/a=L180.

C. Möstl, K. Amla, J. R. Hall, P. C. Liewer, E. M. De Jong, R. C. Colaninno, A. M. Veronig, T. Rollett, M. Temmer, V. Peinhart, J. A. Davies, N. Lugaz, Y. D. Liu, C. J. Farrugia, J. G. Luhmann, B. Vršnak, R. A. Harrison, and A. B. Galvin. CONNECTING SPEEDS, DIRECTIONS AND ARRIVAL TIMES OF 22 CORONAL MASS EJECTIONS FROM THE SUN TO 1 AU. *The Astrophysical Journal*, 787(2):119, 5 2014. ISSN 0004-637X. doi: 10.1088/0004-637X/787/2/119. URL `http://arxiv.org/abs/1404.3579 http://dx.doi.org/10.1088/0004-637X/787/2/119 http://stacks.iop.org/0004-637X/787/i=2/a=119`.

F. Nagai and A. G. Emslie. Gas dynamics in the impulsive phase of solar flares. I Thick-target heating by nonthermal electrons. *Astrophysical Journal*, 279:896–908, April 1984. doi: 10.1086/161960.

W. A. Newcomb. Hydromagnetic stability of a diffuse linear pinch. *Annals of Physics*, 10:232–267, June 1960. doi: 10.1016/0003-4916(60)90023-3.

Chigomezyo M. Ngwira, Antti Pulkkinen, Maria M. Kuznetsova, and Alex Glocer. Modeling extreme Carrington-type space weather events using three-dimensional global MHD simulations. *Journal of Geophysical Research: Space Physics*, 119(6):4456–4474, 6 2014. ISSN 21699380. doi: 10.1002/2013JA019661. URL `http://doi.wiley.com/10.1002/2013JA019661`.

T. Nieves-Chinchilla, R. Colaninno, A. Vourlidas, A. Szabo, R. P. Lepping, S. A. Boardsen, B. J. Anderson, and H. Korth. Remote and in situ observations of an unusual Earth-directed coronal mass ejection from multiple viewpoints. *Journal of Geophysical Research: Space Physics*, 117(A6):n/a–n/a, 6 2012. ISSN 01480227. doi: 10.1029/2011JA017243. URL `http://doi.wiley.com/10.1029/2011JA017243`.

Nariaki V. Nitta, Carolus J. Schrijver, Alan M. Title, and Wei Liu. SDO AIA Observations of Large-Scale Coronal Disturbances in the Form of Propagating Fronts. In *SDO-3: Exploring the Network of SDO Science*, page 111, Mar 2013.

Nariaki V Nitta, Carolus J Schrijver, Alan M Title, and Wei Liu. SDO AIA Observations of Large-Scale Coronal Disturbances in the Form of Propagating Fronts. In *SDO-3: Exploring the Network of SDO Science*, page 111, 3 2013.

Dusan Odstrcil, Victor J. Pizzo, Jon A. Linker, Pete Riley, Roberto Lionello, and Zoran Mikic. Initial coupling of coronal and heliospheric numerical magnetohydrodynamic codes. *Journal of Atmospheric and Solar-Terrestrial Physics*, 66(15-16): 1311–1320, 10 2004. ISSN 13646826. doi: 10.1016/j.jastp.2004.04.007. URL https://linkinghub.elsevier.com/retrieve/pii/S1364682604001415.

Susanna Parenti. Solar prominences: Observations. *Living Reviews in Solar Physics*, 11(1):1, Mar 2014. ISSN 1614-4961. doi: 10.12942/lrsp-2014-1. URL https://doi.org/10.12942/lrsp-2014-1.

E. N. Parker. Sweet's Mechanism for Merging Magnetic Fields in Conducting Fluids. *Journal of Geophysical Research*, 62:509–520, December 1957. doi: 10.1029/JZ062i004p00509.

C. E. Parnell, J. M. Smith, T. Neukirch, and E. R. Priest. The structure of three-dimensional magnetic neutral points. *Physics of Plasmas*, 3:759–770, Mar 1996. doi: 10.1063/1.871810.

S. Patsourakos, A. Vourlidas, and G. Stenborg. The Genesis of an Impulsive Coronal Mass Ejection Observed at Ultra-high Cadence by AIA on SDO. *Astrophysical Journal Letters*, 724:L188–L193, December 2010. doi: 10.1088/2041-8205/724/2/L188.

W. Dean Pesnell, B. J. Thompson, and P. C. Chamberlin. The Solar Dynamics Observatory (SDO). *Solar Physics*, 275(1-2):3–15, Jan 2012. doi: 10.1007/s11207-011-9841-3.

Vahé Petrosian. Stochastic Acceleration by Turbulence. *Space Science Reviews*, 173(1-4):535–556, Nov 2012. doi: 10.1007/s11214-012-9900-6.

Vahé Petrosian and Siming Liu. Stochastic Acceleration of Electrons and Protons. I. Acceleration by Parallel-Propagating Waves. *Astrophysical Journal*, 610(1):550–571, Jul 2004. doi: 10.1086/421486.

Vahé Petrosian, Timothy Q. Donaghy, and James M. McTiernan. Loop Top Hard X-Ray Emission in Solar Flares: Images and Statistics. *Astrophysical Journal*, 569(1):459–473, Apr 2002. doi: 10.1086/339240.

H. E. Petschek. Magnetic Field Annihilation. *NASA Special Publication*, 50:425, 1964.

Alexei A. Pevtsov, Mitchell A. Berger, Alexander Nindos, Aimee A. Norton, and Lidia van Driel-Gesztelyi. Magnetic Helicity, Tilt, and Twist. *Space Science Reviews*, 186(1-4):285–324, Dec 2014. doi: 10.1007/s11214-014-0082-2.

Monique Pick and Nicole Vilmer. Sixty-five years of solar radioastronomy: flares, coronal mass ejections and Sun Earth connection. *Astronomy and Astrophysics Reviews*, 16:1–153, Oct 2008. doi: 10.1007/s00159-008-0013-x.

A. I. Poland, R. A. Howard, M. J. Koomen, D. J. Michels, and Jr. Sheeley, N. R. Coronal Transients Near Sunspot Maximum. *Solar Physics*, 69(1):169–175, Jan 1981. doi: 10.1007/BF00151264.

Jens Pomoell and S. Poedts. EUHFORIA: European heliospheric forecasting information asset. *Journal of Space Weather and Space Climate*, 8:A35, 6 2018. ISSN 2115-7251. doi: 10.1051/swsc/2018020. URL `https://www.swsc-journal.org/10.1051/swsc/2018020`.

D. I. Pontin. Theory of magnetic reconnection in solar and astrophysical plasmas. *Philosophical Transactions of the Royal Society of London Series A*, 370(1970):3169–3192, Jul 2012. doi: 10.1098/rsta.2011.0501.

E. Priest. *Magnetohydrodynamics of the Sun*. Cambridge, UK: Cambridge University Press, 2014, May 2014.

E. Priest and T. Forbes. *Magnetic Reconnection*. Cambridge, UK: Cambridge University Press, June 2000.

E. R. Priest and P. Démoulin. Three-dimensional magnetic reconnection without null points. 1. Basic theory of magnetic flipping. *Journal of Geophysical Research*, 100(A12):23443–23464, Dec 1995. doi: 10.1029/95JA02740.

E. R. Priest and T. G. Forbes. New models for fast steady state magnetic reconnection. *Journal of Geophysical Research*, 91:5579–5588, May 1986. doi: 10.1029/JA091iA05p05579.

E. R. Priest and D. W. Longcope. Flux-Rope Twist in Eruptive Flares and CMEs: Due to Zipper and Main-Phase Reconnection. *Solar Physics*, 292(1):25, Jan 2017. doi: 10.1007/s11207-016-1049-0.

E. R. Priest and V. S. Titov. Magnetic Reconnection at Three-Dimensional Null Points. *Philosophical Transactions of the Royal Society of London Series A*, 354:2951–2992, December 1996. doi: 10.1098/rsta.1996.0136.

F. Pucci and M. Velli. Reconnection of Quasi-singular Current Sheets: The "Ideal" Tearing Mode. *Astrophysical Journal Letters*, 780:L19, January 2014. doi: 10.1088/2041-8205/780/2/L19.

J. Qiu and D. W. Longcope. Long Duration Flare Emission: Impulsive Heating or Gradual Heating? *Astrophysical Journal*, 820:14, March 2016. doi: 10.3847/0004-637X/820/1/14.

J. Qiu, H. Wang, C. Z. Cheng, and D. E. Gary. Magnetic Reconnection and Mass Acceleration in Flare-Coronal Mass Ejection Events. *Astrophysical Journal*, 604:900–905, April 2004. doi: 10.1086/382122.

Jiong Qiu, Qiang Hu, Timothy A. Howard, and Vasyl B. Yurchyshyn. On the Magnetic Flux Budget in Low-Corona Magnetic Reconnection and Interplanetary Coronal Mass Ejections. *Astrophysical Journal*, 659(1):758–772, Apr 2007. doi: 10.1086/512060.

F. Reale. Coronal Loops: Observations and Modeling of Confined Plasma. *Living Reviews in Solar Physics*, 11:4, July 2014. doi: 10.12942/lrsp-2014-4.

J. W. Reep and A. J. B. Russell. Alfvénic Wave Heating of the Upper Chromosphere in Flares. *Astrophysical Journal Letters*, 818(1):L20, Feb 2016. doi: 10.3847/2041-8205/818/1/L20.

J. W. Reep, A. J. B. Russell, L. A. Tarr, and J. E. Leake. A Hydrodynamic Model of Alfvénic Wave Heating in a Coronal Loop and Its Chromospheric Footpoints. *Astrophysical Journal*, 853: 101, February 2018. doi: 10.3847/1538-4357/aaa2fe.

Jeffrey Reep. *Hydrodynamic Modeling of Heating Processes in Solar Flares.* PhD thesis, Rice University, Jan 2014.

A. A. Reinard and D. A. Biesecker. Coronal Mass EjectionAssociated Coronal Dimmings. *The Astrophysical Journal*, 674(1):576–585, 2 2008. ISSN 0004-637X. doi: 10.1086/525269. URL `http://stacks.iop.org/0004-637X/674/i=1/a=576`.

A. A. Reinard and D. A. Biesecker. THE RELATIONSHIP BETWEEN CORONAL DIMMING AND CORONAL MASS EJECTION PROPERTIES. *The Astrophysical Journal*, 705(1):914–919, 11 2009. ISSN 0004-637X. doi: 10.1088/0004-637X/705/1/914. URL http://stacks.iop.org/0004-637X/705/i=1/a=914.

Eva Robbrecht, Spiros Patsourakos, and Angelos Vourlidas. No Trace Left Behind: STEREO Observation of a Coronal Mass Ejection Without Low Coronal Signatures. *Astrophysical Journal*, 701(1):283–291, Aug 2009. doi: 10.1088/0004-637X/701/1/283.

F. Rubio da Costa, W. Liu, V. Petrosian, and M. Carlsson. Combined Modeling of Acceleration, Transport, and Hydrodynamic Response in Solar Flares. II. Inclusion of Radiative Transfer with RADYN. *Astrophysical Journal*, 813:133, November 2015. doi: 10.1088/0004-637X/813/2/133.

Fatima Rubio da Costa, Lucia Kleint, Vahé Petrosian, Wei Liu, and Joel C. Allred. Data-driven Radiative Hydrodynamic Modeling of the 2014 March 29 X1.0 Solar Flare. *Astrophysical Journal*, 827(1):38, Aug 2016. doi: 10.3847/0004-637X/827/1/38.

David M. Rust and Ernest Hildner. Expansion of an X-ray coronal arch into the outer corona. *Solar Physics*, 48(2):381–387, 6 1976. ISSN 0038-0938. doi: 10.1007/BF00152003. URL http://link.springer.com/10.1007/BF00152003.

DavidM. Rust. Coronal disturbances and their terrestrial effects. *Space Science Reviews*, 34(1):21, 1 1983. ISSN 0038-6308. doi: 10.1007/BF00221193. URL http://link.springer.com/10.1007/BF00221193.

D. F. Ryan, P. C. Chamberlin, R. O. Milligan, and P. T. Gallagher. Decay-phase Cooling and Inferred Heating of M- and X-class Solar Flares. *Astrophysical Journal*, 778:68, November 2013. doi: 10.1088/0004-637X/778/1/68.

N. P. Savani, A Vourlidas, I. G. Richardson, A Szabo, B. J. Thompson, A Pulkkinen, M. L. Mays, T Nieves-Chinchilla, and V Bothmer. Predicting the magnetic vectors within coronal mass ejections arriving at Earth: 2. Geomagnetic response. *Space Weather*, 15(2):441–461, 2 2017. doi: 10.1002/2016SW001458.

A. Savcheva, E. Pariat, S. McKillop, P. McCauley, E. Hanson, Y. Su, E. Werner, and E. E. DeLuca. The Relation between Solar Eruption Topologies and Observed Flare Features. I. Flare Ribbons. *Astrophysical Journal*, 810(2):96, Sep 2015. doi: 10.1088/0004-637X/810/2/96.

John Scalo, Lisa Kaltenegger, Antgona Segura, Malcolm Fridlund, Ignasi Ribas, Yu. N. Kulikov, John L. Grenfell, Heike Rauer, Petra Odert, Martin Leitzinger, F. Selsis, Maxim L. Khodachenko, Carlos Eiroa, Jim Kasting, and Helmut Lammer. M Stars as Targets for Terrestrial Exoplanet Searches And Biosignature Detection. *Astrobiology*, 7(1):85–166, 2 2007. ISSN 1531-1074. doi: 10.1089/ast.2006.0125. URL `http://www.liebertpub.com/doi/10.1089/ast.2006.0125`.

P. H. Scherrer, J. Schou, R. I. Bush, A. G. Kosovichev, R. S. Bogart, J. T. Hoeksema, Y. Liu, T. L. Duvall, J. Zhao, A. M. Title, C. J. Schrijver, T. D. Tarbell, and S. Tomczyk. The Helioseismic and Magnetic Imager (HMI) Investigation for the Solar Dynamics Observatory (SDO). *Solar Physics*, 275:207–227, January 2012. doi: 10.1007/s11207-011-9834-2.

B Schmieder, L van Driel-Gesztelyi, J. E. Wiik, T Kucera, B Thompson, C de Forest, C Saint Cyr, and G. M. Simnett. Prominence Activity Related to CME Observed by SOHO, YOHKOH and Ground-Based Observatories. In A Wilson, editor, *Fifth SOHO Workshop: The Corona and Solar Wind Near Minimum Activity*, volume 404 of *ESA Special Publication*, page 663, 1 1997.

B Schmieder, L van Driel-Gesztelyi, G Aulanier, P Démoulin, B Thompson, C De Forest, J. E. Wiik, C Saint Cyr, and J. C. Vial. Relationships between CME's and prominences. *Advances in Space Research*, 29(10):1451–1460, 1 2002. doi: 10.1016/S0273-1177(02)00211-9.

C. J. Schrijver. A Characteristic Magnetic Field Pattern Associated with All Major Solar Flares and Its Use in Flare Forecasting. *Astrophysical Journal Letters*, 655:L117–L120, February 2007. doi: 10.1086/511857.

C. J. Schrijver and A. M. Title. Long-range magnetic couplings between solar flares and coronal mass ejections observed by SDO and STEREO. *Journal of Geophysical Research: Space Physics*, 116(A4):n/a–n/a, 4 2011. ISSN 01480227. doi: 10.1029/2010JA016224. URL `http://doi.wiley.com/10.1029/2010JA016224`.

N. R. Sheeley, J. D. Bohlin, G. E. Brueckner, J. D. Purcell, V. E. Scherrer, R. Tousey,

J. B. Smith, D. M. Speich, E. Tandberg-Hanssen, R. M. Wilson, A. C. De Loach, R. B. Hoover, and J. P. Mc Guire. Coronal changes associated with a disappearing filament. *Solar Physics*, 45(2):377–392, 12 1975. ISSN 0038-0938. doi: 10.1007/BF00158457. URL http://link.springer.com/10.1007/BF00158457.

K. Shibata and T. Magara. Solar Flares: Magnetohydrodynamic Processes. *Living Reviews in Solar Physics*, 8:6, December 2011. doi: 10.12942/lrsp-2011-6.

K. Shibata and S. Tanuma. Plasmoid-induced-reconnection and fractal reconnection. *Earth, Planets, and Space*, 53:473–482, June 2001. doi: 10.1186/BF03353258.

B. V. Somov and T. Kosugi. Collisionless Reconnection and High-Energy Particle Acceleration in Solar Flares. *Astrophysical Journal*, 485:859–868, August 1997. doi: 10.1086/304449.

B. V. Somov, S. I. Syrovatskii, and A. R. Spektor. Hydrodynamic response of the solar chromosphere to an elementary flare burst. I - Heating by accelerated electrons. *Solar Physics*, 73:145–155, September 1981. doi: 10.1007/BF00153151.

Alphonse C. Sterling and Hugh S. Hudson. [ITAL]Yohkoh[/ITAL] SXT Observations of X-Ray Dimming Associated with a Halo Coronal Mass Ejection. *The Astrophysical Journal*, 491(1):L55–L58, 12 1997. ISSN 0004637X. doi: 10.1086/311043. URL http://stacks.iop.org/1538-4357/491/i=1/a=L55.

P. A. Sturrock. Model of the High-Energy Phase of Solar Flares. *Nature*, 211:695–697, August 1966. doi: 10.1038/211695a0.

P. A. Sturrock. Maximum Energy of Semi-infinite Magnetic Field Configurations. *Astrophysical Journal*, 380:655, Oct 1991. doi: 10.1086/170620.

Linhui Sui, Gordon D. Holman, and Brian R. Dennis. Evidence for Magnetic Reconnection in Three Homologous Solar Flares Observed by RHESSI. *Astrophysical Journal*, 612(1):546–556, Sep 2004. doi: 10.1086/422515.

X. Sun, J. T. Hoeksema, Y. Liu, G. Aulanier, Y. Su, I. G. Hannah, and R. A. Hock. Hot Spine Loops and the Nature of a Late-phase Solar Flare. *Astrophysical Journal*, 778:139, December 2013. doi: 10.1088/0004-637X/778/2/139.

X. Sun, M. G. Bobra, J. T. Hoeksema, Y. Liu, Y. Li, C. Shen, S. Couvidat, A. A. Norton, and G. H. Fisher. Why Is the Great Solar Active Region 12192 Flare-rich but CME-poor? *Astrophysical Journal Letters*, 804:L28, May 2015. doi: 10.1088/2041-8205/804/2/L28.

P. A. Sweet. The Neutral Point Theory of Solar Flares. In B. Lehnert, editor, *Electromagnetic Phenomena in Cosmical Physics*, volume 6 of *IAU Symposium*, page 123, 1958.

E. Tandberg-Hanssen. *The Nature of Solar Prominences*. Astrophysics and Space Science Library. Springer Netherlands, 2013. ISBN 9789401733960. URL `https://books.google.com/books?id=b03zCAAAQBAJ`.

E. Tandberg-Hanssen and A. G. Emslie. *The physics of solar flares*. Cambridge and New York, Cambridge University Press, 1988, 286 p., 1988.

M. Temmer, A. M. Veronig, E. P. Kontar, S. Krucker, and B. Vršnak. Combined STEREO/RHESSI Study of Coronal Mass Ejection Acceleration and Particle Acceleration in Solar Flares. *Astrophysical Journal*, 712:1410–1420, April 2010. doi: 10.1088/0004-637X/712/2/1410.

A. Thernisien. Implementation of the Graduated Cylindrical Shell Model for the Three-dimensional Reconstruction of Coronal Mass Ejections. *Astrophysical Journal Supplement*, 194(2):33, Jun 2011. doi: 10.1088/0067-0049/194/2/33.

A. F. R. Thernisien, R. A. Howard, and A. Vourlidas. Modeling of Flux Rope Coronal Mass Ejections. *Astrophysical Journal*, 652(1):763–773, Nov 2006. doi: 10.1086/508254.

B. J. Thompson, S. P. Plunkett, J. B. Gurman, J. S. Newmark, O. C. St. Cyr, and D. J. Michels. SOHO/EIT observations of an Earth-directed coronal mass ejection on May 12, 1997. *Geophysical Research Letters*, 25(14):2465–2468, Jan 1998. doi: 10.1029/98GL50429.

B. J. Thompson, S. P. Plunkett, J. B. Gurman, J. S. Newmark, O. C. St. Cyr, and D. J. Michels. SOHO/EIT observations of an Earth-directed coronal mass ejection on May 12, 1997. *Geophysical Research Letters*, 25(14):2465–2468, 1 1998. doi: 10.1029/98GL50429.

B. J. Thompson, J. B. Gurman, W. M. Neupert, J. S. Newmark, J P. Delaboudinière, O. C. St. Cyr, S Stezelberger, K. P. Dere, R. A. Howard, and D. J. Michels. SOHO/EIT Observations of

the 1997 April 7 Coronal Transient: Possible Evidence of Coronal Moreton Waves. *Astrophysical Journal*, 517(2):L151–L154, 6 1999a. doi: 10.1086/312030.

B. J. Thompson, O. C. St. Cyr, S. P. Plunkett, J. B. Gurman, N. Gopalswamy, H. S. Hudson, R. A. Howard, D. J. Michels, and J.-P. Delaboudinière. The correspondence of EUV and white light observations of coronal mass ejections with SOHO EIT and LASCO. In *Sun-Earth Plasma Connections*, pages 31–46. American Geophysical Union (AGU), 1999b. doi: 10.1029/GM109p0031. URL `http://www.agu.org/books/gm/v109/GM109p0031/GM109p0031.shtml`.

Hui Tian, Scott W. McIntosh, Lidong Xia, Jiansen He, and Xin Wang. WHAT CAN WE LEARN ABOUT SOLAR CORONAL MASS EJECTIONS, CORONAL DIMMINGS, AND EXTREME-ULTRAVIOLET JETS THROUGH SPECTROSCOPIC OBSERVATIONS? *The Astrophysical Journal*, 748(2):106, mar 2012. doi: 10.1088/0004-637x/748/2/106. URL `https://doi.org/10.1088%2F0004-637x%2F748%2F2%2F106`.

Vyacheslav S. Titov, Gunnar Hornig, and Pascal Démoulin. Theory of magnetic connectivity in the solar corona. *Journal of Geophysical Research (Space Physics)*, 107(A8):1164, Aug 2002. doi: 10.1029/2001JA000278.

T. Török and B. Kliem. Confined and Ejective Eruptions of Kink-unstable Flux Ropes. *Astrophysical Journal Letters*, 630:L97–L100, September 2005. doi: 10.1086/462412.

R. Tousey. The solar corona. In *Space Research Conference*, volume 2, pages 713–730, Jan 1973.

S. Tsuneta and T. Naito. Fermi Acceleration at the Fast Shock in a Solar Flare and the Impulsive Loop-Top Hard X-Ray Source. *Astrophysical Journal Letters*, 495:L67–L70, March 1998. doi: 10.1086/311207.

Yutaka Uchida. Propagation of hydromagnetic disturbances in the solar corona and Moreton's wave phenomenon. *Solar Physics*, 4(1):30–44, 5 1968. ISSN 0038-0938. doi: 10.1007/BF00146996. URL `http://link.springer.com/10.1007/BF00146996`.

A. A. van Ballegooijen and P. C. H. Martens. Formation and Eruption of Solar Prominences. *Astrophysical Journal*, 343:971, Aug 1989. doi: 10.1086/167766.

Tom Van Doorsselaere, Elena G. Kupriyanova, and Ding Yuan. Quasi-periodic Pulsations in Solar and Stellar Flares: An Overview of Recent Results (Invited Review). *Solar Physics*, 291(11): 3143–3164, Nov 2016. doi: 10.1007/s11207-016-0977-z.

L. van Driel-Gesztelyi and J. L. Culhane. Magnetic Flux Emergence, Activity, Eruptions and Magnetic Clouds: Following Magnetic Field from the Sun to the Heliosphere. *Space Science Reviews*, 144(1-4):351–381, Apr 2009. doi: 10.1007/s11214-008-9461-x.

L. van Driel-Gesztelyi, D. Baker, T. Török, E. Pariat, L. M. Green, D. R. Williams, J. Carlyle, G. Valori, P. Démoulin, and B. Kliem. Coronal Magnetic Reconnection Driven by CME Expansion—the 2011 June 7 Event. *Astrophysical Journal*, 788(1):85, Jun 2014. doi: 10.1088/0004-637X/788/1/85.

V. M. Vasyliunas. Theoretical models of magnetic field line merging. I. *Reviews of Geophysics and Space Physics*, 13:303–336, February 1975. doi: 10.1029/RG013i001p00303.

C. Verbeke, M. L. Mays, M. Temmer, S. Bingham, R. Steenburgh, M. Dumbović, M. Núñez, L. K. Jian, P. Hess, C. Wiegand, A. Taktakishvili, and J. Andries. Benchmarking CME Arrival Time and Impact: Progress on Metadata, Metrics, and Events. *Space Weather*, 17(1):6–26, 1 2019. ISSN 1542-7390. doi: 10.1029/2018SW002046. URL `http://arxiv.org/abs/1811.10695 http://dx.doi.org/10.1029/2018SW002046 https://onlinelibrary.wiley.com/doi/abs/10.1029/2018SW002046`.

Astrid M. Veronig, Manuela Temmer, and Bojan Vrsnak. High cadence observations of a global coronal wave by EUVI/STEREO. *The Astrophysical Journal*, 681(2):L113–L116, 6 2008. ISSN 0004-637X. doi: 10.1086/590493. URL `http://stacks.iop.org/1538-4357/681/i=2/a=L113 http://arxiv.org/abs/0806.0710 http://dx.doi.org/10.1086/590493`.

Astrid M. Veronig, Tatiana Podladchikova, Karin Dissauer, Manuela Temmer, Daniel B. Seaton, David Long, Jingnan Guo, Bojan Vršnak, Louise Harra, and Bernhard Kliem. Genesis and Impulsive Evolution of the 2017 September 10 Coronal Mass Ejection. *Astrophysical Journal*, 868(2):107, Dec 2018. doi: 10.3847/1538-4357/aaeac5.

A. Vourlidas, P. Subramanian, K. P. Dere, and R. A. Howard. Large-Angle Spectrometric Coron-

agraph Measurements of the Energetics of Coronal Mass Ejections. *Astrophysical Journal*, 534 (1):456–467, May 2000. doi: 10.1086/308747.

A. Vourlidas, B. J. Lynch, R. A. Howard, and Y. Li. How Many CMEs Have Flux Ropes? Deciphering the Signatures of Shocks, Flux Ropes, and Prominences in Coronagraph Observations of CMEs. *Solar Physics*, 8 2012a. ISSN 0038-0938. doi: 10.1007/s11207-012-0084-8. URL http://arxiv.org/abs/1207.1599 http://dx.doi.org/10.1007/s11207-012-0084-8 http://link.springer.com/10.1007/s11207-012-0084-8.

A. Vourlidas, B. J. Lynch, R. A. Howard, and Y. Li. How Many CMEs Have Flux Ropes? Deciphering the Signatures of Shocks, Flux Ropes, and Prominences in Coronagraph Observations of CMEs. *Solar Physics*, 284(1):179, 8 2012b. ISSN 0038-0938. doi: 10.1007/s11207-012-0084-8. URL http://link.springer.com/10.1007/s11207-012-0084-8.

Angelos Vourlidas. The flux rope nature of coronal mass ejections. *Plasma Physics and Controlled Fusion*, 56(6):064001, 6 2014. ISSN 0741-3335. doi: 10.1088/0741-3335/56/6/064001. URL http://stacks.iop.org/0741-3335/56/i=6/a=064001.

Angelos Vourlidas and Russell A. Howard. The proper treatment of coronal mass ejection brightness: A new methodology and implications for observations. *The Astrophysical Journal*, 642(2):1216–1221, may 2006. doi: 10.1086/501122. URL

Angelos Vourlidas, Russ A. Howard, Ed Esfandiari, Spiros Patsourakos, Seiji Yashiro, and Gregorz Michalek. Comprehensive Analysis of Coronal Mass Ejection Mass and Energy Properties Over a Full Solar Cycle. *The Astrophysical Journal, Volume 722, Issue 2, pp. 1522-1538 (2010).*, 722:1522–1538, 8 2010. ISSN 0004-637X. doi: 10.1088/0004-637X/722/2/1522. URL http://arxiv.org/abs/1008.3737 http://dx.doi.org/10.1088/0004-637X/722/2/1522.

Angelos Vourlidas, Russell A. Howard, Simon P. Plunkett, Clarence M. Korendyke, Arnaud F. R. Thernisien, Dennis Wang, Nathan Rich, Michael T. Carter, Damien H. Chua, and Dennis G. Socker. The Wide-Field Imager for Solar Probe Plus (WISPR). *Space Science Reviews*, 204(1-4): 83–130, Dec 2016. doi: 10.1007/s11214-014-0114-y.

Angelos Vourlidas, Laura A. Balmaceda, Guillermo Stenborg, and Alisson Dal Lago. Multi-

viewpoint Coronal Mass Ejection Catalog Based on STEREO COR2 Observations. *Astrophysical Journal*, 838(2):141, Apr 2017. doi: 10.3847/1538-4357/aa67f0.

B. Vršnak, T. Žic, D. Vrbanec, M. Temmer, T. Rollett, C. Möstl, A. Veronig, J. Čalogović, M. Dumbović, S. Lulić, Y.-J. Moon, and A. Shanmugaraju. Propagation of Interplanetary Coronal Mass Ejections: The Drag-Based Model. *Solar Physics*, 285(1-2):295–315, 7 2013. ISSN 0038-0938. doi: 10.1007/s11207-012-0035-4. URL `http://link.springer.com/10.1007/s11207-012-0035-4`.

Zdeněk Švestka. On 'The Solar Flare Myth' postulated by Gosling. *Solar Physics*, 160(1):53–56, Aug 1995. doi: 10.1007/BF00679093.

T. Wang, L. Ofman, X. Sun, E. Provornikova, and J. M. Davila. Evidence of Thermal Conduction Suppression in a Solar Flaring Loop by Coronal Seismology of Slow-mode Waves. *Astrophysical Journal Letters*, 811:L13, September 2015. doi: 10.1088/2041-8205/811/1/L13.

W. Wang, C. Zhu, J. Qiu, R. Liu, K. E. Yang, and Q. Hu. Evolution of a Magnetic Flux Rope toward Eruption. *Astrophysical Journal*, 871:25, January 2019. doi: 10.3847/1538-4357/aaf3ba.

Y.-M. Wang. EIT Waves and Fast-Mode Propagation in the Solar Corona. *The Astrophysical Journal*, 543(1):L89–L93, 11 2000. ISSN 0004637X. doi: 10.1086/318178. URL `http://stacks.iop.org/1538-4357/543/i=1/a=L89`.

A. Warmuth and G. Mann. Constraints on energy release in solar flares from RHESSI and GOES X-ray observations. II. Energetics and energy partition. *Astronomy and Astrophysics*, 588:A116, Apr 2016. doi: 10.1051/0004-6361/201527475.

H. P. Warren. Multithread Hydrodynamic Modeling of a Solar Flare. *Astrophysical Journal*, 637: 522–530, January 2006. doi: 10.1086/497904.

Harry P. Warren, John T. Mariska, and George A. Doschek. Observations of Thermal Flare Plasma with the EUV Variability Experiment. *Astrophysical Journal*, 770(2):116, Jun 2013. doi: 10.1088/0004-637X/770/2/116.

D. F. Webb, A. S. Krieger, and D. M. Rust. Coronal X-ray enhancements associated with H? filament disappearances. *Solar Physics*, 48(1):159–186, 5 1976. ISSN 0038-0938. doi: 10.1007/BF00153342. URL `http://link.springer.com/10.1007/BF00153342`.

D. F. Webb, O. C. St. Cyr, S. P. Plunkett, R. A. Howard, and B. J. Thompson. The Characteristics and Geoeffectiveness of SOHO-LASCO Halo CMEs. In *American Astronomical Society Meeting Abstracts #194*, volume 194 of *American Astronomical Society Meeting Abstracts*, page 17.03, 5 1999.

D. F. Webb, E. W. Cliver, N. U. Crooker, O. C. St. Cry, and B. J. Thompson. Relationship of halo coronal mass ejections, magnetic clouds, and magnetic storms. *Journal of Geophysical Research*, 105(A4):7491–7508, 4 2000. doi: 10.1029/1999JA000275.

David F. Webb and Timothy A. Howard. Coronal Mass Ejections: Observations. *Living Reviews in Solar Physics*, 9(1):3, 2012. ISSN 1614-4961. doi: 10.12942/lrsp-2012-3. URL `http://link.springer.com/10.12942/lrsp-2012-3`.

M. J. Wills-Davey and B. J. Thompson. Observations of a Propagating Disturbance in TRACE. *Solar Physics*, 190:467–483, 12 1999. doi: 10.1023/A:1005201500675.

Reka M. Winslow, No Lugaz, Lydia C. Philpott, Nathan A. Schwadron, Charles J. Farrugia, Brian J. Anderson, and Charles W. Smith. Interplanetary coronal mass ejections from MESSENGER orbital observations at Mercury. *Journal of Geophysical Research: Space Physics*, 120(8):6101–6118, 8 2015. ISSN 21699380. doi: 10.1002/2015JA021200. URL `http://doi.wiley.com/10.1002/2015JA021200`.

Reka M. Winslow, No Lugaz, Nathan A. Schwadron, Charles J. Farrugia, Wenyuan Yu, Jim M. Raines, M. Leila Mays, Antoinette B. Galvin, and Thomas H. Zurbuchen. Longitudinal conjunction between MESSENGER and STEREO A: Development of ICME complexity through stream interactions. *Journal of Geophysical Research: Space Physics*, 121(7):6092–6106, 7 2016. ISSN 21699380. doi: 10.1002/2015JA022307. URL `http://doi.wiley.com/10.1002/2015JA022307`.

G. L. Withbroe. The thermal phase of a large solar flare. *Astrophysical Journal*, 225:641–649, October 1978. doi: 10.1086/156524.

Alexandra M. Wold, M. Leila Mays, Aleksandre Taktakishvili, Lan K. Jian, Dusan Odstrcil, and Peter MacNeice. Verification of real-time WSAENLIL+Cone simulations of CME arrival-time at the CCMC from 2010 to 2016. *Journal of Space Weather and*

Space Climate, 8:A17, 3 2018. ISSN 2115-7251. doi: 10.1051/swsc/2018005. URL https://www.swsc-journal.org/10.1051/swsc/2018005.

L. Woltjer. A Theorem on Force-Free Magnetic Fields. *Proceedings of the National Academy of Science*, 44:489–491, June 1958. doi: 10.1073/pnas.44.6.489.

T. N. Woods. Extreme Ultraviolet Late-Phase Flares: Before and During the Solar Dynamics Observatory Mission. *Solar Physics*, 289:3391–3401, September 2014. doi: 10.1007/s11207-014-0483-0.

T. N. Woods, R. Hock, F. Eparvier, A. R. Jones, P. C. Chamberlin, J. A. Klimchuk, L. Didkovsky, D. Judge, J. Mariska, H. Warren, C. J. Schrijver, D. F. Webb, S. Bailey, and W. K. Tobiska. New Solar Extreme-ultraviolet Irradiance Observations during Flares. *Astrophysical Journal*, 739:59, October 2011. doi: 10.1088/0004-637X/739/2/59.

T. N. Woods, F. G. Eparvier, R. Hock, A. R. Jones, D. Woodraska, D. Judge, L. Didkovsky, J. Lean, J. Mariska, H. Warren, D. McMullin, P. Chamberlin, G. Berthiaume, S. Bailey, T. Fuller-Rowell, J. Sojka, W. K. Tobiska, and R. Viereck. Extreme Ultraviolet Variability Experiment (EVE) on the Solar Dynamics Observatory (SDO): Overview of Science Objectives, Instrument Design, Data Products, and Model Developments. *Solar Physics*, 275:115–143, January 2012. doi: 10.1007/s11207-009-9487-6.

S. Yashiro, N. Gopalswamy, G. Michalek, O. C. St. Cyr, S. P. Plunkett, N. B. Rich, and R. A. Howard. A catalog of white light coronal mass ejections observed by the SOHO spacecraft. *Journal of Geophysical Research (Space Physics)*, 109(A7):A07105, Jul 2004a. doi: 10.1029/2003JA010282.

S. Yashiro, N. Gopalswamy, G. Michalek, O. C. St. Cyr, S. P. Plunkett, N. B. Rich, and R. A. Howard. A catalog of white light coronal mass ejections observed by the SOHO spacecraft. *Journal of Geophysical Research (Space Physics)*, 109(A7):A07105, Jul 2004b. doi: 10.1029/2003JA010282.

Takaaki Yokoyama and Kazunari Shibata. A Two-dimensional Magnetohydrodynamic Simulation of Chromospheric Evaporation in a Solar Flare Based on a Magnetic Reconnection Model. *Astrophysical Journal*, 494(1):L113–L116, Feb 1998. doi: 10.1086/311174.

D. M. Zarro, R. C. Canfield, K. T. Strong, and T. R. Metcalf. Explosive plasma flows in a solar flare. *Astrophysical Journal*, 324:582–589, January 1988. doi: 10.1086/165919.

Dominic M Zarro, Alphonse C Sterling, Barbara J Thompson, Hugh S Hudson, and Nariaki Nitta. SOHO EIT Observations of Extreme-Ultraviolet "Dimming" Associated with a Halo Coronal Mass Ejection. *Astrophysical Journal Letters*, 520(2):L139–L142, 8 1999. doi: 10.1086/312150.

J. Zhang, K. P. Dere, R. A. Howard, M. R. Kundu, and S. M. White. On the Temporal Relationship between Coronal Mass Ejections and Flares. *Astrophysical Journal*, 559:452–462, September 2001. doi: 10.1086/322405.

C. Zhu, J. Qiu, and D. W. Longcope. Two-phase Heating in Flaring Loops. *Astrophysical Journal*, 856:27, March 2018. doi: 10.3847/1538-4357/aaad10.

A. N. Zhukov and F. Auchère. On the nature of EIT waves, EUV dimmings and their link to CMEs. *Astronomy & Astrophysics*, 427(2):705–716, 11 2004. ISSN 0004-6361. doi: 10.1051/0004-6361:20040351. URL `http://www.aanda.org/10.1051/0004-6361:20040351`.

Thomas H. Zurbuchen and Ian G. Richardson. In-Situ Solar Wind and Magnetic Field Signatures of Interplanetary Coronal Mass Ejections. *Space Science Reviews*, 123(1-3):31–43, 11 2006. ISSN 0038-6308. doi: 10.1007/s11214-006-9010-4. URL `http://link.springer.com/10.1007/s11214-006-9010-4`.

Chapter 5

Small-Scale Coronal Activity

Chapter 6

The Coronal Heating Problem

Chapter 7

Solar Wind

Chapter 8

Solar Energetic Particles and Cosmic Rays

Chapter 9

Physics of the Outer Heliosphere